

January 2011

Optimization And Validation Of Direct Analysis In Real Time Mass Spectrometry (dart-Ms) For Quantitation Of Sugars To Advance Biofuel Production

Daudi Sayialel Saang'onyo
Eastern Kentucky University

Follow this and additional works at: <https://encompass.eku.edu/etd>

 Part of the [Analytical Chemistry Commons](#)

Recommended Citation

Saang'onyo, Daudi Sayialel, "Optimization And Validation Of Direct Analysis In Real Time Mass Spectrometry (dart-Ms) For Quantitation Of Sugars To Advance Biofuel Production" (2011). *Online Theses and Dissertations*. 44.
<https://encompass.eku.edu/etd/44>

This Open Access Thesis is brought to you for free and open access by the Student Scholarship at Encompass. It has been accepted for inclusion in Online Theses and Dissertations by an authorized administrator of Encompass. For more information, please contact Linda.Sizemore@eku.edu.

OPTIMIZATION AND VALIDATION OF DIRECT ANALYSIS IN REAL TIME MASS
SPECTROMETRY (DART-MS) FOR QUANTITATION OF SUGARS TO ADVANCE
BIOFUEL PRODUCTION

By

Daudi Sayialel Saang'onyo

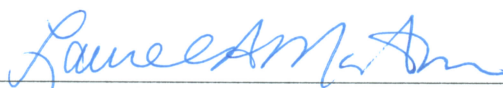
Thesis Approved:



Chair, Advisory Committee



Member, Advisory Committee



Member, Advisory Committee




Dean, Graduate School

STATEMENT OF PERMISSION TO USE

In presenting this thesis in partial fulfillment of the requirements for a Master's degree at Eastern Kentucky University, I agree that the Library shall make it available to borrowers under rules of the Library. Brief quotations from this thesis are allowable without special permission, provided that accurate acknowledgment of the source is made.

Permission for extensive quotation from or reproduction of this thesis may be granted by my major professor, or in his absence, by the Head of Interlibrary Services when, in the opinion of either, the proposed use of the material is for scholarly purposes. Any copying or use of the material in this thesis for financial gain shall not be allowed without my written permission.

Signature 

Date 12-01-2011

OPTIMIZATION AND VALIDATION OF DIRECT ANALYSIS IN REAL TIME
MASS SPECTROMETRY (DART-MS) FOR QUANTITATION OF SUGARS TO
ADVANCE BIOFUEL PRODUCTION

By

Daudi Sayialel Saang'onyo

Bachelor of Education (Science)

Maseno University

Maseno, Kenya

2005

Submitted to the Faculty of the Graduate School of
Eastern Kentucky University
in partial fulfillment of the requirements
for the degree of
MASTER OF SCIENCE
December, 2011

Copyright © Daudi Sayialel Saang'onyo, 2011

All rights reserved

DEDICATION

This thesis is dedicated to my beloved wife, Mary N. Muntet, and my two sons, Vincent

Sanare Saang'onyo and Seth Lempiris Saang'onyo

for their unwavering support and patience in dealing with all of my absence from many

family occasions with a smile,

and above all, love me.

You have been an unending inspiration to me. I love you.

Acknowledgments

I would like to wholeheartedly acknowledge the advice and guidance of my professor and committee chair Dr. Darrin L. Smith. Dr. Smith, thank you for having enough patience to put up with me and my mistakes on DART-MS, allowing me to get to my feet wet until I could take things for myself. Joining your research group was the best decision that I made while at Eastern Kentucky University. I also thank the members of my graduate committee for their guidance and suggestions, Prof. Lori Wilson, Dr. Laurel Morton, and Dr. Nathan Tice for all their advice and encouragement over the past two years. I also thank the Eastern Kentucky University chemistry lab staff, especially Lawrence Miller for ensuring constant availability of MS supplies. Special thanks go to Mr. Jordan Krechmer from IonSense, whose knowledge and assistance in the DART source was instrumental in this study.

I acknowledge the Eastern Kentucky University Chemistry Department and the United States Defense Logistics Agency (through the Center for Renewable Fuel Technologies (CRAFT)) for their financial support for this project.

The major experiment samples for this study were provided by Eastern Kentucky University CRAFT lab. I appreciate the support of Gary Selby in providing the samples required. I also thank Sushma Dendukuri, my fellow graduate student, for her help in initial sugar analysis and optimization experiments. My gratitude also goes to Prof. David O. Sparkman for providing accurate mass spectra for glucose standards.

I would like to thank my parents, Saiyalel Ole Saang'onyo and Mary Enole Saang'onyo for the endless help and love they have given to me over the past years. My brothers and sisters, thank you for supporting and encouraging me to pursue this degree. I am particularly indebted to my wife and best friend Mary Muntet, for her continued love, encouragement, and taking good care of our two sons during my absence over the past two years. Without her inspiration, I would not have finished this degree. Above all, I cannot thank enough my Lord and Savior Jesus Christ for loving me and dying for me to have life so that I can do such an interesting study and that I may live for Him in every way.

Abstract

A direct analysis in real time mass spectrometry method was developed and validated for the analysis and quantitation of sugars that would be generated from pretreated and hydrolyzed switchgrass. This research aspect can be divided into two sections:

i) Literature Review: A review is presented on the status of energy security and how biomass and biofuels can be utilized as a source of transportation fuel. To this end, biomass (specifically switchgrass) can be broken down by pretreatment methods and then enzymatically hydrolyzed to simple sugars. These sugars can assist with algae growth that can eventually be converted into biofuels. Direct Analysis in Real Time Mass Spectrometry (DART-MS), an ambient mass spectrometric method described in this study, can readily analyze these generated simple sugars.

ii) Optimization of DART-MS for the quantitation of glucose: Being the first study to use DART-MS to quantify sugars, the DART-MS instrumental parameters, such as gas heater temperature, helium pressure, linear rail speed, distance of DART source from the mass spectrometer orifice, and the grid voltage were varied to determine the optimal ionization conditions for sugar standards. Reproducibility experiments were performed to determine the robustness of the method. For quantification experiments, a dynamic linear range was developed using sugar standards in matrix-free solvents with the use of internal standards.

iii) Validation of the DART-MS method for quantitation of six-carbon sugars in saccharification matrix: Validation of the DART-MS method was performed to determine the limits of detection/quantitation, investigate matrix effects with respect to instrumental signal suppression when matrix-diluted standards were used, and perform recovery studies for accuracy and precision. Statistical analysis was used to compare calibration curves and recovery results generated from matrix-free and matrix-diluted sugars standards.

The resulting DART-MS method for glucose analysis was found to be precise, fast, and robust for the quantitation with saccharification samples. Since DART-MS requires little to no sample preparation, this technique becomes an attractive option and could be the choice in the quantitation of sugars for biofuel advancement.

KEYWORDS: Biomass, Switchgrass, Biofuels, Lignocelluloses, Saccharification, Direct Analysis in Real Time, Mass Spectrometry

TABLE OF CONTENT

Chapter One: Introduction	1
1.1. Research Objective.....	1
1.2. The Need for Constant Energy Supply.....	2
1.2.1. Energy Demand and Supply.....	3
1.2.2. Fossil Fuels Utilization Challenges.....	5
1.2.3. Renewable Energy Alternatives.....	7
Chapter Two: Background and Significance	10
2.1. Biofuels.....	10
2.1.1. Benefits of Biofuel Utilization.....	10
2.1.2. Classification of Biofuels.....	12
2.1.3. Challenges in the use of Biofuels.....	14
2.2. Biomass.....	16
2.2.1. Composition of biomass.....	16
2.2.1.1. Cellulose.....	17
2.2.1.2. Hemicellulose.....	18
2.2.1.3. Lignin.....	19
2.2.2. Sources of Biomass for Energy Production.....	21
2.2.2.1. Why Switchgrass?.....	21
2.3. Processes for Conversion of Lignocellulosic Biomass to Biofuels.....	26
2.3.1. Goals of Degradation of Lignocellulosic Biomass.....	26
2.3.2. Microwave Pretreatment.....	29
2.3.3. Aqueous Ammonia Pretreatment.....	29
2.3.4. Alkaline Pretreatment.....	30
2.3.5. Dilute Acid Pretreatment.....	30
2.3.6. Methanol and Water Soaks.....	31
2.4. Enzymatic Hydrolysis.....	31
2.4.1. Cellulase Enzyme System.....	32
2.5. Analysis of Sugars and Related Compounds.....	35
2.5.1. Traditional Methods of Sugar Analysis.....	35
2.6. Novel Experimental Methods of Sugar Analysis.....	39
2.6.1. Mass Spectrometry.....	39
2.6.2. Ionization Sources.....	41
2.6.2.1. Direct Analysis in Real Time Mass Spectrometry.....	48
2.6.2.2. Ionization Mechanisms in DART.....	50
2.6.2.3. Applications of Direct Analysis in Real Time.....	54
2.6.3. Mass Analyzers.....	57
2.6.3.1. The Linear Quadrupole Ion Trap (LIT) Mass Analyzer.....	58
2.6.4. Tandem Mass Spectrometry.....	62
2.6.5. Ion Detection.....	64
Chapter Three: Method Validation and Optimization for Sugar Analysis	66
3.1. Introduction.....	66
3.2. Experimental.....	66

3.2.1. Sample Preparation.....	66
3.2.2. Reagents and Chemicals.....	67
3.2.3. Sugar Standards Preparation.....	68
3.3. Instrumentation.....	71
3.3.1. Direct Analysis in Real Time (DART [®]) Ion Source.....	71
3.3.2. The LTQ XL [®] Linear Ion Trap Mass Spectrometer.....	74
3.3.3. Calibration and Tuning of the Mass Spectrometer.....	75
3.3.4. Sample Introduction.....	77
3.4. Method Validation and Optimization.....	78
3.4.1. General Spectral Appearance of Sugar Standards.....	78
3.4.2. Experimental Design Optimization.....	83
3.4.2.1. DART Gas Temperature.....	84
3.4.2.2. Linear Rail Speed.....	89
3.4.2.3. Helium Gas Flow Rate/Pressure.....	90
3.5. Method Precision.....	94
3.6. Linearity and Linear Range Determination.....	97
3.6.1. Calibration Curves.....	97
Chapter Four: Application of DART-MS to Saccharification Samples.....	103
4.1. Introduction.....	103
4.2. Switchgrass Saccharification Samples.....	104
4.2.1. Preliminary Analysis of Switchgrass Samples.....	104
4.2.2. Analysis of Blank Solution from Saccharification Process.....	107
4.2.3. Limit of Detection and Limit of Quantitation Determination.....	108
4.3. Matrix Effects Analysis.....	111
4.3.1. Introduction.....	111
4.3.2. Calibration Curves Comparison.....	112
4.4. Method Accuracy and Recovery.....	118
4.4.1. Introduction.....	118
4.4.2. Recovery of Control Sample Analytes Spiked into Blank Matrices.....	119
Chapter Five: Conclusions and Future Directions.....	132
5.1. Introduction.....	132
5.2. Method Conclusions.....	133
5.2.1. DART Optimization and Validation.....	133
5.2.2. Analytical Challenges of the Method.....	135
5.3. Future Directions.....	137
5.3.1. Real Switchgrass Samples Analysis.....	137
5.3.2. Comparison of Pretreatment Methods.....	138
5.4. Closing Remarks.....	138
List of References.....	140
Appendices.....	152

A. Statistical computation of parameters in matrix-free and matrix-diluted standards.....	152
B. Calibration curves generated from glucose standards prepared from both pure solvents (50:50 methanol/water, v/v) and matrix-diluted solvents (1% BES). The curves were used to determine the percent recoveries of quality control samples (QCs).....	154

LIST OF TABLES

Table 2.1.	Cellulose, hemicellulose, and lignin contents in common agricultural residues and wastes.....	21
Table 2.2.	Gas discharge ionization ambient ionization MS techniques.....	45
Table 2.3.	Common electrospray-based ambient ionization MS techniques.....	46
Table 2.4.	Atmospheric pressure chemical ionization ambient ionization MS techniques.....	47
Table 2.5.	Laser desorption/ablation ambient ionization MS techniques.....	47
Table 2.6.	Summary of the applications of DART.....	56
Table 2.7.	Common types of mass analyzers used in mass spectrometry and their principle of separation.....	57
Table 3.1.	Shows how the working standard solutions prepared from the stock standard solution to create final concentrations for the determination of the dynamic linear range.....	70
Table 3.2.	Comparing theoretical and experimental masses supported ion designations of glucose products.....	83
Table 3.3.	Peak areas and signal-to-noise ratios for three replicates of 1.00×10^{-4} M glucose standards run three times	87
Table 3.4.	Peak area ratios of four trials of nine separate samples of 5.00×10^{-5} M glucose standards spiked with 4.00×10^{-5} M of internal standard	96
Table 3.5.	Peak area ratios of different concentrations of glucose standards spiked with 4.00×10^{-4} M of internal standard (deuterated glucose) and the standard deviation for each measurement ($n = 3$).....	101

LIST OF TABLES – *CONTINUED*

Table 4.1.	The peak area ratios of glucose standards made in methanol/water and 1% blank enzyme solvent (BES) and their respective standard deviations...113
Table 4.2.	Pooled standard errors and <i>t</i> test results for the statistical comparison of linear trend line fits to calibration curves from the matrix-free standards and matrix-diluted standard.....117
Table 4.3.	Peak area ratios and the respective standard deviations from standards spiked into a blank matrix solution analyzed with QCs at three levels of concentration (low, mid, and high).....121
Table 4.4.	Data generated when determining the percent recovery of control samples spiked into blank matrix samples.....124
Table 4.5.	Peak area ratios and the respective standard deviations from standards prepared from matrix-free (methanol/water) solvents analyzed with QCs at three levels of concentration (low, mid, and high).....126
Table 4.6.	Data generated when determining the percent recovery of control samples spiked into matrix-diluted samples. The QCs were analyzed with glucose standards prepared from matrix-free solvents126
Table 4.7.	Replicate sets of measurements for the calculated concentration of the QCs at different levels of concentrations using the matrix-free and matrix-diluted standards.....130
Table 4.8	<i>t</i> test results for the statistical comparison of QCs calculated concentration in two sets of standard samples (matrix-free and matrix-diluted) at the three levels of QCs concentrations.....131

LIST OF TABLES – *CONTINUED*

Table A1.	Computation of statistical values for calculation of Student's t (matrix-free standards).....	153
Table A2.	Computation of statistical values for calculation of Student's t (matrix-diluted standards).....	153

LIST OF FIGURES

Figure 1.1.	World marketed energy consumption, history and predictions for the 1990-2035 period [quadrillion Btu (British thermal units)].....	4
Figure 2.1.	Structure of the monomer units of cellulose molecule.....	18
Figure 2.2.	A simplified structure of hemicellulose showing the different types of sugars present.....	19
Figure 2.3.	Schematic structural formula for lignin	20
Figure 2.4.	Schematic of the conversion of lignocellulosic biomass to biofuels.....	27
Figure 2.5.	Cellulose chain showing the bonds cleaved by the cellulase enzyme.....	33
Figure 2.6.	A block diagram showing the main components of a mass spectrometer.....	41
Figure 2.7.	A schematic showing how a molecule, M, is analyzed by soft ionization and hard ionization and the resulting mass spectra.....	43
Figure 2.8.	A schematic diagram of the DART ion source.....	49
Figure 2.9.	Reactions in positive ion DART.....	54
Figure 2.10.	Schematic representation of a linear quadrupole ion trap mass analyzer..	59
Figure 2.11.	The Mathieu stability diagram for the quadrupole ion trap.....	61
Figure 2.12.	A schematic representation of a tandem mass spectrometry experiment, specifically, a product ion scan.....	63
Figure 3.1.	The molecular structures of (a) deuterated glucose and (b) glucose.....	68
Figure 3.2.	A schematic showing the DART ion source set up. The sample is spiked at the tip of the glass tip placed on a movable rail (not shown) which moves the sample between the source and MS inlet.....	73

LIST OF FIGURES – CONTINUED

- Figure 3.3. A typical positive ion mode DART-LIT mass spectrum generated from 1.00×10^{-4} M glucose standard.....79
- Figure 3.4. A DART-LIT mass spectrum generated from 1.00×10^{-4} M deuterated glucose standard.....80
- Figure 3.5. Tandem mass spectrum (MS/MS) of the precursor ion of m/z 198 generated from glucose standard by the DART source. The insert is the MS³ spectrum of m/z 180 generated (through fragmentation of m/z 180).....82
- Figure 3.6. The TIC DART-LIT mass spectra generated from 1.00×10^{-4} M glucose standard at various helium gas temperatures (showing the 100–265 m/z range).....86
- Figure 3.7. Average peak area (PA) of 1.00×10^{-4} M glucose standards analyzed at various ionizing gas temperatures ($n = 3$). The error bars indicates the standard deviation for the PA of each measurement.....88
- Figure 3.8. Signal-to-noise ratios (S/N) of 1.00×10^{-4} M glucose standards analyzed at different ionizing gas temperatures ($n = 3$). The error bars indicates the standard deviation for the S/N of each measurement.....88
- Figure 3.9. Average peak area of the base peak (m/z 198) produced from 1.00×10^{-4} M glucose standard solution at different linear rail speeds.....90
- Figure 3.10. The average peak areas ($n = 5$) of 1.00×10^{-4} M glucose standards base peak (m/z 198) at different helium pressures. The large error bars indicates a high variability in the peak areas.....92

LIST OF FIGURES – CONTINUED

- Figure 3.11. A line plot of the average peak areas of the base peak at different helium pressures.....93
- Figure 3.12. Reproducibility: Extracted ion chromatogram (m/z 198) for one trial where nine 5.00×10^{-5} M glucose standards spiked with 4.00×10^{-5} M of deuterated glucose were analyzed by DART-LIT.....95
- Figure 3.13. A plot showing the reproducibility in the calculated peak area ratios (PAR) for standard solutions, each trial represents a separate batch of samples ($n = 9$).....96
- Figure 3.14. A graph showing the instrument response as a function of the analyte concentration. After point A the response level starts to deviate making the detected amount less than the expected amount.....99
- Figure 3.15. Calibration curve for a series glucose standards solution spiked with 4.00×10^{-4} M of deuterated glucose (internal standard). Each point represents an average ($n = 3$) peak area ratio with associated standard deviation.....102
- Figure 4.1. A full scan mass spectrum of a switchgrass-saccharification sample showing the generated peaks present using the DART-MS. The analyte of interest (m/z 198) is preliminary designated as the six-carbon sugar.....105
- Figure 4.2. Product ions generated when m/z 198 from a switchgrass-saccharification sample was mass selected and then fragmented giving the tandem mass spectrum (that can be compared with glucose standards).....106
- Figure 4.3. A representative chromatographic peaks showing the signal to noise ratio (S/N) for different concentrations of glucose.....110

LIST OF FIGURES – CONTINUED

Figure 4.4. Calibration curves generated from glucose standards with and without the blank solvent with respective calculated slopes.....113

Figure 4.5. A calibration curve obtained by analyzing blank matrix solutions spiked with glucose standards with high concentration QCs.....121

Figure 4.6. A calibration curve obtained by analyzing blank matrix solutions spiked with glucose standards with mid-range concentration QCs.....122

Figure 4.7. A calibration curve obtained by analyzing blank matrix solutions spiked with glucose standards with low concentration QCs.....122

Figure 4.8. A calibration curve was obtained by analyzing glucose standards in pure solvents with high concentration QCs.....127

Figure 4.9. A calibration curve was obtained by analyzing glucose standards in pure solvents with mid-range concentration QCs.....127

Figure 4.10. A calibration curve was obtained by analyzing glucose standards in pure solvents with low concentration QCs.....128

Figure B1. Trend lines generated from LQC recovery experiments with matrix-free and matrix-diluted glucose standards.....155

Figure B2. Trend lines generated from MQC recovery experiments with matrix-free and matrix-diluted glucose standards155

Figure B3. Trend lines generated from HQC recovery experiments with matrix-free and matrix-diluted glucose standards156

LIST OF ABBREVIATIONS AND SYMBOLS

2D QIT.....	Two-Dimensional Quadrupole Ion Trap
3D QIT.....	Three-Dimensional Quadrupole Ion Trap
APCI.....	Atmospheric Pressure Chemical Ionization
APLI.....	Atmospheric Pressure Laser Ionization
AP-MALDI.....	Atmospheric Pressure Matrix-assisted Laser Desorption Ionization
APPI.....	Atmospheric Pressure Photoionization
ASAP.....	Atmospheric Solids Analysis Probe
BDE.....	Bond Dissociation Energy
BES.....	Blank Enzyme Solvent
BFDP.....	Bioenergy Feedstock Development Program
BTL.....	Biomass to Liquid
CAD.....	Collision-Activated Dissociation
CI.....	Chemical Ionization
CID.....	Collision-Induced Dissociation
CRAFT.....	Center for Renewable and Alternative Fuel Technologies
CV.....	Coefficient of Variation
DAPCI.....	Desorption Atmospheric Pressure Chemical Ionization
DAPPI.....	Desorption Atmospheric Pressure Photoionization
DART.....	Direct Analysis in Real Time
DART-LIT.....	Direct Analysis in Real Time Linear Ion Trap
DART-MS.....	Direct Analysis in Real Time Mass Spectrometry
DBDI.....	Dielectric Barrier Discharge Ionization

LIST OF ABBREVIATIONS AND SYMBOLS - *CONTINUED*

DC.....	Direct Voltage
DEMI.....	Desorption Electrospray Metastable-Induced Ionization
DESI.....	Desorption Electrospray Ionization
DNS.....	Dinitrosalicylic Acid
DOE.....	United States Department of Energy
EASI.....	Easy Ambient Sonic-Spray Ionization
EESI.....	Extractive Electrospray Ionization
EI.....	Electron Ionization
EIA.....	United States Energy Information Administration
ELDI.....	Electrospray-assisted Laser Desorption/ablation Ionization
ELSD.....	Evaporative Light-Scattering Detection
EROI.....	Energy Return on Energy Invested
ESI.....	Electrospray Ionization
FA-APGI.....	Flowing Afterglow-Atmospheric Pressure Glow Discharge
FAB.....	Fast Atom Bombardment
FD.....	Field Desorption
FD-ESI.....	Fused Droplet Electrospray Ionization
FI.....	Field Ionization
FTICR.....	Fourier Transform Ion Cyclotron Resonance
GC.....	Gas Chromatography
GC-MS.....	Gas chromatography/Mass Spectrometry
GDI.....	Gas Discharge Ionization

LIST OF ABBREVIATIONS AND SYMBOLS - *CONTINUED*

GHG.....	Greenhouse Gas
HPLC.....	High Performance Liquid Chromatography
HQC.....	High Concentration Quality Control Sample
ICR.....	Ion Cyclotron Resonance
IR-LADESI.....	Infrared-laser Assisted Desorption Electrospray Ionization
IR-LAMICI.....	Infrared Ablation Metastable-Induced Chemical Ionization
ITMS.....	Ion Trap Mass Spectrometry
LAESI.....	Laser assisted Electrospray Ionization
LC/MS.....	Liquid Chromatography Mass Spectrometry
LDI.....	Laser Desorption/ablation Ionization
LIT.....	Linear Ion Trap
LOD.....	Limit of Detection
LOQ.....	Limit of Quantitation
LQC.....	Low Concentration Quality Control Sample
LTP.....	Low Temperature Plasma
MALDESI.....	Matrix-assisted Laser Desorption Electrospray Ionization
MALDI.....	Matrix-assisted Laser Desorption Ionization
MQC.....	Mid-range Concentration Quality Control Sample
MRFA.....	L-methionyl-arginyl-phenylalanyl-alanine Acetate Monohydrate
MS/MS.....	Mass Spectrometry/Mass Spectrometry
MS.....	Mass Spectrometry
ND-EESI.....	Neutral Desorption Extractive Electrospray Ionization

LIST OF ABBREVIATIONS AND SYMBOLS - *CONTINUED*

OECD.....	Organization for Economic Cooperation and Development
ORNL.....	Oak Ridge National Laboratory
PADI.....	Plasma-Assisted Desorption/Ionization
PAR.....	Peak Area Ratio
PSI.....	Paper Spray Ionization
QC.....	Quality Control
RADIO.....	Radio-Frequency Acoustic Desorption Ionization
RF.....	Radiofrequency
RI.....	Refractive Index
SESI.....	Secondary Electrospray Ionization
SSF.....	Simultaneous Saccharification and Fermentation
SSI.....	Sonic Spray Ionization
SVP.....	Standard Voltage and Pressure
TME.....	Transient Microenvironment
TMEM.....	Transient Micro-Environment Mechanism
TOF.....	Time-of-Flight
UV.....	Ultraviolet
V-EASI.....	Venturi Easy Ambient Sonic-Spray Ionization
XIC.....	Extracted Ion Chromatograms

CHAPTER 1

INTRODUCTION

1.1. RESEARCH OBJECTIVE

It is now widely accepted that use of fossil fuels is unsustainable resulting from diminishing resources, uneven geographical distribution reserves, and accumulation of greenhouse gases in the atmosphere proposed to contribute to climate change. To achieve environmental and economic sustainability, the search for new and/or renewable sources of energy as a substitute for petroleum, coal, and natural gas in the current energy system is inevitable. The new sources of energy should have the potential of effectively replacing fossil fuels in the current energy production system, be renewable, well distributed around the globe, and not contribute to the accumulation of greenhouse gases in the atmosphere. In this respect, natural and renewable resources such as solar energy, hydroelectric power, wind, geothermal activity, and biomass are candidates that meet these requirements.

Being ubiquitous, biomass has spurred enormous research into its possible use as a source of fuel. Switchgrass, a native grass to Central and North America, has been chosen as the biomass model energy crop from its unique characteristics: its perennial nature which reduces management intensity and less consumption of energy and agrochemicals, high cellulose content and less lignin as compared to other woody crops, its soil and wildlife enhancement, adaptability to grow well in poor soils, and the general familiarity with its production processes. The resistance to degradation that protects the

organism from the elements has become the biggest huddle in its utilization as a precursor for biofuel production. However, technologies have been developed for conversion of the sugar polymers (which are formed as a result of photosynthesis) into simple sugars that can further be converted into biofuels. The effectiveness of biomass degradation is gauged by the quantity of sugars produced after conversion. The research presented shows the development and validation of a fast and reliable method for the quantification of six carbon sugars obtained from switchgrass after initial pretreatment and subsequent enzymatic hydrolysis. The sugars thus obtained can be fed to heterotrophic algae for the production of oil, which can be processed into biodiesel and used to supplement or ultimately replace fossil fuels. In this respect, this study is geared towards advancement of biofuels production from initial utilization of biomass.

1.2. THE NEED FOR CONSTANT ENERGY SUPPLY

An adequate, affordable, and reliable supply of energy is the lifeblood of our modern society.¹The fabric of the current economy is dependent upon the questionable supply of fossil fuels. Recent available data of world energy consumption indicates that society still remains highly dependent on fossil fuel at the present time.² These fossil fuels are used to provide energy for various sectors of society (i.e., residential, commercial, industrial, transportation, and electric power), however; the transportation sector is the largest and fastest growing energy sector responsible for almost one third of the energy consumed in the world.³ To achieve a sustainable economy, a constant supply of energy to meet the ever-increasing demand is a fact that needs to be addressed. The following details a comparative perspective on the demand and supply of energy.

1.2.1. Energy Demand and Supply

The demand for the provision of energy is increasing worldwide and will continue to rise due to rapidly rising human population and modernization trends across the globe. In the United States alone, 85% of the energy needs in 2008 were met primarily by the use of non-renewable resources.⁴ In the same period, 80% of the energy consumption in the European Union comprised of non-renewables.⁵ These non-renewable resources comprise of materials such as petroleum, natural gas, coal, and fissionable materials (uranium), all of which are only available in a finite supply. More recent data indicate that a staggering 86.7% of the United States energy needs are being met by the consumption of non-renewable energy sources⁶ consisting of 35.3% provided by petroleum, 23.4% by natural gas, 19.7% by coal, and 8.3% by nuclear power. Currently, only 7.7% of energy needs are being met with renewable energy sources. This is an overwhelming realization considering that the earth has a limited amount of non-renewable sources and if other suitable energy sources are not found, supplies will be depleted and the world will face a loss of basic energy needs.

A study of the world's energy demand and supply provides enlightening facts that should compel everyone to search for alternative energy sources. The US Energy Information Administration (EIA) 2010 International Energy Outlook² shows world marketed energy demand increasing strongly over the projection period of 1990 to 2035, rising by nearly 50% from 2009 through 2035 (**Figure 1.1** below). Most of the growth occurs in emerging economies outside the Organization for Economic Cooperation and Development (OECD), especially in non-OECD Asia. Total non-OECD energy use increases by 84%, compared with a 14% increase in developed OECD nations. Energy

use in non-OECD Asia, led by China and India, shows the most robust growth among the non-OECD regions, rising by 118% over the projection period. However, strong growth is also projected for much of the rest of the non-OECD regions: 82% growth in the Middle East, 63% in Africa, and 63% in Central and South America. In developed OECD economies (where energy consumption patterns are well established), energy use is expected to grow at a much slower average rate of 1.1% per year over the same period. In the transitional economies of Eastern Europe and the former Soviet Union, growth in energy demand is projected to average 1.6% per year.⁷ Overall, the use of energy worldwide from all sources increases over the projection.

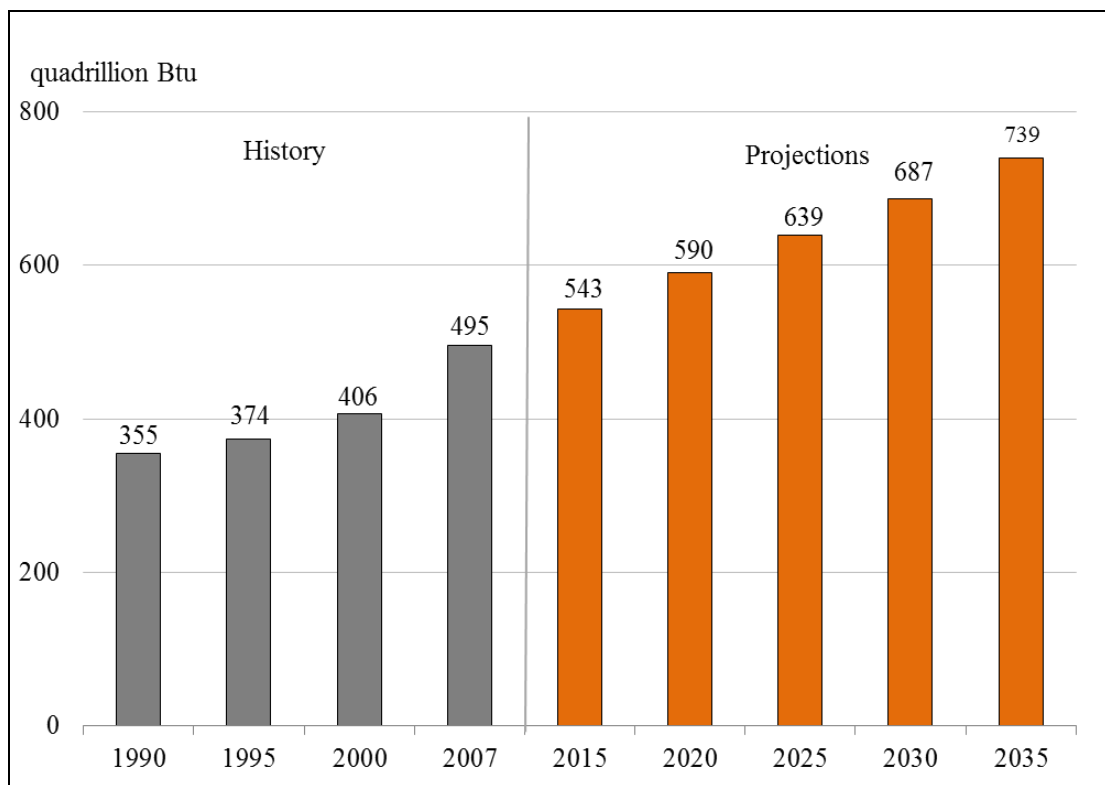


Figure 1.1. World marketed energy consumption, history and predictions for the 1990 – 2035 period [quadrillion Btu (British thermal units)].²

Given expectations that oil prices will remain relatively high, petroleum and similar type liquids are the world's slowest-growing energy sources. The high energy prices and concerns about the environmental consequences of greenhouse gas (GHG) emissions lead a number of national governments to provide incentives in support of the development of alternative energy sources, allowing renewable energy sources the world's fastest-growing source in the outlook. In light of the increasing global energy need against declining fossil fuel reserves, this search for alternative sources of energy is imperative. Renewable resources such as biofuels, hydroelectric power, solar, wind, and geothermal energy offer hope for a viable alternative to non-renewable energy and potentially provide an energy resource that may result in future energy security.

1.2.2. Fossil Fuels Utilization Challenges

The major issues that arise with large-scale use of fossil fuels are: i) availability, ii) climate change, and iii) uneven geographical distribution of reserves. i) Availability: Fossil fuels are finite in nature, and as previously indicated, their current consumption rate is higher than the corresponding regeneration rate, leading to eventual depletion. Considering energy use forecasts and current data of proven reserves, it is estimated that oil, natural gas, and coal will be depleted within the next 40, 60, and 120 years, respectively.⁸ Many researchers predict a more dramatic situation for petroleum and estimated that global production will peak in the year 2020 and decay thereafter. ii) Climate change is, possibly, the most dramatic and known collateral effect produced by the massive utilization of fossil fuels. The term 'global warming' is commonly used to mean 'anthropogenic' global warming; that is, warming caused by human activity.⁹ This

event is attributed when greenhouse gases (carbon dioxide, water vapor, nitrous oxide, and methane) trap heat and light from the sun in the earth's atmosphere, which increases the temperature. The diverse effects or impacts may be physical, ecological, social, or economic and a complete review is outside the scope of this study. When fossil fuels are combusted, they produce a net emission of carbon dioxide (CO₂), a greenhouse gas, into the atmosphere. Thus, the production and utilization of fossil fuels has allowed a large part of the carbon stored in the earth for millions of years to be released in just a few decades. iii) Geographical Distribution: The reserves of fossil fuels are not equally distributed around the globe. Countries in the Middle East control 60% of the oil reserves and 41% of natural gas supplies. Only three countries (US, China, and Russia) account for 60% of the world recoverable coal reserves.³ This situation can lead to economic instabilities, requiring the transportation of fossil fuel resources over long distances, and can cause political and security problems worldwide.

The challenges outlined above, inherently associated with fossil fuels, suggest that society requires new sources of energy to ensure progress and protect the environment for future generations. For the world to have a sustainable energy system and a subsequent secure economy, a shift to focus towards energy alternatives that can reduce and/or eradicate these challenges without affecting the energy supply is necessary. The only solution to these challenges is to embrace the utility of renewable energy alternatives that can be a cornerstone to steer the world's energy system in the direction of sustainability and supply security.

1.2.3. Renewable Energy Alternatives

"Renewable energy" means energy produced from a method that can be continually replenished by utilizing one or more of the following fuels or energy sources: hydrogen produced from sources other than fossil fuels, biomass, solar energy, geothermal energy, wind energy, ocean energy, and hydroelectric power.¹⁰ Renewable sources of energy vary widely in their cost-effectiveness and their availability across the United States. Although water, wind, and other renewables are non-polluting and may appear free, their cost comes in collecting, harnessing, and transporting the energy so it can be consumed. A brief description of the various renewable energy sources is given below.

Solar energy: This energy captured directly from the sun is transformed into electricity. There are two levels of solar energy production, namely; the industrial power plant level and the household supplemental level. On the industrial level, sunlight can be concentrated with mirrors and then used to power steam generators to produce electricity. In household use, sunlight may be converted into electricity via photovoltaic cells manufactured from either silica or organic semiconducting materials.¹¹ The utilization of solar energy to produce electricity in either case can be efficient, but requires direct sunlight and significant space that can be major limitations.

Hydroelectric power (Hydropower): This is the form of mechanical conversion to produce energy from water from high to low altitudes with the use of turbines.¹² The geographical conditions of the regions as well as water conditions, such as available head and flow volume per unit of time, play an important role in assessing the potential of

hydropower. Climatic changes with rainfall variations across world regions can affect the yearly output power of hydropower.

Geothermal Energy: Geothermal power uses the natural sources of heat inside the Earth to produce heat or electricity. Currently, most geothermal power is generated using steam or hot water from underground. This form of energy is mainly obtained by drilling a well into a geothermal reservoir to provide a steady stream of hot water or steam which is channeled to directly drive a turbine to produce electricity.

Wind Energy: Energy from the wind produced with wind turbines that can produce energy on a large or small scale. Electricity from the wind can be produced both day and night (unlike solar energy which can only be produced when the sun is shining). However, the level of energy produced is very sporadic and may be undependable due to lack of energy storage methods and certain methods are still under development.¹³

Ocean Energy: Oceans cover more than 70% of Earth's surface, making them the world's largest solar collectors. Generating technologies for deriving electrical power from the ocean include tidal power, wave power, ocean thermal energy conversion, ocean currents, ocean winds and salinity gradients. As mentioned previously, the three most well developed technologies are tidal power, wave power and ocean thermal energy conversion. Using current technologies, ocean energy is not cost-effective compared to other renewable energy sources, but the ocean remains an important potential energy source that could be developed for the future.¹⁴

Biomass Energy: While a detailed study of energy from biomass is given in the following sections, biomass has been an important source of energy ever since people

first began burning wood to cook food and stay warm against the winter chill. Wood is still the most common source of biomass energy, but other sources of biomass energy can originate from food crops, grasses, agricultural/forestry waste and residues, organic components from municipal and industrial wastes, even methane gas harvested from community landfills. Biomass can be used to produce electricity, fuel for transportation, and/or manufacture products that would otherwise require the use of non-renewable fossil fuels.

Even though solar, wind, hydroelectric, and geothermal have been proposed as excellent alternatives to coal and natural gas for heat and electricity production in stationary power applications,¹⁵ biomass may be the only sustainable source of organic carbon currently available on earth and considered to be an ideal substitute for petroleum in the production of fuels, chemicals, and other carbon-based materials.¹⁶ Consequently, extensive research is required for the development and effective implementation of new technologies for large-scale production of fuels from biomass to be used in the current energy system. The presented research is geared towards advancement of such technologies.

CHAPTER 2

BACKGROUND AND SIGNIFICANCE

2.1. BIOFUELS

Among the most promising replacement for non-renewable fossil fuels (e.g., petroleum, coal, etc.) are fuels derived from organic materials commonly termed as biofuels. The biggest proportion of biofuels is obtained from plant biomass. Biofuels are gaining increased public and scientific attention since they are being driven by factors including i) oil price spikes, ii) increased energy security, iii) concern over climate change from greenhouse gas, iv) and government subsidies.

2.1.1. Benefits of Biofuel Utilization

The use of biofuels instead of fossil fuels offers many benefits with one of the best benefits discussed in literature being the “carbon-neutral” phenomenon.¹⁷ When biomass is burnt, or used after converting it into other types of solid, liquid, and gaseous fuels, the only CO₂ released to the atmosphere is the CO₂ biomass has recently captured from the atmosphere during its photosynthetic growth, therefore; no net addition of CO₂. In contrast, when fossil fuels are burnt, a resulting net addition of CO₂ is released into the atmosphere because fossil fuels are derived from plants and animals that previously lived many years ago. For this reason, fossil fuels have been deemed “carbon positive” for our relative time scale whereas recently grown biomass can be classified as “carbon neutral”.¹⁸ However, it is important to note the production of biomass-based energy is not

always “carbon neutral” since fossil fuel-based energy may currently be utilized at several points with the process of converting biomass into fuels.

Since fossil fuels are finite, one day, the world will run out of fossil fuels and the current primary sources of energy will go up in smoke, figuratively and literally. Since biofuels are derived from renewable biological sources, a sustainable model is achievable. Still, not all biofuels are created equal since some "energy crops" produce more energy than others. For example, rapeseed has a higher oil content than other typical vegetable plants,¹⁹ which means rapeseed can generate more energy when burned. Perennial plants, such as switchgrass, provide an abundant source of power that can be sustainable over a long time.

In 1973, the oil-producing nations of the Middle East stopped exporting oil causing oil prices to rise. As a result economies across the globe suffered. The embargo was a cold slap in the face to the countries that rely on oil imports as their main source of energy. Governments were influenced to find new ways to deal with the energy crisis. The oil-producing countries eventually lifted the embargo. However, that crisis did not change our thirst for oil and today, humans consume approximately 85 million barrels of oil a day.²⁰ While countries can grow sustainable energy crops for conversion to biofuels will lessen the nation's reliance on foreign oil, other factors need to be considered for long- and short-term solutions such as raising fuel economy standards for motor vehicles; enacting tax incentives for hybrids and fuel-cell vehicles; and increasing the use of all renewable fuels.

When oil comes out of the ground, it doesn't automatically transform itself into useable gasoline or home heating oil. Oil refineries must convert crude oil into useable

products and during the process; millions of substances are released into the environment each year. There are 153 of these refineries in the United States and more than 90 million people live within 30 miles but many are not aware of the potential health concern. Refineries have been reported to release many chemicals into the environment such as nickel, lead, sulfur dioxide, and other pollutants that can cause heart disease, asthma and other significant health problems.²¹ Biofuel refineries would dramatically reduce the amount of potential harmful emissions to the surroundings, becoming more environmentally friendly. For example, ethanol plants fueled by natural gas emit very few pollutants, including greenhouse gases. Moreover, ethanol plants fueled by biomass and biogas produce less gas emissions and are cleaner to run.

2.1.2. Classification of Biofuels

Renewable biofuels have been categorized depending on the feedstocks from which they were derived and have also been designated as i) first, ii) second, iii) third, and iv) fourth generation biofuels.

First generation biofuels are fuels whose starting materials are sugars, starch, or oil that include sugar cane, corn, wheat, barley, cassava, palm oil, jatropha, etc. In general terms, they are mainly based on plant sugars, grains, or seeds.²² This category of biofuels comprise of plant-derived oils (lipids), biodiesel produced from transesterification of plant oil with ethanol or methanol, bioethanol from the fermentation of starch and other plant carbohydrates, and biogas (methane and other hydrocarbons) which is mainly obtained from bacterial degradation and physical compression of derived gas.²³

Second generation biofuels are normally categorized as those made from the breakdown of plant cellulose or lignin.²⁴ Such biofuels could be produced from non-food plants but dedicated biofuel crops like switchgrass, other grasses, and/or trees grown on marginal or degraded lands.²⁵ Another source of second generation biofuels includes agricultural residues and wastes (municipal, industrial, and construction waste). Agricultural residues can include remnants of straw of wheat and rice, sugar cane bagasse, stem and roots from food crops, the top ends of trees such as eucalyptus (not used in paper manufacture), and fast developing tall grass. Other alternatives of second generation biofuels that are in various stages of development include the gas-to-liquid Fischer–Tropsh process, which is also overall a biomass to liquid (BTL) process, biohydrogen involving gasification of the biomass and then reforming the methane produced, high temperature upgrading of wet biomass, etc.²⁶

Third generation biofuels are fuels generated from algae, including both microalgae and macroalgae. Microalgae are able to produce 15-300 times more oil for biodiesel production than traditional crops on an area basis. Furthermore compared with conventional crop plants, which are usually harvested once or twice a year, microalgae have a very short harvesting cycle allowing multiple or continuous harvests with significantly increased yields.²⁷ Algae-derived fuels comprise of generating lipids, carbohydrates, and even direct production of hydrocarbons similar to petrol.²³

Recently, fourth generation biofuels have received considerable attention by combining technologies related to genetically optimized feedstocks that are designed to capture large amounts of carbon with genomically synthesized microbes made to efficiently make fuels. An important key to the process is the capture and sequestration of

CO₂ making the fourth generation process a carbon negative source of producing biofuel. Another field that is being researched for fourth generation biofuels is algae metabolic engineering.²⁸

Our research focus is on the second generation fuels in combination with third generation fuels. Plant biomass (switchgrass in this case) is degraded to produce simple sugars which can be precursors for biofuel production. The sugars are fed to heterotrophic algae which then convert the sugars into bio-oil which can be extracted and refined to produce biodiesel and other fuel products. Feeding algae with the sugars is relatively productive than ordinary fermentation to produce ethanol. This is because, algae have a high conversion rate of sugars into oil, and this happens within a relatively short period of time. It is also a green path for bio-oil production because it does not require complex chemical processes that may apply in fermentation.

2.1.3. Challenges in the Use of Biofuels

The rapid growth of biofuel production has not been free of controversy. One of the main challenges is conflict with food agriculture since the use of corn to produce biofuels has raised questions on the competition of food versus fuel. The increase in food prices has been attributed to the use of food crops to produce biofuels and not solely for food production.²⁹ Another aspect of the ‘food versus fuel’ debate is the vast pieces of land required to grow renewable feedstocks. If land is used for growing biomass for fuel (and not food crops), a projected negative effect will result in food production and not as desired when many developing countries are struggling with food shortages.³⁰ Competition with food production can be mitigated by using alternative sources such as

herbaceous crops and aquatic biomass^{27, 31} that are not land intensive and can also utilize marginal lands not fit for food crop production.

While biofuels could significantly contribute to the future energy supply mix, cost is a major barrier to its commercial production in the near to medium term. As compared to fossil fuels, biofuels are typically more expensive in their production. In some cases, it has been reported the energy return on energy invested (EROI) would be too low to invest in biofuels.³² Various costs associated with biofuel production are considered when analyzing cost projections such as capital costs, initial cost and transportation of chosen feedstocks, logging costs, operation and biorefinery maintenance costs (including labor and other energy costs).³³ As reported by Hamelinck and Faaij³⁴, feedstock costs account for about 45–58% of total production costs for second generation biofuels, depending on conversion efficiency and applied technology. The development of energy efficient processing and conversion technologies is necessary to overcome this limitation.

The impact of biofuel production on the environment has also been cited as a challenge that needs to be addressed. The removal of biomass from land and water for energy production increase soil erosion and water degradation, flooding, and removal of nutrients. It also contributes significantly to water pollution through the pesticides and fertilizers that are inevitably needed in sustaining any intensive cultivation.³⁵ Converting natural ecosystems into energy-crop plantations can also influence both the habitat and food sources of wildlife and other biota.³⁶ Even though biomass energy is said to be “carbon neutral”, its production, like any other agricultural activities, can lead to the production of reactive nitrogen compounds with deleterious environmental consequences.³⁷ To illustrate this point, each molecule of N₂O is implicated to have 300

times greater global warming potential compared to a single molecule of CO₂.³⁸ As previously mentioned, fossil fuels are routinely used in biorefinery industries in the production of biofuels and does not support the carbon neutral advocacy for biofuels.

Even though these challenges are pertinent, the depletion of fossil fuels forces modern society with no choice but to seek alternative sources of energy. Being ubiquitous and readily accessible, biomass is a viable and sustainable energy resource envisioned to replace non-renewable sources. However, more research is needed in terms of addressing the challenges described above to make biofuels an attractive energy alternative.

2.2. BIOMASS

Biomass is the general term, which includes *phytomass* or plant biomass and *zoomass* or animal biomass.¹⁸ Biomass is the first renewable fuel used by humankind and was the mainstay of the global fuel economy till the middle of the 18th century. Plants intercept energy from the sun, by the process of photosynthesis, and convert it into chemical energy stored in the form of terrestrial and aquatic vegetation. Generally, animal biomass has very little contribution to the overall biomass potential of the world, therefore; subsequent discussion shall focus on phytomass and will be referred as 'biomass' from this point forward in relation to the production of biofuels.

2.2.1. Composition of Biomass

Plant biomass is mainly composed of cellulose, hemicellulose, and lignin, small amounts of organics (pectin, protein, and extractives), and inorganics (found in ash). The major organic components of biomass and their relative proportions have increasing

interest for the development of fuels as well as a source of value chemical building blocks. The combination of i) cellulose, ii) hemicellulose, and iii) lignin is commonly referred to as lignocellulose and about half of plant matter produced by photosynthesis comprises of lignocellulose. The composition of lignocelluloses can vary from one plant species to another and the ratios between various constituents within a particular plant vary with age, stage of growth, and other conditions.³⁹ A closer discussion of lignocelluloses is given in the following sections.

2.2.1.1. Cellulose

Cellulose is an abundant biopolymer (largest component of lignocellulosic materials) and has unique characteristics including high crystallinity, insolubility in water, and high resistance to depolymerization. It is the main structural constituent of plant cell walls, found in an organized fibrous structure, and a linear polymer composed of repeating D-glucose (dextrose) subunits linked to each other by β -(1,4)-glycosidic linkages. Cellobiose is the repeat unit established through this linkage. The chemical formula of cellulose is $(C_6H_{10}O_5)_n$ and the structure of one chain of the polymer is presented in **Figure 2.1**. The long-chain cellulose polymers are linked together by hydrogen and van der Waals bonds, which make cellulose to be packed into microfibrils.⁴⁰ Cellulose can exist in biomass as two different forms: crystalline (a random orientation of rigid cellulose chains) and amorphous (a random orientation of flexible cellulose chains). Crystalline cellulose comprises the major proportion of cellulose, whereas a small percentage of unorganized cellulose chains form amorphous cellulose.

In wood, cellulose chains contain typically 10,000 glucose molecules where each cellulose chain has one reducing end at the carbon one (C1) position of the terminal D-glucose subunit. The carbon four (C4) position of the other terminal subunit is an alcohol and, therefore, non-reducing. Cellulose has many industrial uses ranging from the production of ethanol to paper, but its uses are often hindered since accessibility is limited by the presence of lignin.

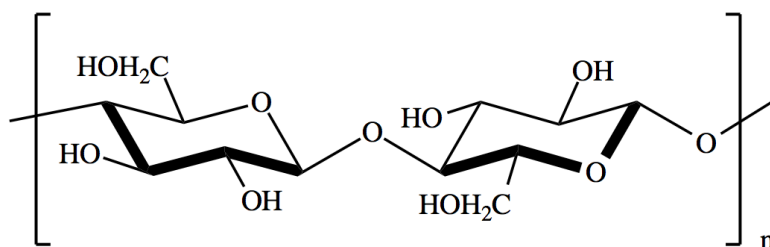


Figure 2.1. Structure of the monomer units of cellulose molecule.

2.2.1.2. Hemicellulose

Hemicellulose is also a major component of plant primary and secondary cell walls and also a sugar polymer but vary significantly from cellulose. The main differentiating feature separating hemicellulose from cellulose is that hemicellulose has branches with short lateral chains consisting of different sugars. **Figure 2.2** shows the structure of hemicellulose.⁴⁰ Hemicellulose is composed of many kinds of sugars including pentoses (D-xylose, L-rhamnose, and D-arabinose), hexoses (D-glucose, D-mannose, and D-galactose), and uronic acids (e.g., 4-o-methylglucuronic, D-glucuronic, and D-galactouronic acids). Hemicellulose backbone is either a homopolymer or a heteropolymer with short branches linked by β -(1,4)-glycosidic bonds and occasionally

by β -(1,3)-glycosidic bonds.⁴¹ In specific cases, hemicellulose can also have some degree of acetylation, and these hemicellulose polymers are easily hydrolyzable.

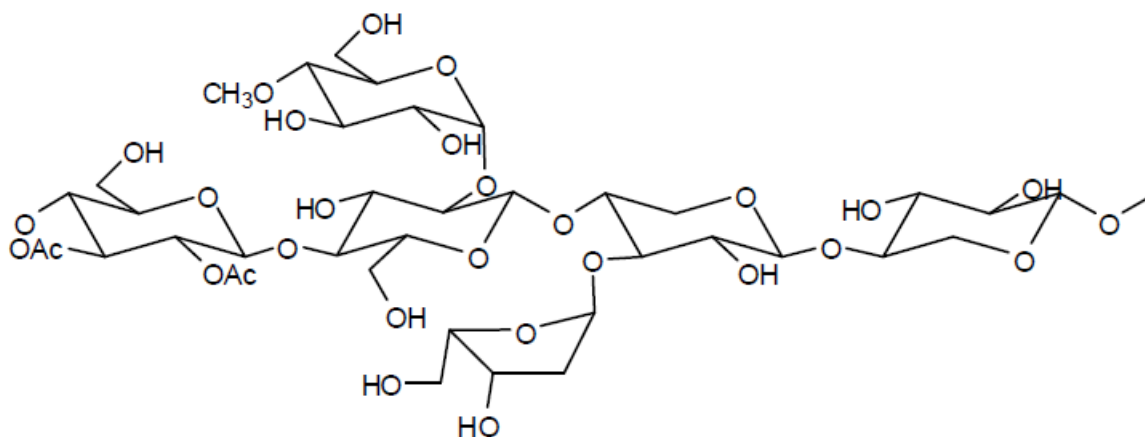


Figure 2.2. A simplified structure of hemicellulose showing the different types of sugars present.⁴⁰

2.2.1.3. Lignin

Lignin is a large three dimensional polymer forming the “glue” that binds cellulose and hemicellulose by intertwining through both the primary and secondary plant tissues and shields the interior of the plant from stimuli. This extremely varied (random polymer), complex, amorphous, and large molecular structure containing cross-linked polymers of phenolic monomers is present in the plant primary cell wall, imparting structural support, impermeability, and resistance against microbial attack. **Figure 2.3** gives a proposed structure of lignin and its monomers. Largely, lignin is unused and even hinders many industrial processes because of the difficulty to break down the polymer or isolate it. The lignin present in biomass is known as native lignin.⁴²

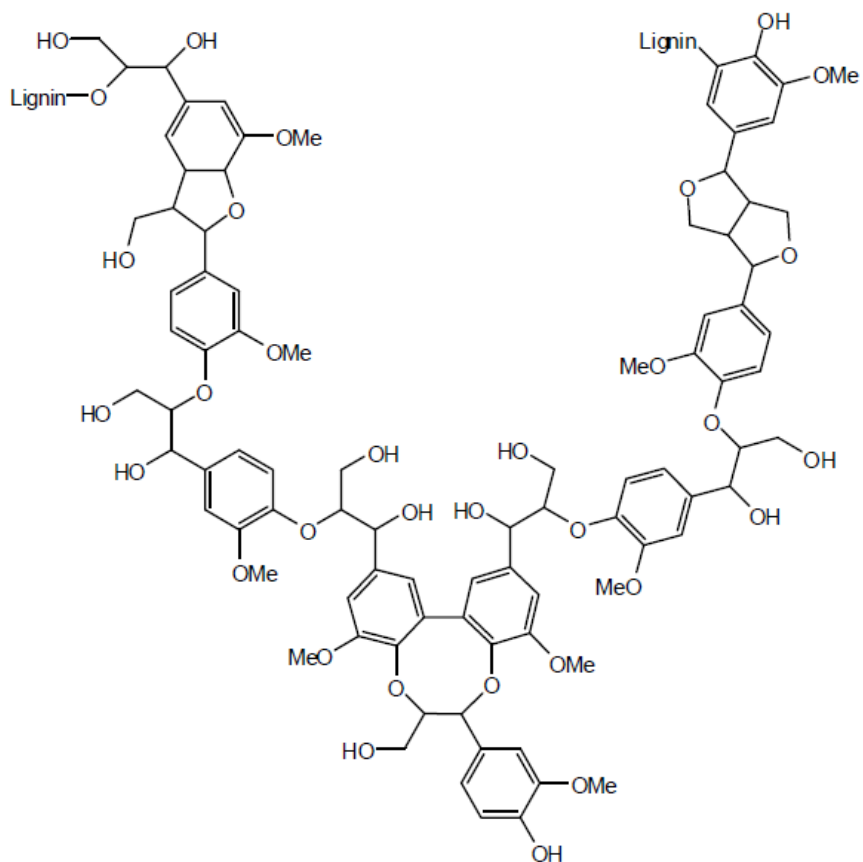


Figure 2.3. Schematic structural formula for lignin.⁴³

Lignin is composed of three monomeric phenyl propionic alcohols: coniferyl alcohol (guaiacyl propanol), coumaryl alcohol (p-hydroxyphenyl propanol), and sinapyl alcohol (syringyl alcohol). These phenolic monomers are linked together by alkyl-alkyl, alkyl-aryl, and aryl-aryl ether bonds. The botanical origin of the biomass dictates the proportion of these phenylpropane units in the lignin. The amount of lignin varies with different sources of plant biomass and generally the lignin content is more in hard and soft wood followed by grasses.

2.2.2. Sources of Biomass for Energy Production

In **Table 2.1**, a summary of the lignocelluloses content in common agricultural residues and wastes is shown. From **Table 2.1**, it is clear that hardwood contains the greater amounts of cellulose, whereas wheat straw and leaves has more hemicellulose. Interestingly, switchgrass is one of the grasses where the cellulose content is close to that from hardwood and softwood and has substantial amount of hemicellulose, but significant lower amounts of lignin.⁴⁴

Table 2.1. Cellulose, hemicellulose, and lignin contents in common agricultural residues and wastes (n/a – not applicable). Reprinted with permission. Source: Kumar, P.; Barrett, D. M.; Delwiche, M. J.; Stroeve, P. *Ind. Eng. Chem. Res.* **2009**, *48*, 3713-3729.

Lignocellulosic Material	Cellulose (%)	Hemicellulose (%)	Lignin (%)
Hardwood stems	40-55	24-40	18-25
Softwood stems	45-50	25-35	25-35
Nut shells	25-30	25-30	30-40
Corn cobs	45	35	15
Grasses	25-40	35-50	10-30
Paper	85-89	0	0-15
Wheat straw	30	50	15
Sorted refuse	60	20	20
Leaves	15-20	80-85	0
Cotton seed hairs	80-95	5-20	0
Newspaper	40-55	25-40	18-30
Waste paper from chemical pulps	60-70	10-20	5-10
Solid cattle manure	1.6-4.7	1.4-3.3	2.7-5.7
Coastal bermudagrass	25	35.7	6.4
Switchgrass	45	31.4	12
Swine waste	6.0	28	n/a

2.2.2.1. Why Switchgrass?

In 1978, the Bioenergy Feedstock Development Program (BFDP) was initiated at Oak Ridge National Laboratory (ORNL) under the sponsorship of the US Department of

Energy (DOE).⁴⁵ The objective of BFDP was to evaluate a wide variety of potential feedstocks other than corn and other food crops that could be grown specifically for bioenergy or bioproduct supply. This was to be achieved by selecting the most promising feedstock species based on actual and potential productivity levels, intensity and type of management requirements, environmental attributes, and the potential economic returns to the producers upon whom production would ultimately depend.⁴⁶ Among the many crops suggested for study as possible feedstocks, switchgrass was one of the herbaceous crops selected for further research.

Over the last few years, switchgrass has received renewed interest as a renewable fuel source.⁴⁷ Switchgrass (*Panicum virgatum*) is a tall, warm-season, perennial grass native for much of the United States and portions of Canada, historically found to grow with several other important native tall-grass prairie plants such as big bluestem, indian grass, little bluestem, sideoatsgrama, eastern gamagrass, and various forbs.⁴⁸ Switchgrass has evolved into two types across its wide native geographic range: (i) lowland ecotypes, which are vigorous, tall, thick-stemmed, and adapted to wet conditions, and (ii) upland ecotypes, which are short, thin-stemmed, and adapted to drier conditions.⁴⁹

Apart from being a native grass to most parts of the United States and some parts of Canada, other factors have made switchgrass to be selected as the “model” herbaceous crop species for energy production based on the following positive qualities:

i) High yields of cellulose: Switchgrass has a higher combined cellulose and hemicellulose content than cool season grasses or legumes (**Table 2.1**). The presence of high amounts of cellulose and hemicellulose is augmented by a low content of lignin allowing pretreatments to easily release cellulose and hemicellulose for hydrolysis (i.e.

low lignin content equal less ‘glue’ holding polymers). When compared to softwoods, herbaceous plants such as grasses have the lowest content of lignin. For switchgrass, the content of cellulose, hemicellulose, and lignin is 45%, 31.4%, and 12%, respectively (**Table 2.1**).

ii) Perennial nature: The perennial nature of switchgrass reduces management intensity, consumption of energy and agrochemicals, a low-input, low-risk energy crop. It does not require annual establishment costs (seed, tillage, etc) and can be harvested and handled with standard farm equipment to provide an annual income.⁵¹ Perennial energy crops are suitable for almost all cropland and potential cropland and can be grown on erosive land (yet achieve acceptable levels of soil protection).⁴⁵

iii) Low fertility needs: A review of literature suggests switchgrass can be grown on soils of moderate fertility without fertilizing (or with minimal fertilizer additions) and still maintain productivity.⁵² Switchgrass has a remarkable ability to extract nitrogen from unfertilized soils and one specific study reported that a field was harvested for seven years with no fertilizer applications, and averaged 53 pounds of nitrogen removed per year with one harvest per year.⁵² This demonstrates that switchgrass has the genetic ability to survive and produce with little to no inputs.⁴⁸ In fact, switchgrass has long-term positive effects on the soil properties and soil nutrient cycles which reduce the need for external nitrogen additions. This has been observed through a buildup of soil organic matter under switchgrass stands over time accompanied by high microbial activity and accumulation of a reservoir of mineral nutrients.⁴⁶

iv) Excellent wildlife habitat: Switchgrass has shown positive impacts on wildlife by providing a suitable habitat for grassland birds⁵³ and causes minimal disturbance to their breeding and nesting, which normally occurs before switchgrass harvesting. Since implementing switchgrass for biofuel production is a long-term investment, a longer-term habitat is also produced that will be tied into the life of an energy production facility (Native grasses, such as switchgrass, are an important habitat component for many species of wildlife that typically use fields because of the structure and cover these grasses provide.⁵⁴ Underneath the forbs and between the grass bunches would be an open environment that would enable small wildlife, such as young wild turkeys, bobwhite quail and field sparrows, to move about and feed unrestricted throughout the field while protected by an overhead canopy.⁵⁵

v) Carbon sequestration: Production and use of switchgrass for bioenergy can help reduce atmospheric CO₂ buildup by carbon sequestration through its deep root system. Soil carbon dynamic studies indicated that soil carbon mineralization, microbial biomass carbon, and carbon turnover tended to increase with time after switchgrass establishment.⁵⁶ Ten years of continuous switchgrass resulted in higher soil carbon level than nearby fallow soils, but several years of continuous grass production may be needed before increases are measurable. Carbon storage in switchgrass generally was observed to increase both in shoots and roots with time after switchgrass establishment, and the rate of increase of carbon storage in roots is higher than that in shoots. The study showed the root/shoot ratio of carbon storage was 2.2, and this implied that carbon partitioning to roots plays a key role in carbon sequestration by switchgrass. Carbon storage in the overall switchgrass-soil system showed an upward trend after switchgrass establishment.

vi) Tolerance to poor soils and wide variations of soil pH: The adaptability of switchgrass to poor and otherwise marginal soils also made it an excellent choice as a model energy crop for further research, since dedicated bioenergy crops were envisioned to be produced mainly on lands not used for primary food and/or cash crops.⁴⁶ Switchgrass can tolerate extremely low pH soils (<5.0) which do not support the growth of cool season grasses or legumes.⁵⁷

vii) Drought and flood tolerance (depending on the ecotype and variety): A unique characteristic of perennials, especially warm-season grasses, is their drought tolerance. The yields of switchgrass, sorghum, sudangrass, and other perennials were compared in different locations in drought years.⁵⁸ It was observed that switchgrass tolerated greater levels of drought stress and its yields maintained a high average yield compared to sorghum whose yields decreased as the drought continued. Switchgrass has also been found to demonstrate good physiological resilience evidenced by a high capability to respond to favorable growing conditions that followed extreme drought.⁵⁹

viii) Efficient water use in grassland/prairie ecosystems: One of the key attributes of switchgrass is its high level of resource allocation to deep root production, as stated previously, while slowing above-the-ground growth during establishment.⁵⁸ This extremely important factor increases the capacity to utilize water and nutrients from deeper soils, increases enrichment of soil associated with high inputs of carbon from root turnover, increases microbial communities activity, and increases the capacity of switchgrass to store and mobilize nutrients needed to re-grow following harvesting.⁴⁷ Switchgrass uses water approximately twice as efficiently as traditional cool season

grasses.⁶⁰ Today, switchgrass and some of the other native prairie grasses have become increasingly important as energy crops in the Midwest because of their capacity to grow in the hot summer months when water availability limits growth of most other grasses and crop species.⁶¹

ix) Resistance to Pests & Diseases: Another unique characteristic of switchgrass is attributed to resistance to pests and diseases. In switchgrass trials conducted in Tennessee, farmers and researchers did not experience significant disease problems and few pests invasion was reported.⁵⁵ However, this does not imply the crop will always be free from attack. As the acreage of switchgrass monocultures increases, a corresponding increase in pests and diseases is likely. The existence of cultivars that are locally adapted and relatively reliable is another factor and research studies have shown that selecting varieties based on location increases the survivability and productivity of a switchgrass stand.^{48, 52}

2.3. PROCESSES FOR CONVERSION OF LIGNOCELLULOSIC BIOMASS TO BIOFUELS

2.3.1. Goals of Degradation of Lignocellulosic Biomass

As stated in previous sections, the degradation and digestibility of cellulose present in lignocellulosic biomass is hampered by many physicochemical, structural, and compositional factors with the most significant factor being high resistance to depolymerization. In the conversion of lignocellulosic biomass to fuel, biomass needs to be treated to expose the cellulose in the plant fibers. Pretreatment refers to the process

that converts lignocellulosic biomass from its native form to a form for which cellulose hydrolysis is much more effective.⁶² Specifically, pretreatment process break down lignin and hemicellulose structures, reduce the crystallinity of cellulose, and increase the porosity of the lignocellulosic materials, so that the acids or enzymes can easily access and hydrolyze cellulose. Pretreatment can be the most expensive process in biomass-to-biofuels conversion, however; it also has great potential for improvements in efficiency and lowering the costs through further research and development. A schematic for the conversion of biomass to fuel is shown in **Figure 2.4**.

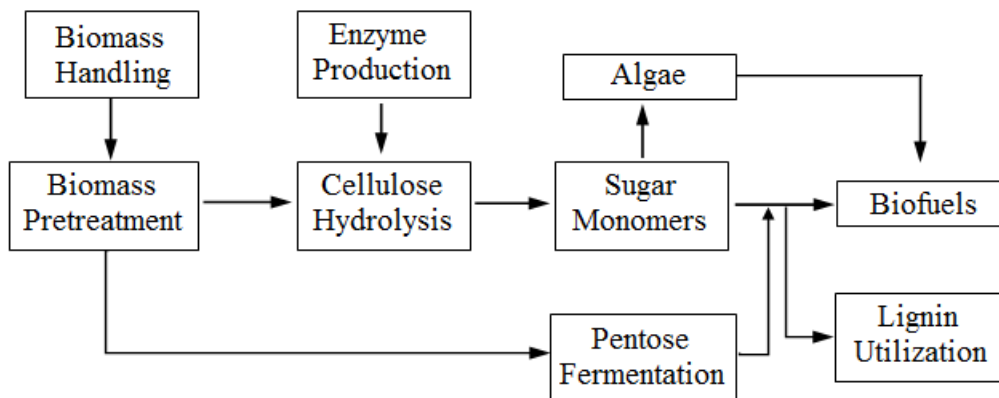


Figure 2.4. Schematic of the conversion of lignocellulosic biomass to biofuels.⁴⁰

The specific objectives of pretreatment are dictated by the overall objectives of a biomass conversion process. Pretreatment must be energetically, chemically, and economically efficient for a biomass conversion process to be profitable.⁶³ Pretreatment must promote effective conversion of available carbohydrates to fermentable sugars so that high product yield can be achieved and it must maximize the formation of sugars or the ability to subsequently form sugars by hydrolysis. Hence degradation or loss of carbohydrate must be avoided. Since it is also desirable to maximize the rate of

enzymatic conversion (when enzymatic hydrolysis used), pretreatment must yield a highly digestible material that is not inhibitory to cell metabolism or extracellular enzyme function. Therefore, it is preferable to avoid the formation of inhibitory product and the need for detoxification or washing (although high sugar losses can occur if pretreated material is washed prior to enzymatic hydrolysis). When using enzymatic hydrolysis as a post-pretreatment conversion process, materials must be efficiently hydrolyzed using low enzyme loadings so the potential of nonspecific binding of enzymes to lignin and other fractions of pretreated biomass are minimized.⁶³ Finally, the pretreatment process needs to be carried out easily without technical limitations.

When evaluating pretreatment efficiency, factors to consider (besides those mentioned above) include recovery of high value-added co-products (from available lignin and proteins), pretreatment catalyst, catalyst recycling, and waste treatment.⁶⁴ In addition, pretreatment results must be weighed against their impact on the ease of operation and cost of the downstream processes and the trade-off between several costs, including operating costs, capital costs, and biomass costs.⁶⁵

Historically, the use of pretreatment to improve lignocellulosic biomass digestibility has been recognized at least since 1919 when a patent for alkali pretreatment using a sodium hydroxide (NaOH) soak for improving *in vitro* digestibility of straw by ruminants was recorded.⁶⁶ Pretreatments currently being used or proposed for use with respect to biofuels and/or chemical production from lignocellulosic materials can be roughly divided into different categories: physical, physicochemical, chemical, biological, electrical, or a combination of techniques. However, none of the pretreatments can be declared a “winner” since each has intrinsic advantages and disadvantages. The

following gives a summary of pretreatment techniques that have been applied to switchgrass in our research, focusing on their mechanism of action.

2.3.2. Microwave Pretreatment

Microwave irradiation have non-thermal or thermal effects arising from the heating rate “hot spots”, acceleration of ions and collision with other molecules, and rapid rotation of dipoles such as water with an alternating electric field.⁶⁷ Microwave pretreatment works by partially disrupting lignin structure and expose more accessible surface area of cellulose to the hydrolytic enzyme. Moreover, it disrupts silicified waxy surfaces (for biomass that accumulates high silicon in the shoot), break down lignin-hemicellulose complex, and could reduce unproductive binding of cellulase to lignin.⁶⁸ The method applied for microwave pretreatment was a response surface methodology described by Wu and coworkers, with some modifications.⁶⁷

2.3.3. Aqueous Ammonia Pretreatment

Ground Alamo switchgrass (35 g/L) was soaked for 5 days at room temperature in 30% aqueous ammonium hydroxide without any agitation. After the soak was completed the slurry was filtered, washed, and the solids were retained for enzymatic saccharification. Aqueous ammonium hydroxide is an effective technique for removing lignin whereas preserving the cellulose fraction. Isci and coworkers⁶⁹ also observed that nearly half of the hemicellulose was removed with ammonia pretreatment. Removal of hemicellulose is advantageous in biomass pretreatment because it reduces inhibitory

compounds such as furfural resulting from hemicellulose degradation via dilute acid treatment at high temperature and pressures.

2.3.4. Alkaline Pretreatment

The method applied in this study for alkaline pretreatment of switchgrass is described by Wang *et al.*⁷⁰ Slake lime (calcium hydroxide, Ca(OH)₂) and sodium hydroxide (NaOH) were used. The mechanism of alkaline pretreatment is believed to be the saponification of intermolecular ester bonds crosslinking hemicellulose and other components⁷¹ and the pretreatment depends on the lignin content of the material.⁶³ Delignification of lignocellulosic biomass is another effect of alkaline pretreatment. This enhances enzyme effectiveness by eliminating nonproductive adsorption sites and by increasing access to cellulose and hemicellulose. Alkaline pretreatment also removes acetyl and different types of uronic acid substitutions on hemicellulose, thus lowering the extent of enzymatic hydrolysis of cellulose and hemicellulose. NaOH effectively promotes lignocellulose digestibility by causing swelling of lignocellulosic materials thus increasing the internal surface area, reducing the degree of polymerization and the crystallinity of cellulose, and breaking structural linkages between lignin and carbohydrates.^{70, 72}

2.3.5. Dilute Acid Pretreatment

Concentrated and dilute acid pretreatment has been successfully developed for the pretreatment of lignocelluloses.^{73, 74} The most commonly used acid is sulfuric acid (H₂SO₄). Dilute H₂SO₄ pretreatment effectively removes and recovers most of the

hemicellulose as dissolved sugars, and the glucose yield is almost 100% from cellulose when hemicellulose is removed because cellulose will be readily exposed to the hydrolysis enzymes. Both high and low temperature processes are used in dilute acid pretreatment. The process applied in our study is a modification of Dien *et al.*⁷⁵ in which 2.5% H₂SO₄ was added to samples of mature switchgrass that was previously ground at a substrate concentration of 35 g/L. The solution was then cooked at 121 °C for 1 h, after which it was washed in preparation for hydrolysis.

2.3.6. Methanol and Water Soaks

Another pretreatment process that was considered in this study was soaking of switchgrass in methanol. Even though this was not a pretreatment per se, it was done to determine whether there was any degradation of lignocelluloses. 35 g/L of switchgrass was soaked in 90:10 (v/v) methanol:water at room temperature for 12 h. This process has not been reported in literature and the objective of this process was to find out if a methanol soak would lead to the formation of any sugars after enzymatic hydrolysis. Another set of switchgrass samples (35 g/L) was soaked in distilled water at room temperature for 1 h. This was treated as a control set in that it was not expected to make available much of carbohydrates (cellulose and hemicellulose) for hydrolysis.

2.4. ENZYMATIC HYDROLYSIS

Enzymatic hydrolysis of cellulose and hemicellulose to sugar monomers is carried out using cellulase and hemicellulase enzymes (glycosylhydrolases) that are highly specific catalysts. This hydrolysis is carried out under mild conditions (e.g., pH 4.5–5.0

and temperature 40–50 °C) leading to advantages such as low corrosion problems, low utility consumption, and low toxicity of hydrolyzates.

2.4.1. Cellulase Enzyme System

Enzymatic degradation of cellulose to simple sugars is generally accomplished by a synergic action of a cellulase enzyme system consisting of three major components: 1,4- β -D-glucanoglucanohydrolase, 1,4- β -D-glucanocellobiohydrolase, and β -glucosidase commonly referred to as endoglucanase, exoglucanase, and cellobiase, respectively.^{76, 77} A random scission of cellulose yielding glucose, cellobiose, and cellotriose is achieved by endoglucanases. Hydrolysis is initiated by a random attack of the β ,1-4 linkages of the cellulose polymer by endoglucanases to create free-chain ends. Exoglucanases perform an endwise attack on the non-reducing end of free-chain cellulose polymer generating cellobiose, a disaccharide comprised of glucose, as the primary product. With endoglucanases, disruption of cellulose hydrogen bonding occurs allowing hydrolysis of the accessible cellulose. The cellobiose units are further digested by β -glucosidases to produce glucose with high activity.^{78, 79}

It is also widely reported that all the three components of the cellulase system can hydrolyze cellulose as well as cellodextrins. Cellobiose is hydrolyzed to glucose by both endoglucanases and cellobiase. Cellobiase also hydrolyzes soluble cellotriose and cellotetraose to give cellobiose and glucose, or cellobiose, respectively, as products.⁷⁶

Enzymatic hydrolysis of cellulose consists of cellulase adsorption onto the surface of the cellulose, the biodegradation of cellulose to fermentable sugars, and then desorption of cellulase. Mechanistically, the cellulase enzymatic hydrolysis reaction

works through the addition of a water molecule to the anomeric (1) carbon of a glucose unit in the cellulose, causing the bridge oxygen to go off with the other (4) carbons, severing the chain (**Figure 2.5**). This process occurs towards the end of the chains, separating one or two glucose molecules at a time; if two glucose molecules are freed this way then another enzyme will cleave the dimer into two monomers.

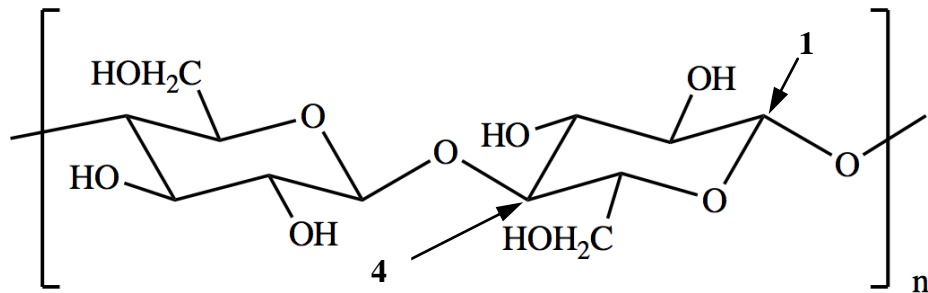


Figure 2.5. Cellulose chain showing the bonds cleaved by the cellulase enzyme. The 1 refers to the anomeric carbon (C1) and 4 is the carbon bridging one glucose monomer to another.

There are several factors to consider when performing enzymatic hydrolysis. These factors include substrate (cellulose and/or hemicellulose) quality and concentration, applied pretreatment method, cellulase activity, and hydrolysis conditions such as temperature and pH. Substrate concentration in a slurry solution is the main factor that affects the yield and initial rate of enzymatic hydrolysis. High substrate concentration has been found to inhibit the hydrolysis thus lowering the yield of sugars. The extent of inhibition depends on the total enzyme to total substrate ratio. The optimum temperatures and pH of different cellulases are usually reported to be in the range of 40 to 50 °C and pH of 4 to 5, respectively, but optimum residence time and pH might affect

each other, even though these conditions vary depending on the biomass feedstock used and the enzyme source.⁸⁰

A comparison of enzymatic hydrolysis with other common hydrolytic techniques highlights some of the advantages and disadvantages of enzymatic hydrolysis. Enzymatic hydrolysis is carried out in mild conditions as compared to dilute acid (H_2SO_4) hydrolysis, which requires high temperature and low pH while resulting in corrosive and toxic conditions.⁸¹ It is possible to achieve cellulose hydrolysis at almost 100% efficiency by enzymatic hydrolysis, but this efficiency is difficult to obtain with acid hydrolyses. Moreover, several inhibitory compounds are formed during acid hydrolysis whereas this limitation is not severe for enzymatic hydrolysis.

On the other hand, enzymatic hydrolysis has its own disadvantages compared to acid hydrolysis including time required for enzymatic hydrolysis (order of days with enzymes opposed to a few minutes for acid hydrolysis) as well as cost since the price of enzymes are much higher than sulfuric acid (commonly used in acid hydrolysis). With enzymatic hydrolysis, the resulting sugar products are reported to inhibit the hydrolytic reaction but in acid hydrolysis, the products do not inhibit the reaction.^{80, 82, 83} To overcome these limitations, simultaneous saccharification and fermentation (SSF) was developed, in which the sugars produced by hydrolysis are directly consumed by present microorganisms. However, since fermentation and hydrolysis usually have different optimum conditions, separate enzymatic hydrolysis and fermentation is still considered as a choice.

2.5. ANALYSIS OF SUGARS AND RELATED COMPOUNDS

After pretreatment and enzymatic hydrolysis processes with biomass are complete, the next step in the biomass-to-biofuels conversion process (**Figure 2.4**) is to determine the quantity of sugars obtained. At such a stage, the amount of liberated sugar measured appraises a given pretreatment followed by enzymatic hydrolysis. There is an increasing impetus to develop rapid and reliable quantitative analyses for individual degradation products from complex matrices in order to advance a fundamental understanding of lignocellulose pretreatment as well as subsequent processes for converting pretreatment hydrolysates into biofuels. The goal of the presented research was to develop and validate a new mass spectrometric technique utilizing Direct Analysis in Real Time, an ambient ionization source for sugar quantification obtained from switchgrass after enzymatic hydrolysis. This technique was chosen as an alternative to the traditional methods of sugar analysis that can be time and cost consuming. Descriptions on the analytical equipment and instrumentation used for traditional methods of sugar analysis as well as method used to develop and validate the novel technique for the analysis of sugar from hydrolysis are presented.

2.5.1. Traditional Methods of Sugar Analysis

Carbohydrates are among the most abundant compounds found in nature and qualitative and quantitative analysis of sugars (typically found as mixtures) has significant importance to the biofuels industry. The existing analytical methods for sugar compounds fall into five categories: colorimetric methods, gas chromatography (GC)-based methods, high performance liquid chromatography (HPLC)-based methods, direct

mass spectrometric methods, and liquid chromatography mass spectrometry (LC/MS) methods.

i) *Colorimetric Detection*: Reduction of sugars using dinitrosalicylic acid for a colorimetric assay is one of the earliest carbohydrate analysis available.⁸⁴ A dinitrosalicylic acid (DNS) assay has been available since 1955 and is still useful for the quantitative determination of reducing sugars.⁸⁵ The DNS reacts with reducing sugars and other reducing molecules to form 3-amino-5-nitrosalicylic acid, which absorbs light strongly at 540 nm. It was first introduced as a method to detect reducing substances in urine and has since been widely used, for example, for quantification sugars from poplar wood and newspapers after enzymatic hydrolysis following chemical pretreatments.⁴⁴ In general, carbohydrates do not absorb ultraviolet (UV) light because they lack chromophores and fluorophores, thus limiting the use of traditional of spectrophotometric methods to identify and quantify these compounds. Thus chemical attachment of a chromophore to the hydroxyl groups of carbohydrate molecules is often required to promote volatility and provide UV absorptivity at selected wavelengths.⁸⁶ More recently several enzymatic assays for glucose⁸⁷ have been developed. Poor specificity pertaining to a lack of differentiation among mono- and oligosaccharides, differences in efficacy of measuring total carbohydrate, and errors with control blanks are some of the challenges associated with this method.⁸⁸

ii) *Gas Chromatography (GC)*: Numerous analyses of sugars using GC-based methods have been reported in literature.⁸⁹⁻⁹² GC coupled with flame ionization, ultraviolet, pulsed amperometric, and mass spectrometry detection have been the most commonly used methods for analysis. These methods have been used successfully for decades in the

determination and quantitation of sugars from biomass. The use of derivatization enables chromatographic analysis to be done with high sensitivity especially at low concentrations. However, the derivatization step is a labor-intensive process, which at times, is prone to sample contamination. It involves additional sample preparation, handling, and manipulation that are time-consuming (usually characterized by long hours or days of analysis) and additional costs are necessary with the purchase of derivatization reagents. Moreover, the occurrence of overlapping chromatographic peaks with sugar anomers and/or mixtures is a limitation of GC-based methodologies.⁹³

iii) *High Performance Liquid Chromatography (HPLC)*: This technique utilizes a suitable column for separation of the samples where a variety of detection methods have been used including electrochemical detection,⁹⁴ refractive index (RI),^{86, 95} pulsed amperometric detection,⁹⁶ and evaporative light-scattering detection (ELSD).⁹⁷ These techniques have been successful to some extent for the quantitative analysis of sugars, however; limitations can be attributed to analysis times for a chromatographic run that can vary from 6 to 15 minutes (per sample), incomplete resolution of analytes, and the inability to use readily accessible wavelengths for the detection of these samples which lack chromophoric and fluorophoric moieties required for UV and fluorescence detection. As a result, less selective universal detection methods (such as RI and ELSD) are used and these detection methods typically provide detection limits in the range of 0.05–1.2 µg/injection.⁹⁸

In order to improve and avoid the limitations of HPLC analysis of sugars using universal detection methods, coupling mass spectrometry to the HPLC have been embraced in the recent past. With direct MS methods, sample is injected into system

where no chromatography column exists. This is accomplished with either the HPLC pumping system or using a syringe connected to an appropriate pump. A few examples of HPLC with MS for sugar analysis include distinction of monosaccharide stereoisomers using ion trap mass spectrometry (ITMS),⁹⁹ determination of glucose concentration in tear fluid with electrospray ionization,¹⁰⁰ study of fragmentation profiles of sugars with atmospheric pressure chemical ionization,¹⁰¹ and the use desorption electrospray for the analysis of carbohydrates.¹⁰²

With analysis by HPLC, sample preparation, extractions, and modifications may need to be performed before analysis including matrix removal and sample pre-concentration. The matrices present in the various samples that pass through a chromatography column can significantly influence the quality and sensitivity of the column. Prior removal of specific matrices may be required before analysis with the HPLC can occur. A cost hindrance is the need for mobile phase solvents (typically some percentage exist as organic solvent) that has initial cost as well as the cost associated to store and dispose of these solvents. Time for analysis can also be compounded taking into account mobile phase preparation.

Despite the accessibility of user-friendly equipment and more streamlined protocols for sample preparation, pressure to increase productivity and quality is dependent on sample-preparation. As chromatography has become faster and more sensitive, sample preparation has become a vital step in order to receive the benefits from these advances. However, researchers and scientists have become more interested in getting their answers and data directly without spending the time preparing samples. The result has been recent advances analytical methods to increase throughput by

significantly reducing sample preparation or eliminating it completely – while holding a high level of selectivity and sensitivity. Therefore, current investigations employ a technique that requires little to no sample preparation in the analysis of sugars from biomass. The use of the ambient ionization source, Direct Analysis in Real Time (DART), (coupled to a mass spectrometer) described in the following sections will eliminate the stringent considerations of sample preparation required by traditional analytical methods.

2.6. NOVEL EXPERIMENTAL METHODS FOR SUGAR ANALYSIS

The main focus of this section is to describe the analytical techniques and instrumentation that were necessary to develop and validate a quantitative method for six-carbon sugars derived from switchgrass. Specifically, instrumentation includes linear ion trap mass spectrometry, with special emphasis using the ambient ionization method of Direct Analysis in Real Time (DART). Diagrams, basic theories, and operation of the analytical instrumentation will be described as well as listed advantageous over other ion sources for mass spectrometry. While brief descriptions of are provided, readers are encouraged to consult the provided literature sources for a more comprehensive description.

2.6.1. Mass Spectrometry

In analytical instrumentation, mass spectrometry can be considered as one of the fastest growing fields. While an established analytical tool in analytical, organic, synthetic, and pharmaceutical chemistry, it can be extensively applied for material

science, forensic, toxicological, biotechnology, and environmental research. Mass Spectrometry (MS) is an analytical tool for identifying unknown compounds by measuring the molecular mass of compounds as well as interrogating molecular structure. It is essentially a technique for "weighing" molecules – obviously, this is not done with a conventional balance or scale. Instead, MS is based upon the motion and monitoring of charged particles, e.g. ions, in an electric or magnetic field. Typically, the result of mass spectrometric analysis (generated with a mass spectrometer) is reported as a mass spectrum where the molecular mass of a sample is given as a mass-to-charge ratio, m/z , where m is the relative mass and z is the charge of a specific ion. The mass spectrum is a graph where the x -axis represents the m/z of detected ions and the y -axis represents the abundance of each ion. Typically, the unit of the y -axis is listed as percent relative intensity since each peak is assigned an intensity relative to a base peak (the most intense peak that is automatically designated with an intensity of 100%).

The mass spectrometer consists of four basic components: the ion source, the mass analyzer, a detector, and a vacuum system (**Figure 2.6**). The vacuum system is a vital component of the mass spectrometer since a vacuum must be present so ions can transverse from the ion source to the detector, e.g. decrease the possibilities of collision events of the ions of interest with residual gas molecules. The ideal operating pressure needed provides an average distance an ion travels before colliding with a gas molecule (its *mean free path*) that is longer than the distance from the source to the detector.¹⁰³ The role of the ion (or ionization) source is to convert molecules from an innate neutral state to a charged or ionized form before they can enter the mass analyzer. Depending on the nature of ionization, the ion source may or may not be held under vacuum. The role of

the mass analyzer is to separate ions, either in space or in time, according to their m/z employing electric and/or magnetic fields. Once separated, ions proceed to an ion detector where ions are converted to produce an electrical current that can be amplified and detected and then transferred to a computer/data processor to produce and record the resulting mass spectrum.

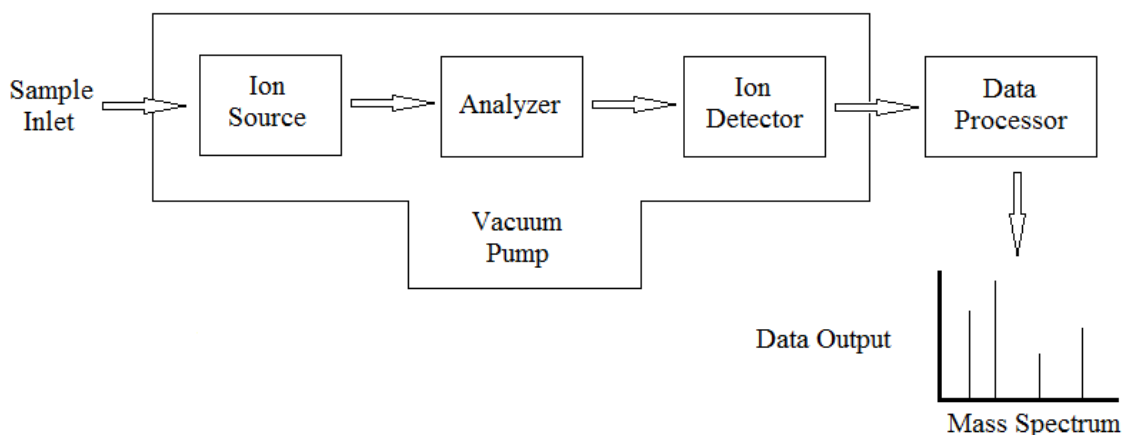


Figure 2.6. A block diagram showing the main components of a mass spectrometer.

2.6.2. Ionization Sources

While a review of all ionization techniques used with mass spectrometry is beyond the scope of this thesis, it is important to briefly discuss the classifications of ionization. Ionization sources have undergone an evolution as more efficient and user-friendly sources have been developed. This section will therefore give a summary of the ionization process with focus on ambient ionization. Since the starting point with mass spectrometry is the formation of gaseous analyte ions, the ionization process dictates utility and scope of a mass spectrometric method.¹⁰⁴ An ion source produce molecular ions mainly by ionizing a neutral molecule in the gas phase through electron ejection,

electron capture, protonation, deprotonation, adduct formation or by the transfer of a charged species from a condensed phase to the gas phase.¹⁰⁵

Ion sources are generally classified as being either “hard ionization” or “soft ionization” sources. With hard ionization sources, most commonly used is electron ionization (EI), sources impart sufficient energy to target molecules to eject an electron resulting in a charged radical (M^+). Available excess energy will rupture molecular bonds resulting in fragment ions that have mass-to-charge ratios less than the molecular ion. Soft ionization techniques such as chemical ionization (CI), electrospray ionization (ESI), matrix-assisted laser desorption/ionization (MALDI), photoionization (PI), field ionization (FI) and field desorption (FD), and fast atom bombardment (FAB) produce molecular ions that represent an intact molecule, usually in the form of a protonated molecule, $[M+H]^+$.¹⁰⁶ With soft ionization, the energy imparted on the molecule is less than its bond dissociation energy (BDE) resulting with little to no fragmentation. If fragmentation of a molecular ion is required, then tandem mass spectrometry experiments are normally performed (discussed in detail in Section 2.6.4). In **Figure 2.7**, a schematic illustrates the differences in mass spectra formed using soft and hard ionization processes.

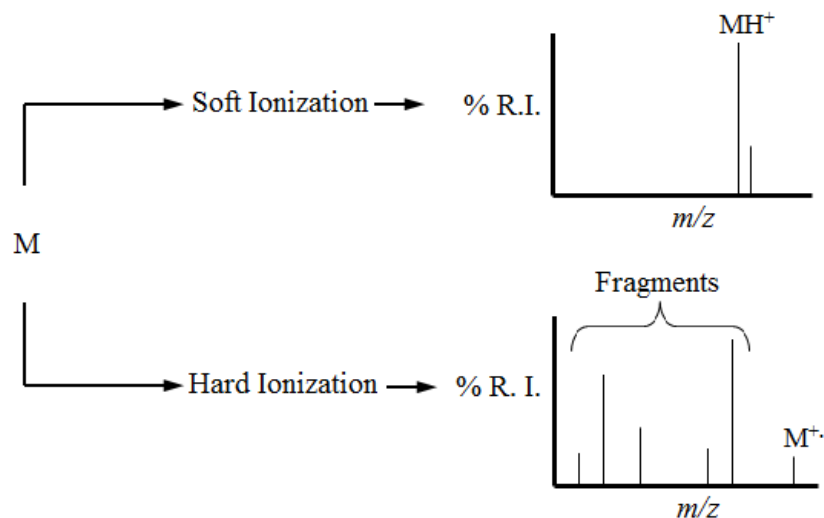


Figure 2.7. A schematic showing how a molecule, M, is analyzed by soft ionization and hard ionization and the resulting mass spectra.

Ion sources can also be classified depending on the pressure in which they are operated. Atmospheric pressure ionization sources ionize compounds and transmit those ions into the mass analyzer at atmospheric pressure. Since the mass analyzer usually operates in a high vacuum ($\leq 10^{-5}$ Torr), an atmospheric interface equipped with a differential pumping system must be present to transfer ions into the vacuum region.¹⁰⁵ Examples of traditional atmospheric ionization include: electrospray (ESI), atmospheric pressure chemical ionization (APCI), atmospheric pressure photoionization (APPI), atmospheric pressure–MALDI.

In the recent past, mass spectrometry has undergone a contemporary revolution with the introduction of a new group of desorption/ionization techniques known collectively as “ambient ionization mass spectrometry”. These techniques are performed in an open atmosphere directly on samples in their natural environments or matrices, or by using auxiliary surfaces. The development of ambient MS has greatly simplified and

increased the speed of MS analysis. Basic characteristics have been presented for a technique to be included as an “ambient ionization” thus distinguishing it from atmospheric pressure ionization techniques.¹⁰⁷ Ambient ionization techniques with MS should enable: i) ionization in the absence of enclosures such as those typically found in ESI, APPI, APCI, or AP-MALDI sources and operate in the open air or ambient environment. This is significant when analyzing samples of unusual shape or size that could not be easily fit inside of an ion source enclosure or that would be critically disrupted or damaged when placed under vacuum. ii) Allow direct ionization with minimum sample preparation. iii) Can be interfaced to most types of mass spectrometers without substantial modification to the ion transfer optics or vacuum interface. iv) Allow soft ionization to occur where the amount of internal energy deposited is equal to or lower than that in traditional atmospheric pressure ionization techniques.

From rapid growth of ambient MS, many techniques are being utilized in a myriad of applications and detailed reviews of these techniques are found in literature¹⁰⁷,¹⁰⁸ **Tables 2.2 - 2.5**, adapted from refs.¹⁰⁷⁻¹⁰⁹ summarize the current techniques that are considered highly significant to ambient MS field stemming from their originality in terms of their fundamental insights and applicability.

Other ambient mass spectrometric sources that do not fit in any of the groups in the tables above are known as “sonic spray ionization” (SSI). SSI was unique and revolutionary because it introduced a new concept of ionization (ion production by spraying an acidified solution of the analyte in methanol at sonic speed without the assistance of voltage, radiation, or heating) to MS.¹¹⁰ SSI-based techniques include: desorption atmospheric pressure photoionization (DAPPI), radio-frequency acoustic

desorption ionization and ionization (RADIO), easy ambient sonic-spray ionization (EASI), and Venturi easy ambient sonic-spray ionization (V-EASI).^{107, 108} More data and applications have been developed for the originally introduced ambient ionization techniques, Direct Analysis in Real Time (DART) and Desorption Electrospray Ionization (DESI). The goal of this research is to develop and validate a DART-MS method for the quantitation of sugars from switchgrass saccharification samples.

Table 2.2. Gas discharge ionization ambient ionization MS techniques.

Gas Discharge Ionization (GDI)-based Techniques		
Acronym	Description	Summary of the Mode of Operation
DART	Direct analysis in real time	A heated gas plasma generated via atmospheric glow discharge ionization impinges on the analyte thus causing desorption and ionization (see Section 2.6.2.1)
DEMI	Desorption electrospray metastable-induced ionization	A dual ionization source integrating the advantages of DART and DESI
FA-APGI	Flowing afterglow-atmospheric pressure glow discharge	Somewhat similar to DART. A plasma from a discharge chamber (with two glow discharge electrode) excites helium molecules which causes desorption and ionization of the analyte
LTP and DBDI	Low temperature plasma and dielectric barrier discharge ionization	These techniques use plasma generated by a dielectric barrier discharge between two isolated electrodes. An alternating potential at a specific frequency ionizes the sample via desorption
PADI	Plasma-assisted desorption/ionization	Similar to DART and DBDI except that a radio frequency is applied to a needle end to generate a low power plasma to ionize samples

Table 2.3. Common electrospray-based ambient ionization MS techniques.

Electrospray (ESI)-based Techniques		
Acronym	Description	Summary of the Mode of Operation
DESI	Desorption electrospray ionization <ul style="list-style-type: none">• Reactive DESI• DESI Imaging	Analyte droplet pickup/splashing from a surface followed by ESI-like ion evaporation from secondary droplets
SESI	Secondary electrospray ionization	Interaction of neutral analyte gaseous molecules with charged particles created by ESI
EESI	Extractive electrospray ionization	Introduction of volatile vapors of neutral analyte molecules from a solution into a stream of charged droplets produced by ESI
ND-EESI	Neutral desorption EESI	Desorption of analyte molecules into a neutral gas stream coincident with the ESI plume
FD-ESI	Fused droplet electrospray ionization	Merging an ESI stream with aerosols carrying the analyte
PSI	Paper spray ionization	Capillary action in a porous material with a macroscopically sharp point is used to transport the analyte. Ionization is performed using a high electric field applied on the porous material

Table 2.4. Atmospheric pressure chemical ionization ambient ionization MS techniques.

Atmospheric Pressure Chemical Ionization (APCI)-based Techniques		
Acronym	Description	Summary of the Mode of Operation
ASAP	Atmospheric solids analysis probe	A solvent spray or hot stream of nitrogen gas impinges a solid sample on a solid probe producing analyte molecules which are ionized under corona discharge-based APCI conditions
DAPCI	Desorption atmospheric pressure chemical ionization	Similar to ASAP but in DAPCI gaseous analyte ions generated by the corona discharge are directed to condensed-phase samples causing desorption and ionization of neutral target molecules

Table 2.5. Laser desorption/ablation ambient ionization MS techniques.

Laser desorption/ablation Ionization (LDI)-based Techniques		
Acronym	Description	Summary of the Mode of Operation
ELDI	Electrospray-assisted LDI	A laser desorbs and partially ionizes a matrix-free analyte forming a plume of neutral and mono-charged species that are subjected to ESI to produce multi-charged analyte species
MALDESI	Matrix-assisted laser desorption electrospray ionization	Same as ELDI but differs in that the plume of neutral and charged species is formed via MALDI
LAESI	Laser assisted ESI	A UV laser is used to ablate a matrix-free analyte forming neutral species which are ionized by ESI
IR-LADESI	Infrared-laser assisted desorption ESI	Same as LAESI but an IR laser is used to desorb and ablate the sample
IR-LAMICI	Infrared ablation metastable-induced chemical ionization	A glow discharge generates metastables (which causes ionization) that are directed to a neutral sample plume desorbed by an IR laser

2.6.2.1. Direct Analysis in Real Time Mass Spectrometry

While techniques like liquid chromatography mass spectrometry (LC-MS) and gas chromatography (GC-MS) give reliable and reproducible results, they can involve multiple sample preparation steps (extractions, derivatization, etc.) and can require significant time for chromatography run (8 to 15 minutes per sampler pertaining to sugar analysis). Given the fact that specific government agencies and industrial laboratories are responsible for monitoring thousands of samples, the time intensive nature of LC-MS and GC-MS limits their effectiveness. Consequently, a need for a rapid and accurate test that can quickly determine the presence of an analyte of interest is desired. Furthermore, the ideal technique would involve minimal sample preparation, allow sampling under atmospheric conditions, and provide a response within seconds of sample introduction.

DART is a mass spectrometric atmospheric pressure ion source that instantaneously ionizes gases, liquids and solids in open air under ambient conditions. Its development was motivated by the need to replace the radioactive sources used in hand-held spectrometers with an atmospheric ion source. After several trials in different laboratories of its applicability as ion source, DART was introduced as a commercial product in early 2005.^{111, 112}

The operation of DART involves the atmospheric pressure interactions of long-lived electronic excited-state atoms or vibronic excited-state molecules with the sample and atmospheric gases.¹¹³ A schematic illustration of the DART ion source is shown in **Figure 2.8**. In the DART ion source, a gas flows through an enclosed chamber where an electrical glow discharge produced by an applied potential of several kilovolts (1–5 kV), generates ions, electrons, and excited-state neutral species (atoms and molecules)

commonly referred to as metastables. The gases used in DART include helium, nitrogen, and/or argon. The chamber has perforated intermediate lenses or grids (**Figure 2.8, a**) in which the excited-state species passes through removing most of the charged species. However, neutral gas atoms/molecules including metastable species remain in the chamber. These gaseous species exiting the discharge chamber pass through an optional gas heater which adjusts the gas temperature (thermal analyte desorption) from room temperature up to the desired value with a maximum of 500 °C.^{108, 114}

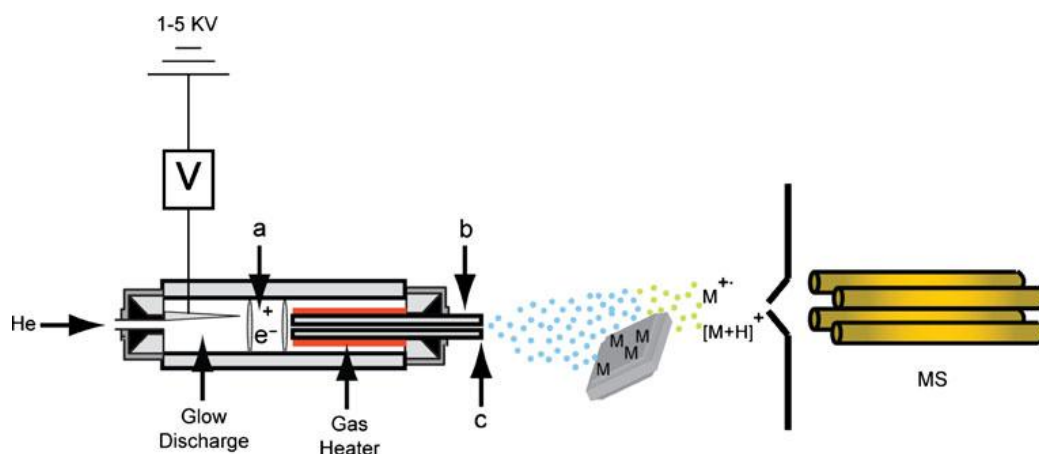


Figure 2.8. A schematic diagram of the DART ion source adapted from reference.¹⁰⁸ The **a** is a perforated intermediate lens, **b** is a grid electrode, **c** is the insulation cap, and **M** is the analyte.

At the exit of the DART source, there is a grid electrode (**Figure 2.8, b**) which serves to remove ions with opposite polarity to prevent signal loss by ion–ion interaction and ion–electron recombination, acting therefore as an ion repeler, and acts as an electrode promoting drifting of ions towards the inlet of the mass spectrometer’s atmospheric interface. and an insulation cap (**Figure 2.8, c**), whose functions is to protect the sample and the operator from any exposure to the grid.¹¹³ Ionization occurs when the DART gas

makes contact with the sample at a contact angle of 0° or reflected off a sample surface at approximately 45° .

The DART ion source can operate in either positive or negative mode and ions formed by DART depend on the nature of the gas, ion polarity, and whether dopants are present.¹¹¹ In positive ion mode, molecular ions (M^+) are mainly observed for low-polarity or nonpolar molecules compounds when nitrogen is used while protonated $[M + H]^+$ cations are typically formed when helium is used. Adducts have also been observed when an ammonia source is present nearby the DART source while analyzing samples, $[M + NH_4]^+$. In negative ion mode, mass spectra are mainly dominated by deprotonated $[M - H]^-$ anions for most compounds while some negative charge ions (M^-) are observed for specific compounds. Other adducts, such as $[M + Cl]^-$, are observed when a suitable dopant is used. Since only a few ionized species are formed with DART, the interpretation of mass spectra for unknown compounds is simpler when compared to electrospray ionization, where multiple ionization species can form.^{111, 115} Even though fragment ions are not observed for most compounds when using DART, fragmentation can be induced by increasing the voltage and the capillary temperature on orifice of the mass spectrometer atmospheric pressure interface.

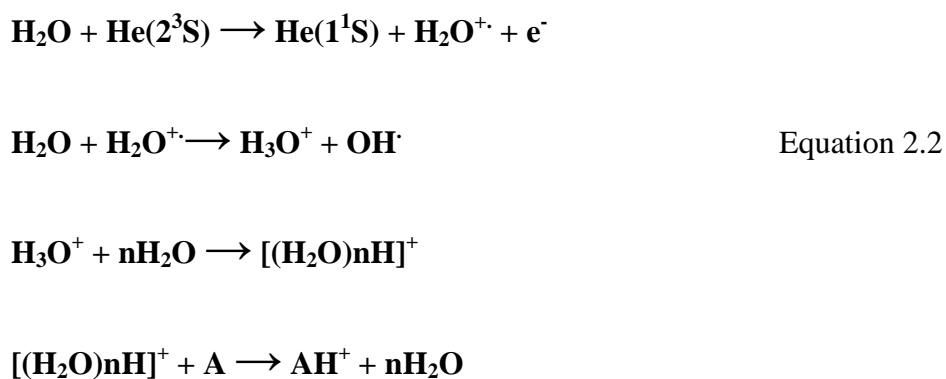
2.6.2.2. Ionization Mechanisms in DART

Several ionization mechanisms in DART have been reported and are dependent on the polarity of the ionizing gas, the proton affinity of the sample, the presence of additives or dopants, and the ionization potential of the analyte.

As proposed,¹¹¹ the first ionization mechanism is referred to as Penning ionization which involves the transfer of energy from an excited gas M* to an analyte A with an ionization potential lower than the energy of M*. This leads to the formation of a radical molecular cation A⁺ and an electron (e⁻), as shown by Equation 2.1. This mechanism is proposed predominantly to occur when the DART ionization gas is either nitrogen or neon.¹¹³

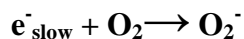
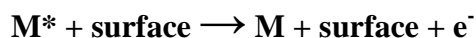


Secondly, DART ionization can occur through proton transfer mechanism. This mainly takes place in the positive ion mode when helium is used as the ionizing gas. In this mechanism, water clusters are generated by the interaction of helium metastables (He, 2³S) with atmospheric water vapor followed by proton transfer reactions (Equation 2.2).¹¹³



This mechanism occurs because helium metastables (He, 2³S) have a higher energy potential (19.8 eV) and its reaction with water is highly efficient. This indicates that the performance of DART is not affected by humidity.¹¹¹

The third mechanism proposed in DART ionization is commonly known as electron capture where electrons (e^-) that are produced by Penning ionization (ionization that occurs through the interaction of two or more neutral gaseous species, at least one of which is internally excited usually to a high energy state) or surface Penning ionization (refers to the interaction of the excited-state gas with a surface, resulting in the release of an electron) are readily thermalized by collision with atmospheric pressure gas as shown in Equation 2.3. These electrons are captured by atmospheric oxygen to produce O_2^- . The formed O_2^- can react with interacting analyte molecules to produce negatively charged anions.



It is reported that¹¹³ the DART negative-ion reagent mass spectra are virtually identical for nitrogen, neon, and helium. However, negative-ion sensitivity increases for DART gases in the following order:

nitrogen < neon < helium

This phenomenon results from increased efficiency in forming electrons by Penning ionization and surface Penning ionization as the internal energy of the metastable species increases. Other negative ion mode mechanisms were also investigated.¹¹⁶

Another reported mechanism in correlation with DART is the Transient Micro-Environment Mechanism (TMEM).¹¹⁷ The proposed mechanism takes into account the DART ionizing gas stream contains both metastable helium atoms and water clusters while in contact with a sample. A transient microenvironment (TME) is then created that can shield the analytes from direct ionization by the DART gas stream. The TME may be generated through desorption and ionization of volatile matrix molecules (containing the analyte), and analytes are then ionized by the matrix ion species through gas-phase ion/molecule reactions.¹¹⁷

A nine-stage reaction mechanism, shown in **Figure 2.9** can be grouped into three steps for the TMEM.¹¹⁷ In step one, molecular ions of water are formed (reaction 1 in **Figure 2.9**) when the helium metastable atoms are in contact with atmospheric water that generate protonated water clusters (reaction 2 in **Figure 2.9**). In step two, helium metastables, He*, come into contact with solvent molecules, S, producing solvent molecular ions (reaction 3 in **Figure 2.9**). Solvent molecular ions react with other solvent molecules to produce protonated solvent molecules (reaction 4 in **Figure 2.9**). Protonated water clusters can also react with solvent molecules to produce protonated solvent molecules as well (reaction 5 in **Figure 2.9**). The third step constitute the ionization of analyte molecules, A, to form protonated molecules through gas-phase ion/molecule reactions with protonated solvent molecules (reaction 6 in **Figure 2.9**). The solvent molecular ions can react with analyte molecules to produce both protonated analyte molecules and analyte molecular ions, (reactions 7 and 8 in **Figure 2.9**) or protonated analyte molecular ions if the TME is thin (reaction 9 in **Figure 2.9**).

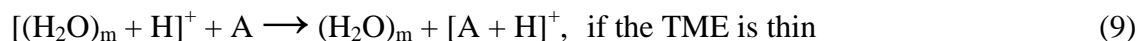
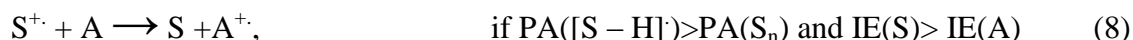
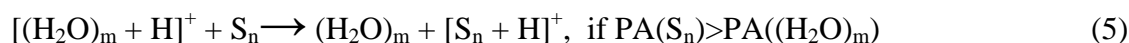


Figure 2.9. Reactions in positive ion DART. ^aME(He) is helium's metastable energy, 19.8 eV; $m = 1, 2,$ or 3 ; $n = 1$ or 2 . Reaction 4 has a few variants for alkanes and chlorinated methanes. ^bIE is the ionization energy and ^cPA is the proton affinity of the specified species. Reprinted with permission from reference.¹¹⁷

2.6.2.3. Application of Direct Analysis in Real Time

Since its introduction as a readily available commercial product with the versatility in ionizing a wide range of chemicals without the need of extensive sample preparation, DART has been used for a multitude of applications. The speed with which data is obtained with DART, as compared with conventional GC-MS and LC-MS, has motivated mass spectrometric practitioners to apply this technique in various fields where

appropriate. The DART-MS has been successfully used both in qualitative and quantitative chemical analysis and readers are directed to the cited literature for more information on a specific set of applications mentioned in **Table 2.6**. The presented table is by no means an inclusive complete description of all the possible applications that have been performed with DART-MS, but provides a broad survey of recent applications.

Table 2.6. Summary of the applications of DART.

Field	Specific Applications	Refs.
Pharmaceuticals	Quantitation of drugs in biological matrices	118
	Detection of counterfeit antimalarial drugs	119
	Preclinical pharmaceutical analysis for impurities, degradation products, isotopic abundance and drug loading	120
Bioanalysis	Ovarian cancer metabolomics fingerprinting of blood samples	121
	Screening of insect terpenoids	122
Homeland security and law enforcement	Detection of “date rape drug” in alcoholic and nonalcoholic drinks	123
	Separation and quantitation of chemical warfare agents	124, 125
	Analysis and detection of explosives	126
	Monitoring of the release of adenine in ricin activity assay	127
Forensics	Detection of cocaine and its metabolites in human urine	128
	Forensic screening of illegal drugs	129
Environment	Determination of sulfur-containing materials in drywall	130
	Analysis of water contamination by UV filters	131
	Detection of organometallic compounds	132
	Screening of insoluble polycyclic aromatic hydrocarbon contaminants	133
	Analysis of poplar pyrolysis products	134
Food, flavor, and fragrances	Identification of food packaging additives	135
	Detection of melamine and cyanuric acid contamination in powdered milk	136, 137
	Detection of mycotoxins in cereals, grains, flours, and beer	138, 139
	Detection of pesticides on fruit surfaces	140
	Release kinetics of taste-refreshing compound in chewing gum	141
Polymer and additives	Stabilizers in polypropylene samples	142
	Detection of restricted phthalic acid esters in toys	143
	Detection of additives in polyvinyl chloride lid gaskets	144

2.6.3. Mass Analyzers

Once gas-phase ions are produced from the ion source, they need to be separated according to their mass-to-charge ratio (m/z) based on their characteristic behavior in electric and/or magnetic fields. Just as a great variety of ion sources exist, several types of mass analyzers have been developed using either electric fields or a serial combination of magnetic and electric fields for the sorting of ions according to their m/z . **Table 2.7** lists the major categories of mass analyzers according to their ion separation processes. Scanning mass analyzers transmit the ions of different masses successively along a time scale. They are either magnetic sector instruments with an ion guide path in the magnetic field, allowing only the ions of a given m/z to go through at a given time, or quadrupole instruments. However, other analyzers allow the simultaneous transmission of all ions, such as the dispersive magnetic analyzer, the time-of-flight (TOF) mass analyzer and the trapped-ion mass analyzers that corresponds to the ion traps, the ion cyclotron resonance (ICR) or the orbitrap instruments(only ICR and orbitraps have simultaneous detection of ions but these are not transmission type instruments).¹⁰⁶

Table 2.7. Common types of mass analyzers used in mass spectrometry and their principle of separation.¹⁰⁵

Type of Analyzer	Symbol	Principle of Separation
Time-of-flight	TOF	Velocity (flight time)
Quadrupole	Q	m/z (trajectory stability)
Ion trap	IT	m/z (resonance frequency)
Electric sector	E or ESA	Kinetic energy
Magnetic sector	B	Momentum
Fourier transform ion cyclotron resonance	FTICR	m/z (resonance frequency)
Orbitrap	OT	m/z (resonance frequency)

When describing and measuring the performance of a mass analyzer, five parameters are present including: i) mass range – the limit of m/z over which the mass analyzer can manipulate and separate ions, ii) scan speed – the rate at which the analyzer measures over a particular mass range, iii) transmission – the ratio of the number of ions reaching the detector and the number of ions entering the mass analyzer, iv) mass accuracy – the ability to measure the accuracy of the m/z provided by the mass analyzer (the difference that is observed between the theoretical m/z and the measured m/z), and v) resolution/resolving power – the ability of a mass analyzer to yield distinct signals for two adjacent ions where a measurable m/z difference exists.¹⁰³ More detailed explanation of these parameters with respect to each type of mass analyzer can be found in literature or in reference text. The following section focuses on the type of mass analyzer used with the presented research, the linear ion trap.

2.6.3.1. The Linear Quadrupole Ion Trap (LIT) Mass Analyzer

The linear ion trap (LIT), also referred as a two-dimensional quadrupole ion trap (2D QIT), was initially developed as a collision cell of a triple quadrupole instrument.¹⁴⁵ An LIT consist of two conical lenses or electrodes (commonly referred to as endcaps) and one “donut-shaped” ring lens (ring electrode), **Figure 2.10** shows a representation of the LIT. In an LIT, ions transmitted from the ion source are held or trapped in the small interior volume between the front and back sections of the trap (the center section, **Figure 2.10**). When the voltages are lowered or raised on the entrance and exit sections, ions can pass into the trap, be stored for some period of time (usually μs), and then ejected to the

detector. The trap is usually operated in the mass selective stability mode where ions of a particular m/z are selectively and systematically ejected from the trap.

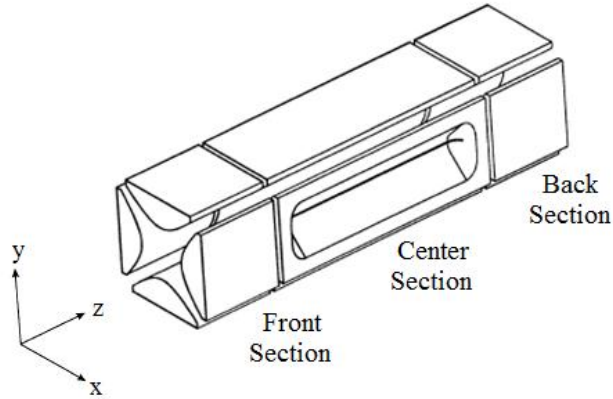


Figure 2.10. Schematic representation of a linear quadrupole ion trap mass analyzer. Reprinted with permission from reference.¹⁴⁶

Within the trap ions undergo a complex sinusoidal motion with the application of an oscillating radiofrequency (RF) potential to the outer sections of the trap. The storage of an ion in the trap depends on the value of the mass, m , and charge, z , of the ion, and the potentials applied on the entrance and exit sections. The ion trajectories and ejection can be described by solutions to derivations of the Mathieu equations a and q (Equation 2.4 and 2.5).¹⁰³

$$a_z = -2a_r = -16 \frac{zU}{m(r_0^2 + z_0^2)\omega^2} \quad \text{Equation 2.4}$$

$$q_z = -2q_r = 8 \frac{zV_{RF}}{m(r_0^2 + z_0^2)\omega^2} \quad \text{Equation 2.5}$$

where a_z and q_z are Mathieu equation functions that define a stable trajectory for which ions do not collide with the trap walls across a range of values for U (the direct voltage,

DC) and V_{RF} (the RF voltage). r_0 the radial distance from the center of the trap, z_0 the axial radius of the center section of the trap, and ω is the RF frequency.

An ion stability diagram can be constructed to define the coordinates (a , q) for which ions are stored in the trap (**Figure 2.11**). Ions possessing values of a and q that give both axial (along the z -axis, parallel to ion trap walls) and radial (oscillation in the xy plane) stability will remain trapped. For example, if the front and back sections are sufficiently positive with respect to the center section, cations become trapped in the center section. Once the ions are in the trap, they are dampened by collision with an inert gas, usually helium (added to a pressure of about 10^{-3} Torr, or 0.1 Pa; helium is also a collision activation agent), and fly along the z -axis while simultaneously oscillating in the xy plane owing to the application of an RF-only potential on the front and back sections (axial ejection, for the detection process). On the other hand, by manipulation of the voltages, ions of a specific m/z value can be expelled through the slits in the x direction (radial ejection, in the isolation/scanning process).¹⁰⁵

The LITs have one great advantage over three-dimensional quadrupole ion traps (3D QIT); a more than 10-fold higher ion trapping efficiency. This higher trapping capacity is combined with the ability to contain many more ions before space charge effects (this arises when there are too many ions which cause great repulsions of neighboring ions) occur owing to a greater volume of the trap. Moreover, the ion ejection and collection to the detector is almost 100% efficient for an LIT.

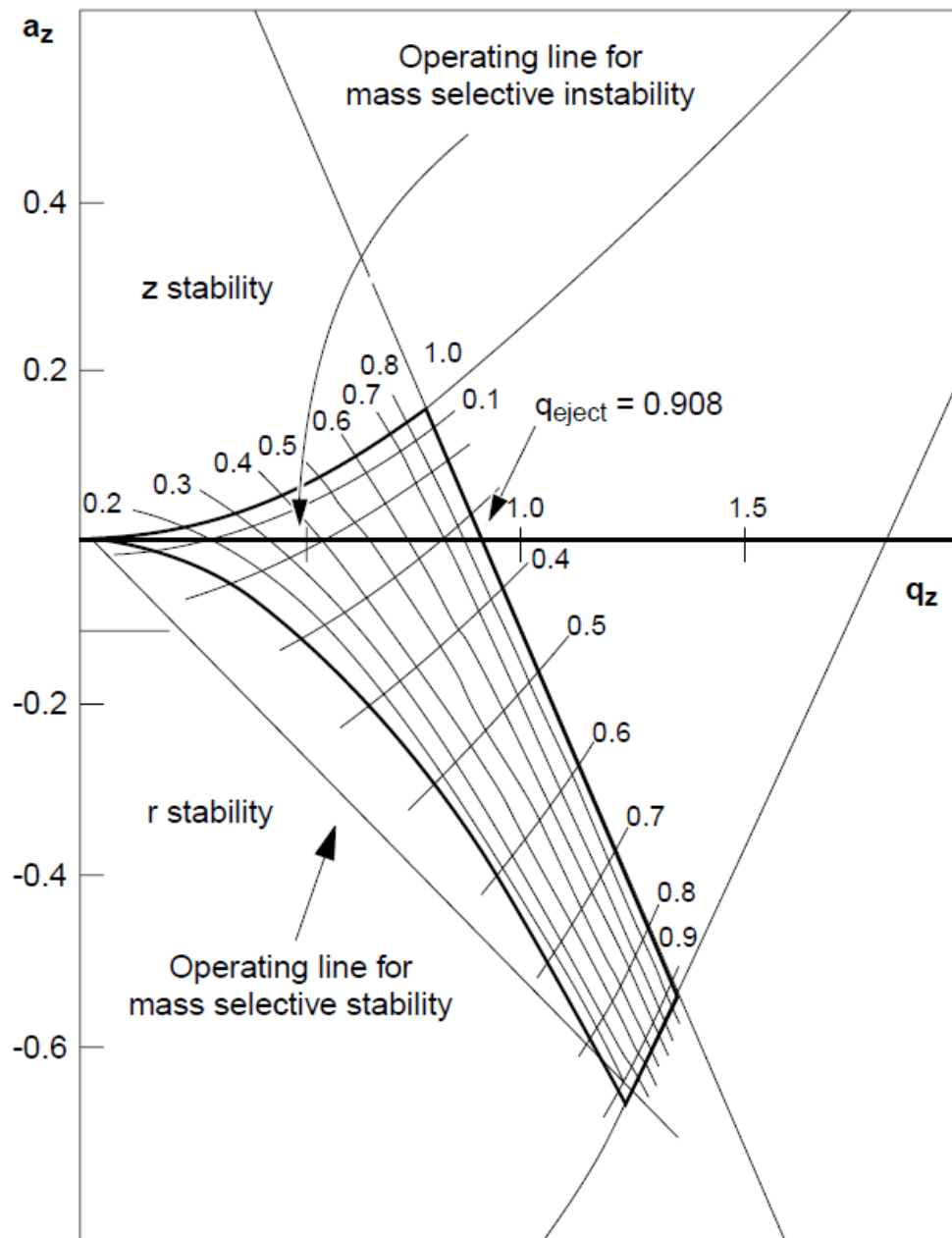


Figure 2.11. The Mathieu stability diagram for the quadrupole ion trap is shown. Ions are stable in the r - and z -direction if their Mathieu parameters a_z and q_z fall within the shaded area in the diagram. The common mode of mass analysis is the mass-selective instability scan where the RF potential is raised to increase the value of q_z to the instability point $q_z = 0.908$, while $a_z = 0$.¹⁴⁷

The other advantages of the LIT in chemical analysis include (1) high sensitivity, (2) compactness and mechanical simplicity in a device which is nevertheless capable of high performance, (3) ion/molecule reactions can be studied for mass-selected ions, (4) high resolution ($>10^6$ at $m/z >1000$) is accessible through slow scans, but mass measurement accuracy is relatively poor, and (5) ions of high mass/charge are accessible using resonance experiments.^{148, 149}

2.6.4. Tandem Mass Spectrometry

With the exception of hard ionization methods, all “soft” ionization methods lead to the formation of a molecular ion species with limited fragmentation.¹⁰³ While this is important in determining the molecular weight of the compound, it is not conducive with determining structural information of a compound. Tandem mass spectrometry (MS/MS) is a method where more than one stage of mass analysis occurs, typically to induce fragmentation of a selected ion of interest and then analyze the generated fragments. Structure elucidation can take place after interpretation of the fragmentation pattern of the selected intact ion.¹⁰⁵

A schematic representation of a tandem mass spectrometry experiment to achieve structure elucidation is shown in **Figure 2.12**. The ions generated from the ion source are directed to the first stage of mass analysis, MS1, (**Figure 2.12**) which is set to select and isolate only ions of a specific m/z ratio into a collision cell where dissociation/fragmentation of the ions occurs by bond cleavage through various energetic excitation processes. The ion selected for fragmentation is called the precursor ion and the ions generated through bond cleavage of the precursor ion are referred to as product

(fragment) ions. The second stage of mass analysis, MS2, is then scanned to transmit the products of fragmentation to the detector. A mass spectrum is generated with the m/z ratios of the fragments and the data obtained can determine the structural information of a compound.

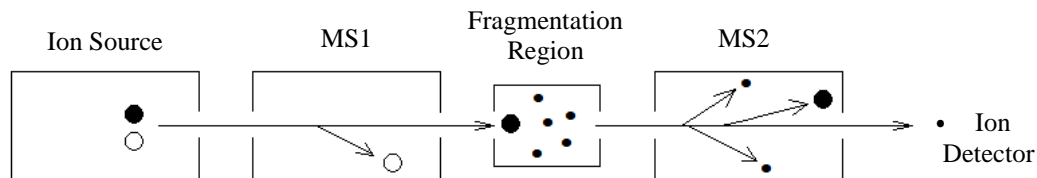


Figure 2.12. A schematic representation of a tandem mass spectrometry experiment, specifically, a product ion scan.

When the described MS/MS experiment occurs with multiple mass analyzers for every stage of mass analysis, the experiment is performed as “tandem in space”.¹⁵⁰ In contrast, the described linear ion trap mass spectrometer (specifically, a Thermo LTQ XL used in the presented research) allows all stages of mass analysis to be conducted within the same physical space and referred as “tandem in time”. For “tandem in time” with a linear ion trap, product ion scan experiment involves: (1) the transmission of ions from the ion source into the ion trap where their exit is prevented by the voltages applied to the endcaps of the ion trap. (2) selective isolation of the precursor ions by ramping the RF voltage of the ion trap above and below a particular value to store ions of a specific m/z . (3) applying a resonance excitation RF voltage to the endcaps to induce faster and more extensive ion trajectories of the selected precursor ions. If fragmentation of the selected precursor ion is desired, collision activation with a collision gas (typically helium) to increase internal energy will induce bonds to break to generate product ions. This

process is termed collision-induced dissociation (CID), also known as collision-activated dissociation (CAD). (4) Finally, lowering the voltage applied to the endcaps, with simultaneous ramping of the RF voltage applied to the ring electrode, will eject the remaining precursor and fragment ions to the ion detector.¹⁰³ Ion traps can also allow multiple stages of mass analysis and dissociation to be carried out in the so-called MSⁿ experiments (e.g. MS³ equivalent to three separate stages of mass analysis and so on). As many as ten stages ($n = 10$) of tandem mass spectrometry have been performed on commercial instruments.¹⁵¹

2.6.5. Ion Detection

When ions pass through the mass analyzer, they must be detected and transformed into a usable signal by a detector to generate a mass spectrum. A detector is able to generate an electric current that is proportional to the incident ions. While many types of detectors exist,¹⁵² the choice of a detector mainly depends on the design of the instrument and the analytical application that will be performed.

For the utilized mass spectrometer, the ion detection system includes a conversion dynode and an electron multiplier. A set of ion detection systems is located on opposite sides of the linear ion trap so collection efficiency is approximately 100% when ions are ejected from the trap. The conversion dynode is a concave metal surface located at a right angle to the ion beam. The ions are attracted to the conversion dynode by holding a positive potential for negative ions and a negative potential for positive ion detection. Once an ion strikes the surface of the conversion dynode, secondary particles (typically electrons) are produced. The curved surface of the conversion dynode focuses these

secondary particles and the voltage gradient accelerates them into the electron multiplier. Secondary particles from the conversion dynode strike the inner walls of the electron multiplier cathode with sufficient energy to eject electrons. The ejected electrons strike the inner surface of the cathode further up, which creates a cascade of even more ejected electrons. The final result is a measurable current at the anode. The current collected by the anode is proportional to the number of secondary particles striking the cathode.¹⁵³ The current that leaves the electron multiplier via the anode is recorded by the data system. Because of the off-axis orientation of the ion detection system relative to the mass analyzer, neutral molecules from the mass analyzer tend not to strike the conversion dynode or electron multiplier and reduce noise from neutral molecules.

CHAPTER THREE

METHOD VALIDATION AND OPTIMIZATION FOR SUGAR ANALYSIS

3.1. INTRODUCTION

The main objective of this research was to develop, optimize, and validate a simple, high throughput, and rapid method for the detection and quantitation of sugars extracted from switchgrass. In this study, DART was used as the analytical method for achieving this objective. DART has been widely used in various fields, as stated in Section 2.6.2.3, because of its versatility in the wide range of compounds it can analyze. However, there is no published literature showing any application of DART for qualitative and quantitative analysis of sugars. The different sections that follow describe the experiments performed with sugar standards to optimize and proof the feasibility of DART in sugar analysis. The chapter ends with a demonstration of the application of the method for quantitation of sugars.

3.2. EXPERIMENTAL

3.2.1. Sample Preparation

Six-carbon sugars from the biomass feedstock used were the compounds of interest. Since cellulose is the major component of switchgrass, glucose, a monomer unit of cellulose was used for the optimization and validation processes. Little to no sample preparation is the main advantage of DART. Therefore, a section dedicated to specific

sample preparation procedures was not necessary. Moreover, this chapter describes the development of the method. For this reason, sugar standards were used.

3.2.2. Reagents and Chemicals

The sugar standard used was D-(+)-glucose (hereafter referred as glucose), m/z 180. Glucose, $C_6H_{12}O_6$, (**Figure 3.1, b**) is by far the most common carbohydrate in nature. It is classified as a monosaccharide, an aldose, a hexose, and is a reducing sugar. It is also known as dextrose, because it is dextrorotatory (meaning that as an optical isomer it rotates plane polarized light to the right, as shown by the + sign above, and also is an origin for the D designation. In plants glucose is synthesized by chlorophyll using carbon dioxide from the air and sunlight as an energy source. Glucose is further converted to cellulose or starch. 99% glucose was purchased from Sigma-Aldrich (St. Louis, MO, USA). An internal standard was required for quantitation and calibration experiments. D-glucose-6,6-D₂ (hereafter referred as deuterated glucose), $C_6D_2H_{10}O_6$, was selected as the internal standard. Deuterated glucose (Figure 3.1, a), m/z 182, was selected because of two main reasons: (1) deuterated glucose is ionized in a similar fashion as glucose, and (2) the chemical structure of deuterated glucose is similar that of glucose except for the two deuterium atoms attached to carbon number 6. This causes a shift of two mass units more than glucose. Deuterated glucose (98%) was also purchased from Sigma-Aldrich (St. Louis, MO, USA).

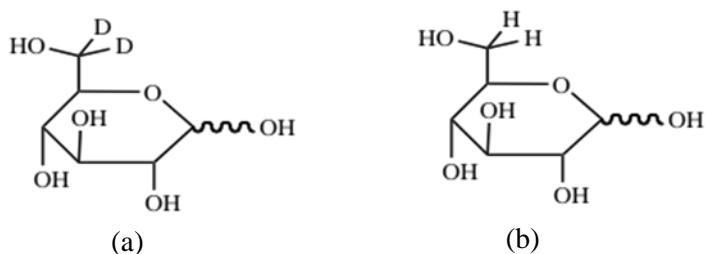


Figure 3.1. The molecular structures of (a) deuterated glucose and (b) glucose.

HPLC-grade methanol was purchased from Thermo Fischer Scientific (Fair Lawn, NJ, USA). Ultra-pure water (18.0 M Ω) was produced in-house with a NANOpure Ultra Water Purification System (Barnstead/Thermolyne Inc., Dubuque, IA, USA). All the chemicals and reagents were used without further purification.

3.2.3. Sugar Standards Preparation

Glucose and deuterated glucose standard stock solutions were prepared and stored in a refrigerator at temperature below 10 °C when not in use to prevent decomposition that may occur at room temperature. Working solutions were prepared from these stock standards ranging from 5.00×10^{-6} to 5.00×10^{-3} M, depending on the specific experiments performed. Initially, the working standard solutions were prepared from ultra-pure water. However, the solvent was later on changed to a mixture of methanol/ultra-pure water (1:1, v/v) (due to production of a higher signal when methanol/water was used, data not shown). The mass of each sugar standard was weighed out on a microbalance (Denver Instrument Co., Arvada, CO, USA) which had the ability to measure micrograms to 4 decimal places. Mass measurements were done to prepare a 1.00×10^{-2} M solution of glucose (180.16 g/mol) and deuterated glucose, (182.15 g/mol)

according to Equations 3.1 and 3.2 respectively, (deuterated glucose is designated d-glucose in Equation 3.2) with the only difference being the change in the molar mass. Each sugar standard was measured depending on their degree of purity. 0.1820g and 0.1859g of glucose and deuterated glucose were weighed, respectively. The granules were dissolved in ultra-pure water and made up to 100 mL in a volumetric flask. The reason for using 0.99 and 0.98 in the equations was to account for the purity level of the sugar standards stated above.

$$0.1 \text{ L} \times \frac{0.01 \text{ mole glucose}}{1.0 \text{ L}} \times \frac{180.16 \text{ g glucose}}{1 \text{ mole glucose}} \times \frac{100}{99} = 0.1820 \text{ g} \quad \text{Equation 3.1}$$

$$0.1 \text{ L} \times \frac{0.01 \text{ mole d-glucose}}{1.0 \text{ L}} \times \frac{182.17 \text{ g d-glucose}}{1 \text{ mole d-glucose}} \times \frac{100}{98} = 0.1859 \text{ g} \quad \text{Equation 3.2}$$

When working standard solutions were needed, the stock solutions were brought out of the refrigerator, shaken for a few seconds, and then allowed to equilibrate to room temperature. For initial peak identification and optimization experiments 1.00×10^{-4} M glucose standard working solutions were prepared in triplicate from the stock solution. The internal standard was prepared the same way. However, for calibration experiments, various concentrations of working standard solutions were prepared in methanol/water (1:1, v/v). The following sets of standards, in increasing order were prepared: 1.00×10^{-5} , 4.00×10^{-5} , 6.00×10^{-5} , 1.00×10^{-4} , 4.00×10^{-4} , 6.00×10^{-4} , 1.00×10^{-3} , 2.00×10^{-3} , 3.00×10^{-3} , and 5.00×10^{-3} M. These solutions were prepared to contain 4.00×10^{-5} M of the internal standard. **Table 3.1** shows the initial and final concentrations of standard solutions prepared. These standards were prepared to determine the dynamic linear range

for the sugar standards. The working solutions were prepared by measuring out the specific volume of glucose/deuterated glucose using disposable plastic micropipettes. The highest concentration prepared was 5.00×10^{-3} M and the lowest was 1.00×10^{-5} M. The concentration of the internal standard was the same (4.0×10^{-5} M) for each of the samples prepared.

Table 3.1. Show how the working standard solutions prepared from the stock standard solution to create final concentrations for the determination of the dynamic linear range.

Glucose Concentration (M)			Deuterated Glucose Concentration (M)		
Initial	Volume (μ L)	Final	Initial	Volume (μ L)	Final
1.00×10^{-2}	500	5.00×10^{-3}	1.00×10^{-2}	40	4.00×10^{-4}
1.00×10^{-2}	300	3.00×10^{-3}	1.00×10^{-2}	40	4.00×10^{-4}
1.00×10^{-2}	200	2.00×10^{-3}	1.00×10^{-2}	40	4.00×10^{-4}
1.00×10^{-2}	100	1.00×10^{-3}	1.00×10^{-2}	40	4.00×10^{-4}
1.00×10^{-2}	60	6.00×10^{-4}	1.00×10^{-2}	40	4.00×10^{-4}
1.00×10^{-2}	40	4.00×10^{-4}	1.00×10^{-2}	40	4.00×10^{-4}
1.00×10^{-2}	10	1.00×10^{-4}	1.00×10^{-2}	40	4.00×10^{-4}
1.00×10^{-2}	6	6.00×10^{-5}	1.00×10^{-2}	40	4.00×10^{-4}
1.00×10^{-2}	4	4.00×10^{-5}	1.00×10^{-2}	40	4.00×10^{-4}
1.00×10^{-2}	1	1.00×10^{-5}	1.00×10^{-2}	40	4.00×10^{-4}

The working standard solutions were placed in 1.5 mL clear screw septum vials using micropipettes as follows: 4.00×10^{-5} M of the internal standard was placed in each vial. Then a specified volume of glucose is added depending on the desired concentration (**Table 3.1**). The vial was then filled with the solvent [methanol/water (1:1, v/v)] to a final volume of 1.0 mL. The samples were then shaken for a few seconds to ensure even

mixing of the vial's content and were placed into a sample holding rack ready for analysis.

3.3. INSTRUMENTATION

The instrument used in this study was an LTQ XL linear ion trap (Thermo Scientific, San Jose, CA, USA) mass spectrometer. The fundamentals of the operation of a linear ion trap are described in Section 2.6.3.1. The LTQ XL was either interfaced to a DART ion source or an ESI source. The ESI source was only used for tuning and calibration of the mass spectrometer whereas the DART ion source was used for the analysis. The tuning and calibration of the mass spectrometer depends on the type of samples being analyzed. The DART ion source parameters were also a function of the analytical samples. This section describes these instrumentation and their parameters.

3.3.1. Direct Analysis in Real Time (DART[®]) Ion Source

The DART source was purchased from IonSense Inc. (Saugus, MA, USA). The specific model of the DART source used was referred to as the DART[®]SVP (Standardized Voltage and Pressure) ion source, hereafter referred to as the DART source. The ion source is covered by cylindrical metal casing enclosing the discharge glow chamber with electrodes and a heater. Towards the opening of the ion source is a steel casing with a conical shape and a ceramic tube is connected to the end of the cone, which is the opening of the ion source. The heater is enclosed in this cone-shaped casing. Heated gaseous metastables are released from the ion source through an opening with a grid held in place by the ceramic tube.

On the other side of the ion source is an adapter flange. The adapter flange is used to mount, support and align the DART source in place. A ceramic tube which is in line with the opening of the DART source is screwed to a circular opening at the center of the flange. The ionizing gas that comes out of the source is directed into the ceramic tube attached to the adapter flange. A metallic base connects the DART source and the adapter flange. The side of the adapter flange facing away from the DART source also serves as the interface of the source to the mass spectrometer. When the DART source is mounted on the mass spectrometer, a small hollow space exists between the adapter flange and the mass spectrometer inlet. A rubber tubing is connected to a built-in valve on the adapter flange. The other end of tubing is connected to a small membrane pump (Vacuubrand, Wertheim, Germany) which is used to create a partial vacuum between the Vapur[®] flange and the mass spectrometer inlet. A movable linear rail, which is the sample holding system, is connected to the metal block holding the adapter flange and the DART source. On the rail is a rectangular metal block with 12 holes in it which are used to hold the Dip It[®] tips in place. A schematic diagram of the DART ion source is shown in **Figure 3.2**.

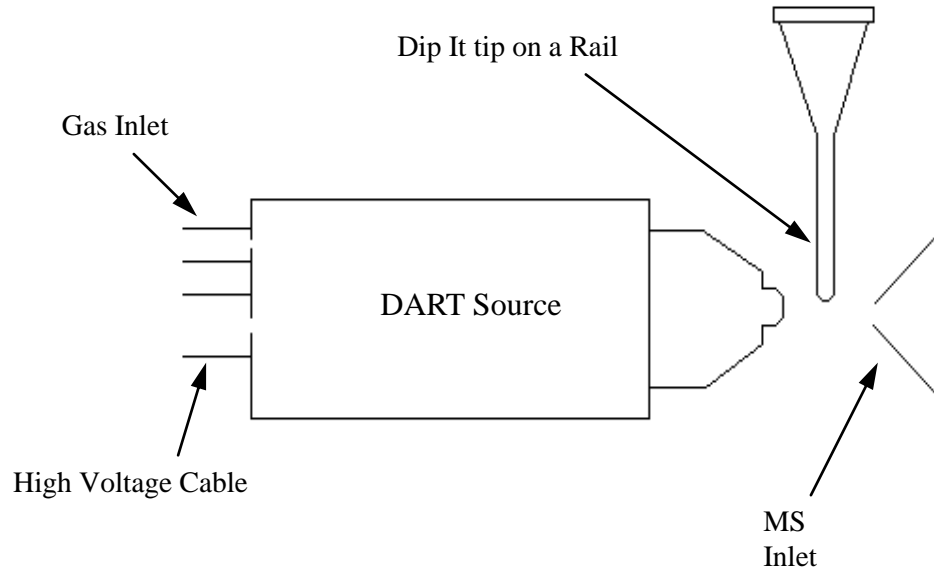


Figure 3.2. A schematic showing the DART ion source set up. The sample is spiked at the tip of the glass tip placed on a movable rail (not shown) which moves the sample between the source and MS inlet.

Operational control of the DART source is completed by using the SVP controller box (referred here as the controller). The controller is the software “management center” for the DART source. The flow on nitrogen and helium gases is regulated by the controller. Output and input cables for the gasses, a voltage cable, and a linear rail control cable are connected to the controller. The other ends of these cables are connected to the end of the DART source facing away from the mass spectrometer. An Apple iPod touch is used to operate the DART source. It is the user interface for the DART SVP system and has in-built software for the DART SVP operation. It is used for all the operations of the DART source such as temperature and voltage regulation, manipulation of the linear rail, setting up an analytical method, selecting the ionization mode, turning on/off of the DART source, etc. The iPod operates with a wireless Wi-Fi connection to the controller.

The following instrument settings were those recommended by the manufacturer and all parameters were measured using the DART SVP interface software. Optimization of the DART source parameters for sugar analysis was performed to determine the optimum conditions for obtaining the highest signals with little fragmentation. Unless otherwise noted, the DART source settings were: positive ion mode; nitrogen/helium gas pressure: 80 psi; gas temperature: 450°C; discharge needle voltage, +1.5 kV; and grid electrode voltage, 200V. These values are the optimum conditions for the DART source for the experiments performed in this study; their optimization is discussed in Section 3.4. High purity nitrogen (99.998%) was used as the standby gas and the gas was automatically switched to high purity helium (99.998%) in run mode.

3.3.2. The LTQ XL[®] Linear Ion Trap Mass Spectrometer

An LTQ XL[®] linear ion trap mass spectrometer (Thermo Scientific, San Jose, CA, USA) was used to obtain the mass spectra of all the compounds analyzed. The mass range of the mass spectrometer was between m/z 50 to 2000. Even though it is not a high resolution spectrometer the mass spectra were obtainable up to 2 decimal places. All data analysis and peak integration was accomplished through the user friendly Thermo Xcalibur software. The software was used to view and upload the data, either in form of mass spectra, chromatograms, or both. Before any analysis was, the mass spectrometer was tuned and calibrated using a standard procedure explained in the following section.

3.3.3. Calibration and Tuning of the Mass Spectrometer

In order to optimize the performance of data acquisition on the LTQ XL[®] mass spectrometer, tuning and calibration was done. Tuning was done manually with a calibration solution to establish a stable spray of solution and to ensure that enough ions are detected to calibrate the MS detector. Before tuning and/or calibration are done, the DART ion source is removed and an ESI source is mounted on the mass spectrometer. It was not possible to do any tuning and/or calibration with the DART ion source.

Tuning and calibration involved a three step process. First, the mass spectrometer was tuned in ESI mode by infusing a calibration solution. In this step, automatic tuning procedure in Tune Plus (Xcalibur software) was used to establish a stable spray of ions into the spectrometer and to demonstrate that the transmission of ions into the MS detector is optimum. A calibration solution was infused into the mass spectrometer directly from a syringe pump at a steady rate of 5.0 $\mu\text{L}/\text{min}$ for several minutes. For tuning and calibration of the LTQ XL[®] mass spectrometer in the ESI mode, calibration was done as instructed by the instrument manual utilizing the manufacturer's calibration solution. The calibration solution (Pierce[®] LTQ ESI Positive Ion calibration solution) used consisted of caffeine, MRFA (L-methionyl-arginyl-phenylalanyl-alanine acetate monohydrate), and Ultramark 1621 (covered m/z range: 150 – 2000) in an acetonitrile/methanol/water solution containing 1% acetic acid (Thermo Scientific, Rockford, IL, USA). A peak at m/z 195, the mass-to-charge of caffeine, was chosen in the calibration solution. This peak was chosen because it was one of the ions in the calibration solution that was closest to the mass-to-charge ratio for the ion of interest in our analytes (e.g., m/z 198 for sugar samples).

Secondly, the mass spectrometer was calibrated in the ESI mode using the same calibration solution to automatically optimize its performance. The purpose of the calibration of the MS detector was to optimize the parameters that affect ion detection thus optimizing its performance. In this step, it was ensured that the calibration parameters complete automatic calibration successfully, which took about 45 minutes. Calibration parameters are instrument parameters whose values do not vary with the type of experiment. The calibration dialog box in the Tune Plus provided a readback of the status of the calibration parameters, both during the automatic calibration and when the calibration was complete.

The third step involves maximizing the detection of one or more particular ions (if necessary). This is done by optimizing the tune of the mass spectrometer detector with the analyte of interest in the ESI mode. A significant mass-to-charge ratio of the analyte of interest is chosen. This step was not performed in our study because the m/z of 195 for caffeine was closest to the mass-to-charge ratio for our ions of interest. Calibration was performed periodically, every one to three months, for optimum performance of the MS detector.

For a typical experiment, the mass spectrometer settings included: capillary voltage, 30 V; tube lens voltage, 100 V; capillary temperature, 200 °C. The ion optics settings were as follows: multipole 1 offset voltage, -4.5 V; multipole 2 offset voltage, -8.0 V; lens 1 voltage, -4.2 V; lens 2 voltage, -15.0 V; gate lens voltage, -35.0 V; and front lens voltage, -5.25 V. The detector voltage was set to +15 kV. The mass range in which the mass spectra were acquired was m/z 50 – 400. Tandem experiments were done when the elemental composition of a compound were necessary. Fragmentation of

selected precursor ions was possible in the ion trap with collision–induced dissociation (CID) of 30.0 normalized collision energy, by colliding the precursor ion with helium atoms. The ion trap collision cell was supplied with ultra–high purity helium gas (99.999% purity).

3.3.4. Sample Introduction

After samples were prepared and ready for analysis, the DART source is powered on and set at the required temperature using the iPod touch interface. A DART source file in the Xcalibur software was opened for data collection. Glass Dip It[®] (purchased from IonSense, Saugus, MA, USA) tips were used for sample introduction. A typical experiment would entail spiking a sample on the tip of a glass Dip It[®] tip (hereafter referred to as a glass tip) placed on a movable linear rail which could move in a left-to-right direction and vice versa. **Figure 3.2** (Section 3.3.1) shows a simplified schematic view of the sample introduction system. The orientation of the DART source was such that the exit of the DART source was in line with the ceramic tube leading to the Vapor adapter flange hyphenated with the inlet of the spectrometer. The linear rail was a 12 Dip It[®] block that ran between the DART source and the ceramic tube.

In all the experiments performed, 1.0 μL of a given sample solution was pipette–deposited on the tip of the glass tip which was secured on a block engineered to hold the glass tips on the movable rail whose movements can be set at a specific speed. The rail holding the glass tips with samples would then move from left to right at a constant speed such that the sample on the glass tips came into contact with the helium gas stream from the DART source outlet, producing a signal as it moves across the ionization region. The

glass tips moved perpendicular to the gas stream but were adjusted (by adjusting the height of the linear rail block) to ensure that the gas stream was not entirely blocked by the glass tips. For optimization and quantitation measurements, a constant speed of 0.5 mm/s (unless otherwise stated) was maintained for all samples analyzed with the Dip-It tip rail system. The samples could also be introduced manually without using the rail by hand (with the sample placed on the glass tip) or by use of an adjustable tweezers (for solid samples). Manual sample introduction was not performed because of the errors involved in placing the sample at the right position.

3.4. METHOD VALIDATION AND OPTIMIZATION

3.4.1. General Spectral Appearance of Sugar Standards

Before validation and optimization experiments were performed, it was necessary to carry out initial analysis of sugar standards to determine the mass spectral peaks that are produced. From the sugar standard stock solutions, 1.00×10^{-4} M of both glucose and deuterated glucose working solutions were prepared in 1.5 mL clear glass vials. The DART ion source was run in the positive ion mode and the temperature, gas pressure, and voltage were set at 450 °C, 80 psi, and 200 V, respectively. These temperature and voltage values were chosen randomly whereas the gas pressure was the value recommended by the DART source manufacturer. The mass spectrometer settings were as explained previously.

After the sugar solutions equilibrated to room temperature and the glass tips set on the linear rail, 1.0 μ L of glucose and deuterated glucose solution was pipette-deposited on the tip of the glass tip. The speed of the linear rail was set at 1.0 mm/s (chosen

randomly). The data was acquired separately for each standard solution. The mass spectra obtained for glucose and deuterated glucose are shown in **Figures 3.3** and **3.4**, respectively. Several runs were done (data not shown) to confirm that the same peaks were formed.

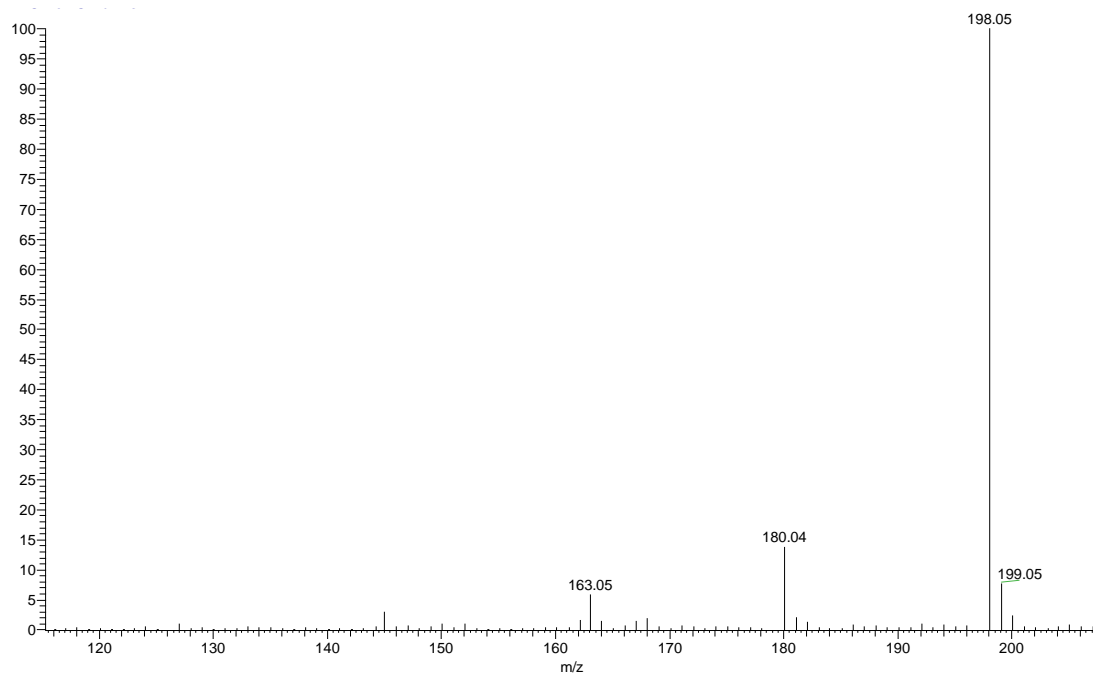


Figure 3.3. A typical positive ion mode DART-LIT mass spectrum generated from 1.00×10^{-4} M glucose standard.

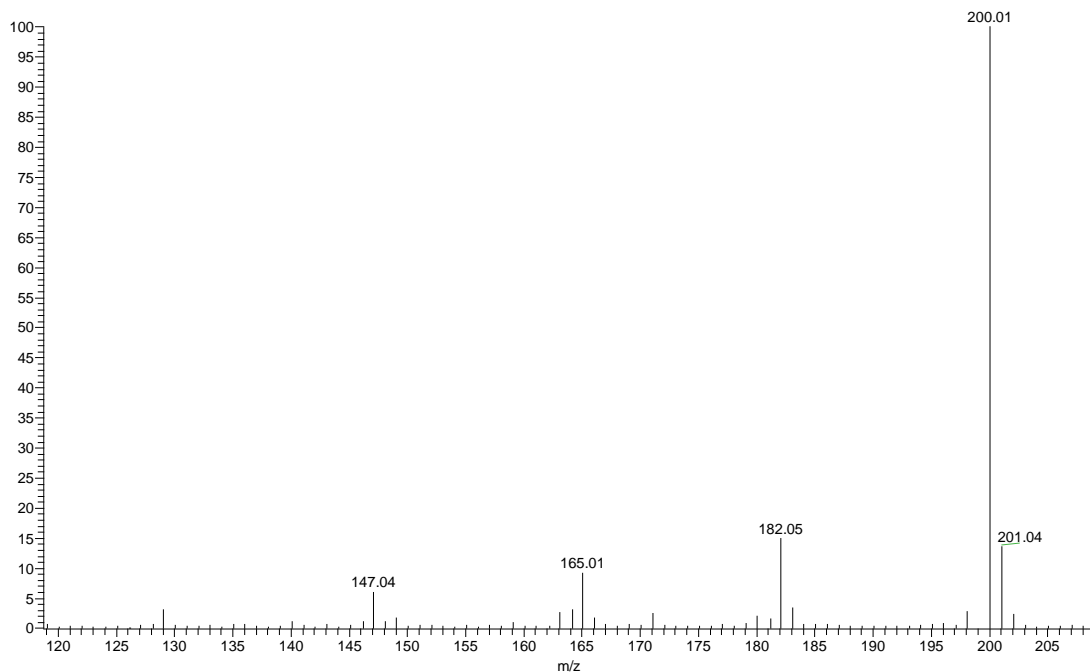


Figure 3.4. A DART-LIT mass spectrum generated from 1.00×10^{-4} M deuterated glucose standard.

The DART-LIT mass spectrum of a 1.00×10^{-4} M glucose standard solution generated after introduction into the DART ionizing gas stream, **Figure 3.3**, primarily formed a base peak at m/z 198 and small peaks (less than 20% relative abundance (RA)) at m/z of 163 and 180. Glucose has a nominal molecular mass of 180 and therefore the peak formed at m/z 180 may be thought to be that of a molecular ion, M^+ , in the first instance. However, our studies have shown that the peak at m/z 180 may not a molecular ion. The peak at m/z 198 is actually an ammonium adduct of glucose, $[M + NH_4]^+$, and the peak at m/z 180 is a loss of a water molecule from the ammonium adduct forming $[M + NH_4 - H_2O]^+$. The same pattern was also observed for deuterated glucose, **Figure 3.4**, (with a nominal molecular mass of 182); a base peak at m/z 200, $[M-d_2 + NH_4]^+$ and another peak at m/z 182, $[M-d_2 + NH_4 - H_2O]^+$, in which a molecule of water is lost ($-d_2$

is inserted in the deuterated glucose ion to distinguish it from glucose). The mass shift is stemming from the two deuterium atoms on the deuterated glucose molecule.

Studies shows that ammoniated adducts are commonly observed in polar compounds containing carbonyl functional groups such as acids, esters, ketones, and peroxides.¹⁵⁴ Simple sugars such as glucose can exist in aqueous solution in different anomeric forms in which cyclic hemiacetals and an open carbonyl form exist in equilibrium. An interesting aspect of the ammonium adduct is that formation occurred without the introduction of an ammonia dopant that has been reported necessary to modify DART ionization for other compounds.¹¹⁴ The other observed peak at m/z 180 (or m/z 182 for deuterated glucose) could either be attributed to the formation of a radical molecular ion through Penning Ionization¹⁵⁵ or a fragment of the glucose ammonium adduct. Tandem mass spectrometry of the peak at m/z 198 produced fragmentation profiles with a base peak at m/z 180 (**Figure 3.5**) suggesting this peak is formed through fragmentation (loss of water) rather than ionization of the innate molecule. Further fragmentation (MS^3) of the peak at m/z 180 produced a base peak at m/z 163 and another peak at m/z 145, **Figure 3.5** (insert), which could be attributed to ammonia and then a subsequent water loss, respectively.

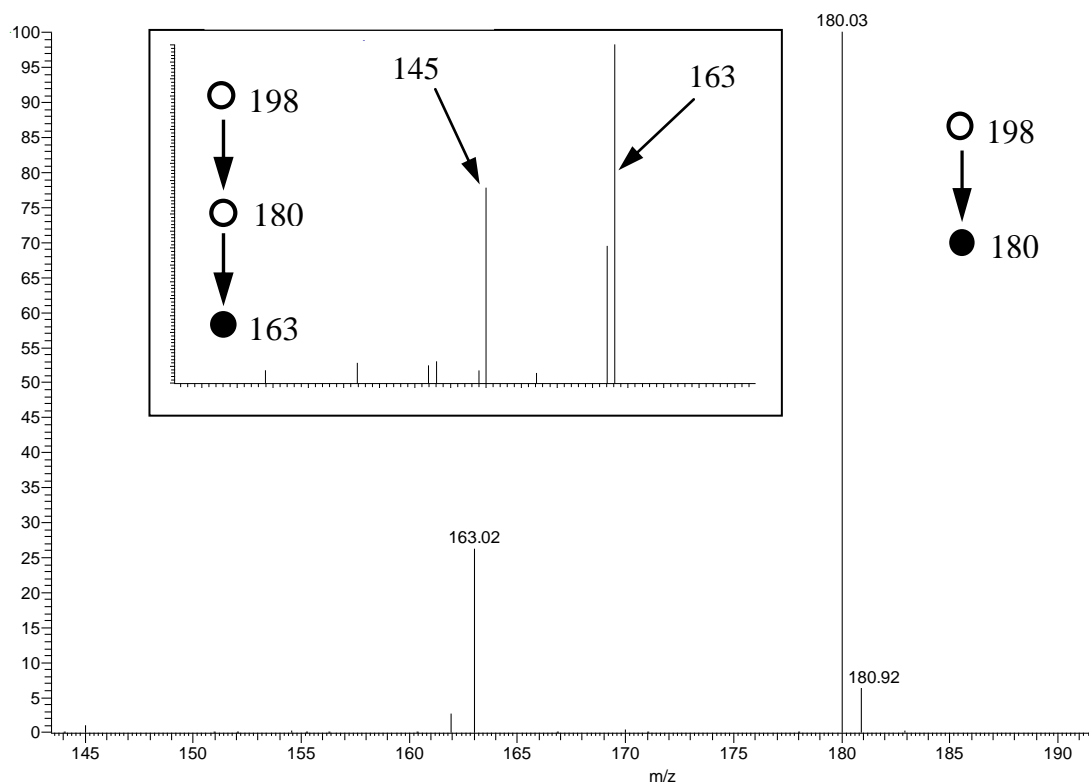


Figure 3.5. Tandem mass spectrum (MS/MS) of the precursor ion of m/z 198 generated from glucose standard by the DART source. The insert is the MS³ spectrum of m/z 180 generated (through fragmentation of m/z 180).

The ion designations for the adduct species and fragmentation are supported by accurate mass measurements using a DART JEOL AccuTOFTM (with in-source fragmentation) experimentally determined at an independent laboratory as shown in **Table 3.2**. The theoretical mass was calculated from provided exact mass isotopes.¹⁰⁶

The sensitivity of DART, as with any ambient ionization techniques, is a function of the ion yield and the ion transmission efficiency from the ambient pressure region into the vacuum regions of the mass spectrometer. Reported factors that have influenced ion transmission in DART include molecule ionizability, helium gas flow rate, gas temperature, the distance from the DART outlet to mass spectrometer inlet, and the

DART exit grid voltage.¹²² To validate DART-LIT for the analysis of sugars, these factors must be optimized so that a high instrument signal can be obtained for these specific samples. The optimization of these factors is discussed in the following sections.

Table 3.2. Comparing theoretical and experimental masses supported ion designations of glucose products. An independent laboratory acquired the accurate mass measurements reported for the experimental masses with a DART coupled to an AccuTOFTM. ^aM for glucose, ^btheoretical mass calculated from exact mass isotopes,¹⁰⁶ ^cexperimental mass average with standard deviation (n = 4). ^d difference between theoretical mass and experimental mass average.

Ion Designation ^a	Theoretical Mass (<i>m/z</i>) ^b	Experimental Mass (<i>m/z</i>) ^c	Difference (<i>m/z</i>) ^d
[M + NH ₄] ⁺	198.0978	198.0975 ± 0.0008	0.0003
[M + NH ₄ - H ₂ O] ⁺	180.0872	180.0869 ± 0.0006	0.0003
[M + NH ₄ - H ₂ O - NH ₃] ⁺	163.0606	163.0611 ± 0.0002	-0.0005
[M + NH ₄ - 2H ₂ O - NH ₃] ⁺	145.0501	145.0519 ± 0.0001	-0.0018

3.4.2. Experimental Design Optimization

This section deals with optimization of instrument parameters, that is optimization employed to provide the maximum amount of instrument signal for the samples being analyzed. A review of optimization in relationship to experiments in four aspects has been reported by Haftka et al.¹⁵⁶ These aspects include the use of optimization for designing efficient experiments (called “analytical optimization”), the use of experiments to perform optimization (called “experimental optimization”, the subject of this section), the use of techniques developed for experimental optimization in numerical optimization and eventually, the importance of experimental validation of optimization. The main parameters optimized were those related to the DART ion source such as gas temperature, exit grid voltage, linear rail speed, gas flow rate, and the distance from the

DART exit to the inlet of the mass spectrometer. Precision and linearity experiments will also be discussed as a validation of the optimized experimental parameters.

3.4.2.1. DART Gas Temperature

Among the parameters that affect the formation and transmission of ions in DART, the temperature of the ionizing gas (helium) is a significant factor. The following experiment was performed to determine the extent with which this parameter affects DART ionization. The DART source gas heater temperature was raised in increments of 50 °C from 200 °C to 450 °C (i.e., 200, 250, 300, 350, 400, and 450 °C). The DART source software was set such that the temperature could only be changed by 50 °C from one value to the next. All the other parameters were held constant, i.e., the grid voltage was kept at 200 V, the linear rail speed was 1.0 mm/s, the helium gas pressure was 80 psi (recommended by the DART manufacturer), and the capillary ion transfer tube in the mass spectrometer orifice was maintained at 200 °C (this was the temperature determined to give the least fragmentation of the sugar standards being analyzed). A 1.00×10^{-4} M glucose working standard solution was analyzed by spiking 1.0 μL of the sample on the tip of the glass tips. The purpose of this experiment was to determine the appearance of the mass spectra observed in relation to the background at the selected temperature. The same sample was analyzed three times at the specific temperature to determine the consistency of the mass spectra observed. The highest temperature applicable for the DART ion source that could be used was 500 °C but was not used since it was the upper temperature limit for the source software.

Figure 3.6 shows DART-LIT total ion chromatogram (TIC) mass spectra for the glucose standards at various helium gas temperatures. The peak that was monitored is the glucose base peak at m/z 198. As the temperature was increased, the total signals observed increased including the signals of interest. At low temperatures, the background signals were higher and this made the signal for the sugar standards lower. At 200 °C, a signal was observed for the sugar standards but the background spectra were higher thus affecting the total signal intensity of the analyte. However, increasing the temperature caused the signal intensity for the sugar standards to increase while the background signals decreased. The greatest signal intensity was observed at a temperature of 450 °C.

The temperature values quoted here refers to set values in the software. The temperature readout in the DART software is from a thermocouple embedded in the ceramic heater, not in the gas stream. Therefore the actual gas temperature was lower than this readout and is a function of the heater core temperature, gas flow rate and heat capacity of the gas. The actual temperature where the sample was exposed to the ionizing helium gas stream has been observed to be lower through finite simulations of ion transport in an ambient DART-type metastable-induced chemical ionization source.¹⁵⁷

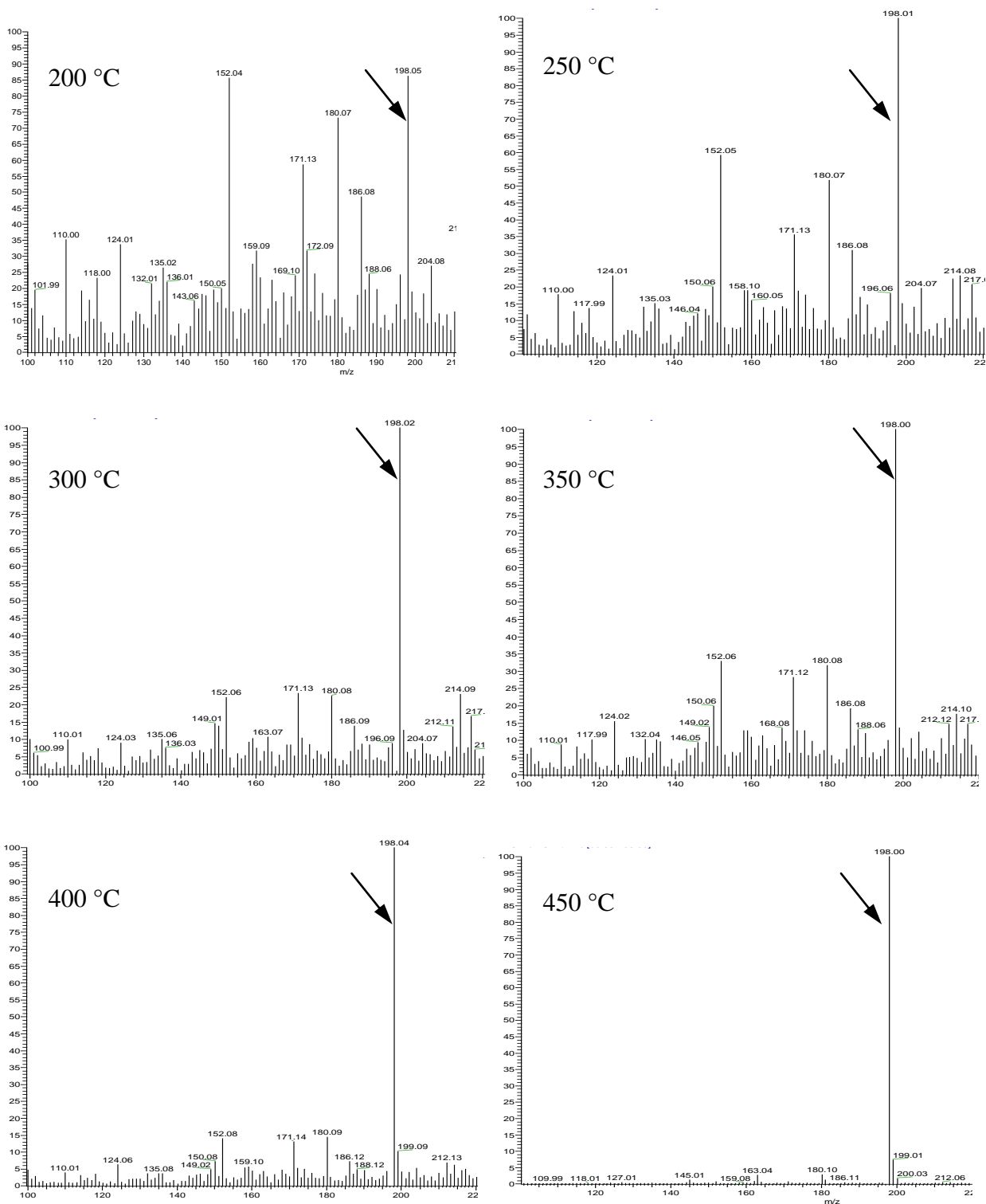


Figure 3.6. The TIC DART-LIT mass spectra generated from 1.00×10^{-4} M glucose standard at various helium gas temperatures (showing the 100–265 m/z range).

The effect of temperature was further verified and quantified by monitoring the peak area of the base peak (m/z 198). Three separate trials of three replicates of 1.0×10^{-4} M glucose standards were analyzed and their peak area (PA) was computed using the Xcalibur™ software. The average peak area was calculated for the three separate runs at each temperature, as shown in **Table 3.3**. **Figure 3.7** shows a plot of the average peak areas against temperature. It was observed that as temperatures increases, the signal intensity for the sugar standards increased and the greatest signal intensity was observed at a temperature of 450°C. This was chosen as the optimum temperature for analyzing samples in this study.

Table 3.3. Peak areas and signal-to-noise ratios for three replicates of 1.00×10^{-4} M glucose standards run three times.

Temperature (°C)	Peak Area (PA)				Signal-to-noise Ratio (S/N)			
	Trials				Trials			
	1	2	3	Average	1	2	3	Average
200	0	0	0	0	0	0	0	0
250	64116	98676	91519	84770.3	11	15	10	12
300	658047	868855	340448	622450	72	100	20	64
350	1213763	1172226	267466	884485	172	177	41	130
400	919837	1027423	1276846	1074702	121	130	150	133.7
450	1381658	1175708	1407598	1321655	173	119	270	187.3

The signal-to-noise ratio (S/N) was also computed for the peaks reported in **Figure 3.7** and a plot of the average S/N (**Table 3.3**) against temperature is shown in **Figure 3.8**. It is clear that at lower temperatures, the signal-to-noise (S/N) ratio of the sugar standards was lower and it increased as the temperature was raised. A high S/N ratio is required to differentiate the peaks of the analyte from the background.

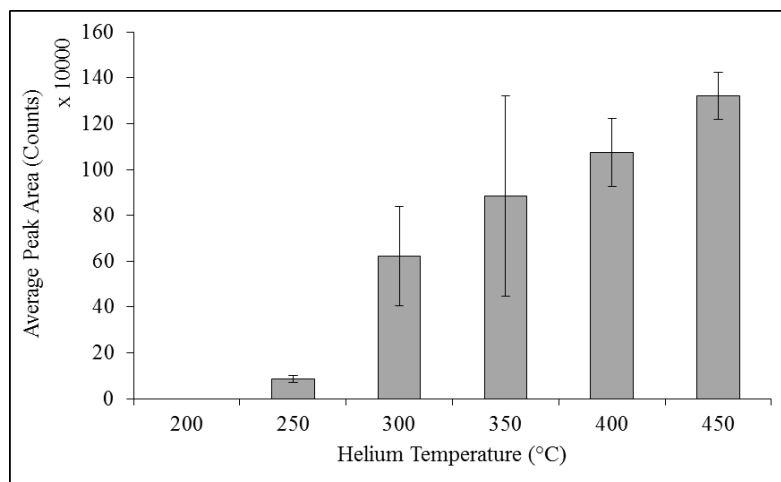


Figure 3.7. Average peak area (PA) of 1.00×10^{-4} M glucose standards analyzed at various ionizing gas temperatures ($n = 3$). The error bars indicate the standard deviation for the PA of each measurement.

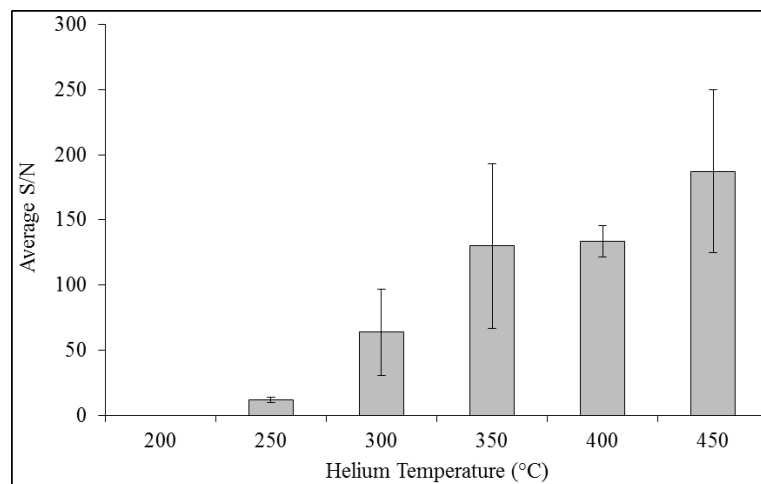


Figure 3.8. Signal-to-noise ratios (S/N) of 1.00×10^{-4} M glucose standards analyzed at different ionizing gas temperatures ($n = 3$). The error bars indicates the standard deviation for the S/N of each measurement.

Three observations have been previously reported with DART ionization:¹⁵⁸ (i) high gas temperatures accelerate sample drying and analyte thermal desorption rates, (ii) high temperatures causes samples to desorb quickly, resulting in signal loss if the spectral

acquisition rate is not high enough, and (iii) high gas temperatures could lead to sample charring on the glass tip surface, leading to irreversible sample degradation. From the optimization studies with the DART-LIT, the 450 °C seems to readily desorb the glucose from the glass tip without visible charring of sample. The charring was not a concern since of the diluted concentration and use of small volumes (1.0 µL) on the glass tips in the experiments.

3.4.2.2. Linear Rail Speed

The analytes were introduced into the ionization region using glass tips mounted on a software operated linear rail which is a component of the commercial DART-SVP ion source. The speed of the linear rail ranged from 0.2 mm/s to 10.0 mm/s. The speed with which the analyte passes through the ionization region and the time for interaction with the excited helium gas stream determines the number of ions formed by thermal desorption. To achieve optimal rail speed to ensure adequate sample interaction with the gas stream, a series of experiments with a 1.00×10^{-4} M glucose standard solution was performed at different rail speeds, ranging from 0.2 to 2.0 mm/s in increments of 0.5 mm/s (except with the initial 0.3 mm/s increment from 0.2 to 0.5 mm/s). The rail speeds used include 0.2, 0.5, 1.0, 1.5, and 2.0 mm/s.

The glass tips placed on the rail were applied with 1.0 µL of glucose and allowed to pass through the ionization region perpendicular to the helium gas stream. Three replicate standards were analyzed at a specific rail speed, each run five times and the peak areas of the base peak (m/z 198) were measured by mass-selecting the chromatogram which corresponds to the peak. For each run the peak area was computed

using the instrument software and the average peak area calculated. **Figure 3.9** demonstrates that the average peak area was observed to vary with the rail speed applied. A rail speed of 2.0 mm/s gave the least signal whereas the highest signal was observed when a rail speed of 0.2 mm/s was used. Longer residence time in the ionizing gas increases the probability for analyte molecules to reactively collide causing efficient ionization by causing substantial increase in ions produced that are detected by the mass spectrometer. Even though a speed of 0.2 mm/s produced the highest signal, a speed of 0.5 mm/s that also gave a relatively high signal was chosen for subsequent calibration experiments since analysis time was significantly reduced by at least two minutes for each batch of samples run.

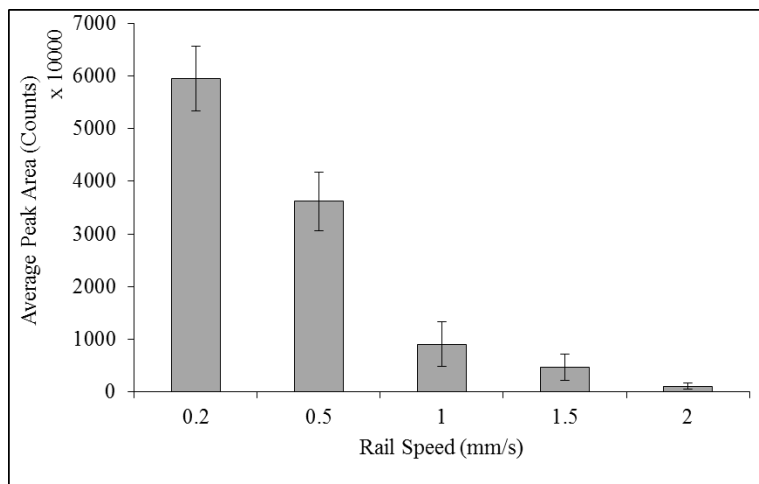


Figure 3.9. Average peak area of the base peak (m/z 198) produced from 1.00×10^{-4} M glucose standard solution at different linear rail speeds.

3.4.2.3. Helium Gas Flow Rate/Pressure

The helium flow rate is another parameter to consider when doing experiments with the DART source. Several reports on how the flow of the ionizing gas affects the

ionization in DART are found in literature. Helium has been the gas in use with major publications on DART application, even though the use of argon has also been reported.¹³⁷ Even though relatively high flow rates have been used before,¹¹⁴ our study shows that only minimal gas flow rates are necessary to ensure a constant flow of gas through the glow discharge region of the DART ion source. In this study the helium pressure was varied from 40 to 100 psi (the pressure was set at the gas tank regulator) in increments of 10 units to determine the optimum gas pressure. Three replicates of glucose standards were analyzed using the optimum gas temperature and rail speed described previously.

From the data obtained, it was observed that there were no major differences in the appearance of the mass spectra, including the background. However, the peak areas of the base peaks studied were found to fluctuate at different pressures. Minimal fluctuation was observed with a pressure of 60 psi. **Figures 3.10** and **3.11** show the variation in the average peak areas for the base peak of glucose standards at different helium pressures, as illustrated by the large error bars in **Figure 3.10**. A similar study¹⁵⁸ showed that increasing the flow rate increased the number of metabolites detected in a sample, but high gas pressures caused sample particle dispersion and may lead to the contamination of the mass spectrometer inlet when remaining solvents are pushed directly into the inlet. **Figure 3.10** shows that there are high variations in the average peak areas when high gas pressure is used (large error bars). This may be due to strong turbulence produce by high gas pressure which was also found to affects experimental reproducibility. **Figure 3.11** shows that the optimum helium gas pressure falls in the range of 55–65 psi. The assumption made in this experiment was that there was no software control on the gas

flow rate entering the DART ion source. However, we believe that the DART controller box regulates the gas flow rate entering the ion source. Therefore, when a high gas pressure is used, there may be a counterbalancing that takes place to ensure that the required flow rate is maintained. Due to the unconfirmed effect of the controller box on the gas flow rate, a gas pressure of 80 psi, recommended by the ion source manufacturer, was maintained for calibration and quantification experiments.

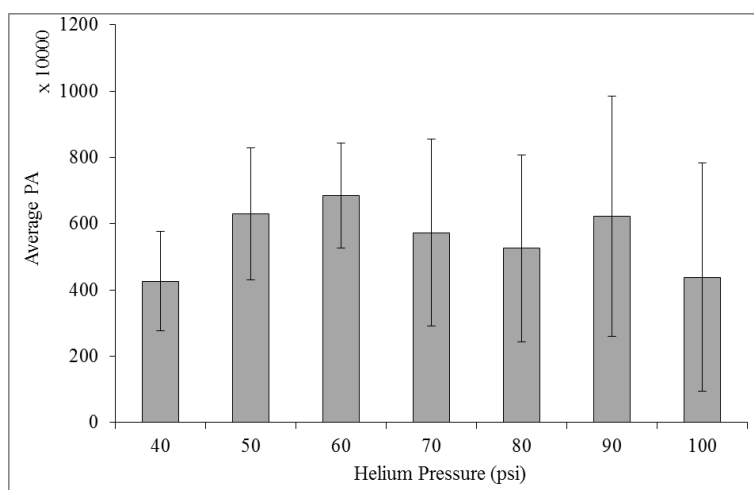


Figure 3.10. The average peak areas ($n = 5$) of 1.00×10^{-4} M glucose standards base peak (m/z 198) at different helium pressures. The large error bars indicates a high variability in the peak areas.

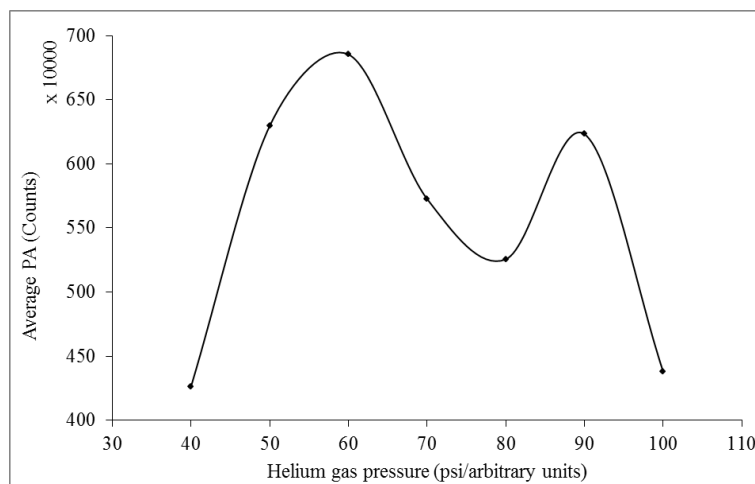


Figure 3.11. A line plot of the average peak areas of the base peak at different helium pressures.

The only advantage of using high gas flow rate/pressure is to speed up the transport of ions formed within the gas stream into the mass spectrometer. In this study, moderate gas pressure was used due to the configuration on the DART source which incorporated a small membrane pump. The DART adapter flange was connected to a small diaphragm pump which created a partial vacuum region just outside mass spectrometer inlet. This pumping system on the DART ion source improved ion transport from the ionization region into the mass spectrometer. The ions formed in the excited helium gas are drawn towards the partial vacuum region and channeled towards the inlet of the mass spectrometer. This configuration enables the DART user to operate at significantly reduced helium flow rates, while improving overall ion transmission into the spectrometer.¹⁵⁹ This reduces the consumption of the expensive helium gas.

3.5. METHOD PRECISION

The other important process in method development is to determine the reproducibility of quantification (or precision) of sugar standards. Once a method is established, it must be demonstrated that it is robust to give reliable, reproducible results from the instrument over time. The precision of an analytical method is the amount of scatter in the results obtained from multiple analyses of a homogeneous sample. To be meaningful, the precision study must be performed using the exact sample and standard preparation procedures that will be used in the final method. To validate the DART-LIT system as a method for glucose analysis, several experiments were performed to determine data reproducibility. Nine separate runs of 5.00×10^{-5} M glucose standard samples spiked with 4.00×10^{-5} M of the internal standard were performed. In **Figure 3.12**, the extracted ion chromatograms (XIC) using m/z 198 are shown for the nine separate glucose standards.

The observed peak height for the samples initially appears to have a high degree of variation. However, to validate the reproducibility of the method for quantitation purposes, a peak area ratio (PAR) was calculated. First, mass ranges of the analyte and internal standard were selected to obtain their XIC. The peak area for each XIC was computed using XcaliburTM software for both glucose (m/z 198), and deuterated glucose (m/z 200). The peak area ratio (PAR) was obtained by dividing the peak area of glucose by the peak area of deuterated glucose (Equation 3.3) and the data is shown in **Table 3.4**.

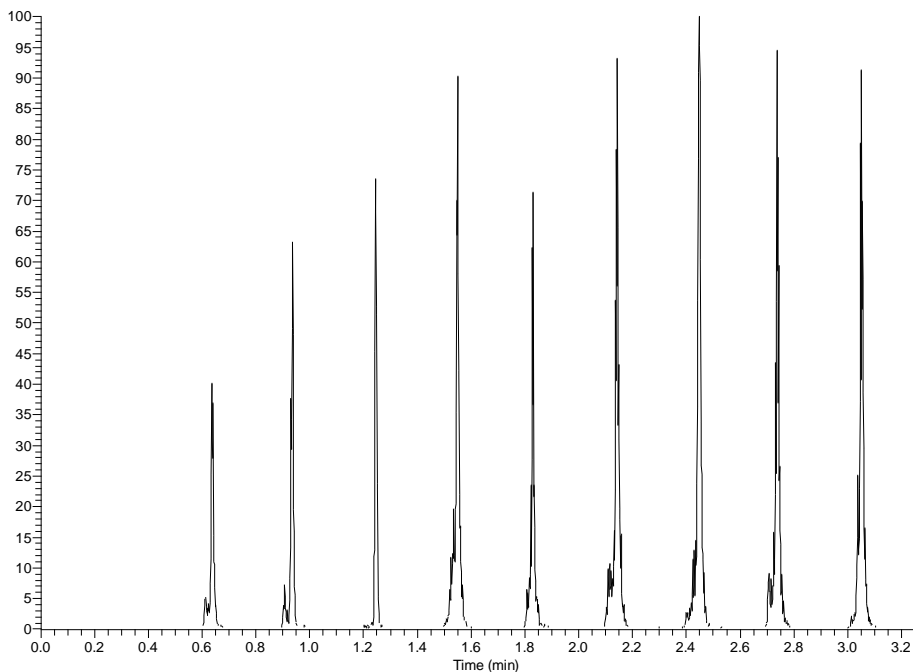


Figure 3.12. Reproducibility: Extracted ion chromatogram (m/z 198) for one trial where nine 5.00×10^{-5} M glucose standards spiked with 4.00×10^{-5} M of deuterated glucose were analyzed by DART-LIT.

In **Figure 3.13**, a plot of the calculated PARs for four trials (each trial contained nine standards) shows that a specific concentration of glucose compared to an internal standard have low levels of deviation. While a good amount of variation can be observed measuring the absolute peak area or peak height, see deviations in **Figures 3.7**, this variation can be dramatically reduced using an internal standard and calculating PARs with the DART ion source.

$$\text{PAR} = \frac{\text{Peak Area of Glucose (}m/z\text{ 198)}}{\text{Peak Area of Deuterated Glucose (}m/z\text{ 200)}} \quad \text{Equation 3.3}$$

Table 3.4. Peak area ratios of four trials of nine separate samples of 5.00×10^{-5} M glucose standards spiked with 4.00×10^{-5} M of internal standard. ^astandard deviation of the respective trials, ^bcoefficient of variance.

Peak Area Ratios (PAR) of <i>m/z</i> 198 and 200							
Trial 1		Trial 2		Trial 3		Trial 4	
1.1835		1.1032		1.1439		1.1896	
1.1831		1.1843		1.1635		1.1381	
1.1776		1.2043		1.1942		1.1535	
1.1757		1.1565		1.1565		1.1710	
1.1656		1.1427		1.1250		1.1644	
1.1696		1.1626		1.2001		1.1616	
1.1995		1.1957		1.1518		1.1701	
1.1921		1.1427		1.1832		1.1507	
1.1931		1.1574		1.1935		1.1727	
Average	1.8221	Average	1.1611	Average	1.1680	Average	1.1635
STD ^a	0.0113	STD	0.0310	STD	0.0261	STD	0.0149
CV ^b	0.95	CV	2.67	CV	2.23	CV	1.28

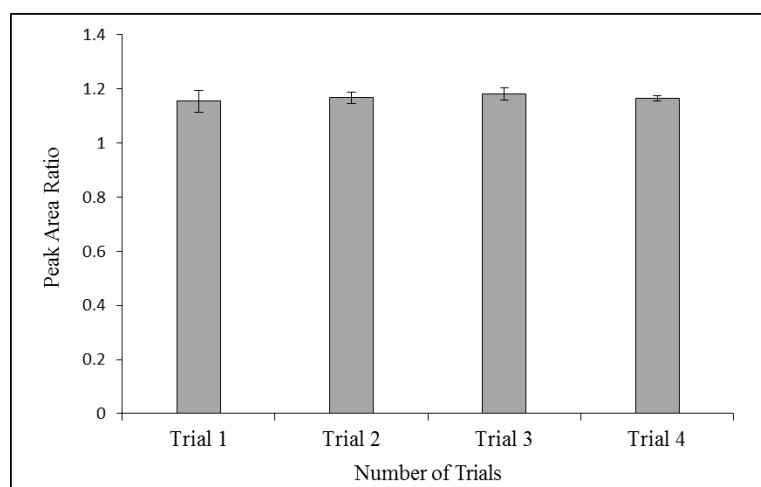


Figure 3.13. A plot showing the reproducibility in the calculated peak area ratios (PAR) for standard solutions, each trial represents a separate batch of samples (n = 9).

Since the experiment was repeated three different times, the average PARs and standard deviations were calculated for each sample. The precision of the method can be evaluated with the coefficient of variation (CV), usually expressed as a percentage for

each sample (**Table 3.4**) according to Equation 3.4. The CVs obtained ranged from 0.95 to 2.67%. The CV represents the ratio of the standard deviation to the mean, and it is a useful statistical value for comparing the degree of variation from one data series to another, even if the means are drastically different from each other. The smaller the coefficient of variation, the more precise is a set of measurements. The small CV values support that the method is fairly robust and quantification of sugars can be done.

$$CV = \frac{\text{Standard Deviation}}{\text{Mean}} \times 100 \% \quad \text{Equation 3.4}$$

3.6. LINEARITY AND LINEAR RANGE DETERMINATION

3.6.1. Calibration Curves

A linearity study verifies that the sample solutions are in a concentration range where analyte response is linearly proportional to concentration. This study is generally performed by preparing standard solutions at five concentration levels (at least), from 50 to 150% of the target analyte concentration to construct a calibration curve. A minimum of five levels are required to allow detection of curvature in the plotted data. The standards are evaluated using the instrumental conditions determined during the specificity studies.

The first step in developing a calibration curve is to make a set of standard solutions of known concentrations to be analyzed to determine the range. The range needs to be set such that any sample analyzed with an unknown concentration will have its instrumental signal within the range of the standard curve. To accomplish this serial dilution of standards is often necessary. This is because if the range is set too high, there

may be competitive inhibition in the ionization of the sample due to its high concentration which creates a curve in the line causing a large deviation from the actual line. A highly concentrated sample will have too many molecules to be ionized and not all of them will be sufficiently ionized before transmitted into the mass spectrometer. And since the spectrometer only detects charged molecules, the great number of molecules present actually inhibits their ionization thus creating a point in the curve with significant deviation from the tangent line.

The linear range of an analytical method is the analyte concentration range over which the detector response is proportional to the analyte concentration. This is demonstrated in **Figure 3.14**. The point in the line at which the concentration starts to deviate from the tangent line (point A in **Figure 3.14**) marks the end of the linear range. The concentration at point B will be too high and will therefore give incorrect results because it falls outside the linear range. The level on analyte concentration should remain below this point to ensure a least square multiple (R^2) of at least ≥ 0.990 . The lowest concentration on the curve should produce a peak of at least ten times greater than the noise to be valid for use in quantification. A related quantity is the dynamic range, the range of analyte concentration over which a change in concentration gives a change in detector response, but the response is not linear.

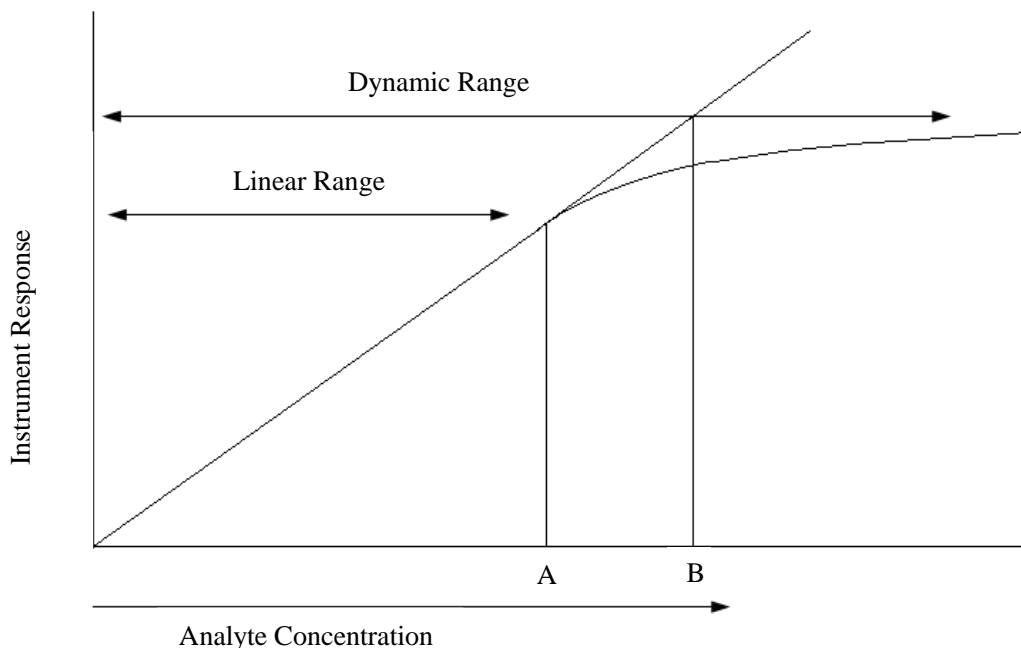


Figure 3.14. A graph showing the instrument response as a function of the analyte concentration. After point A the response level starts to deviate making the detected amount less than the expected amount.

In generating calibration curves, reproducibility is very important. To prove that a generated calibration curve is reproducible, a set of working standards should be made in triplicate and analyzed separately. The slopes of the three sets are compared to determine if they agree or not. If the slopes do not agree, then a *t*-test should be used to determine the degree of deviation to conclude whether the slopes are significantly different or not. A significant difference in the slopes indicates that further experimental investigations are needed to eliminate any possible systematic or random errors that may be present.

Like any other analytical technique, the signal obtained from a sample with DART ionization is directly proportional to the number of ions formed and transferred to the mass spectrometer for further detection, which in turn is proportional to the concentration of the sample being analyzed. The range of glucose standards

concentrations used to build a calibration curve was from 5.00×10^{-6} to 5.00×10^{-3} M, each sample spiked with deuterated glucose (the internal standard) such that its final concentration was 4.00×10^{-4} M. The curve was generated by plotting the detector response versus the concentration of the sugar standards. In this case the detector response was reported as the peak area ratio (PAR). The PAR was obtained by dividing the peak area of glucose by the peak area of the internal standard (Equation 3.3) by using the extracted ion chromatograms of glucose (m/z 198) and the internal standard (m/z 200).

After several experimental trials using sugar standards ranging from 5.00×10^{-6} to 5.00×10^{-3} M, it was observed calibration curves started to deviate from the required linear relationship once the concentration passed 3.00×10^{-3} M (data not shown). Concentrations beyond 3.00×10^{-3} M constituted the dynamic range which caused the correlation coefficient to go below the required value. It was also observed solutions having concentrations below 1.00×10^{-5} M were barely detected, e.g. S/N values were below levels of quantification. Therefore, the acceptable linear range used in generating calibration curves for glucose standards was 1.00×10^{-5} to 3.00×10^{-3} M. This is equivalent to 1.80 ng to 540 ng of glucose since 1.0 μ L was applied in all cases.

Three replicates of the linear dynamic range standards were analyzed and the PARs computed to obtain an average. In **Table 3.5**, a representative set of data obtained by analyzing glucose standards along with their average PAR and standard deviations is presented. A calibration curve using values in **Table 3.5** was generated, as shown in **Figure 3.15**, by plotting the average (with error bars) PAR values against the glucose concentrations. The calibration curves were generated by using the triplicate set of standards for two more days to confirm reproducibility. All the calibration curves

generated had a linear regression value ≥ 0.998 . Some of the error bars may not be visible because their values were simply low and will not appear beyond the shape of the graph point. From the three-days calibration curves generated using the linear range concentrations, it was observed that the sugar standards are stable molecules in solution and can be readily quantified.

Table 3.5. Peak area ratios of different concentrations of glucose standards spiked with 4.00×10^{-4} M of internal standard (deuterated glucose) and the standard deviation for each measurement (n = 3).

Concentration (M)	Average Peak Area Ratio (PAR)	PAR Standard Deviation
3.00×10^{-3}	6.17329	0.13575
2.00×10^{-3}	4.20513	0.01533
1.00×10^{-3}	2.14244	0.10152
6.00×10^{-4}	1.49796	0.01856
1.00×10^{-4}	0.46486	0.19118
6.00×10^{-5}	0.15259	0.01214
4.00×10^{-5}	0.09267	0.01995
1.00×10^{-5}	0.04111	0.00396

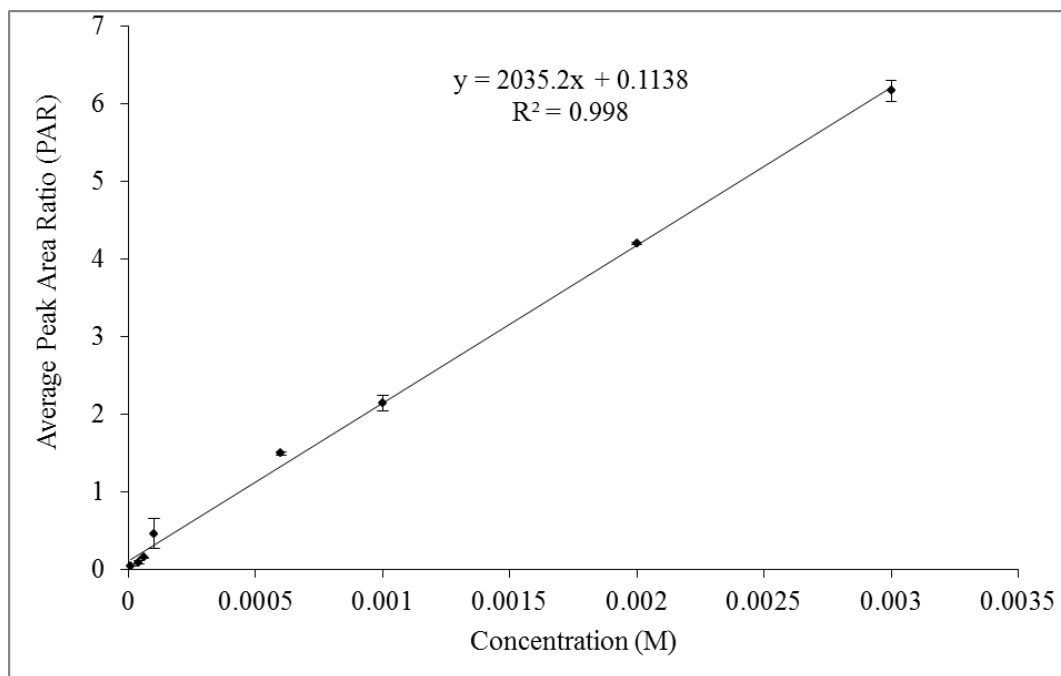


Figure 3.15. Calibration curve for a series glucose standards solution spiked with 4.00×10^{-4} M of deuterated glucose (internal standard). Each point represents an average ($n = 3$) peak area ratio with associated standard deviation.

CHAPTER FOUR

APPLICATION OF DART-MS TO SACCHARIFICATION SAMPLES

4.1. INTRODUCTION

In chemical analysis, most of the samples analyzed exist as a mixture of multiple components (e.g. analytes of interest contained in matrix). The production of the analyte signal by an instrument can be affected by the presence of any form of impurities present in the matrix, typically referred to as matrix effects. In developing a method of analysis, sample preparation is an important process that will influence the accuracy and precision of generated data. This process entails extracting the analyte from a complex matrix, preconcentrating dilute analytes, removing or masking interfering species, or chemically transforming (derivatizing) analyte into a more easily detected form.¹⁶⁰

One objective of the study was to quantify six-carbon sugars produced after pretreatment and saccharification of switchgrass using DART-MS. The switchgrass samples after the saccharification process are still biological in nature and, apart from the sugars to be quantified, contain other components in solution that may lead to matrix effect. Therefore, a series of experiments were developed involving limits of detection and quantitation, recovery trials, and matrix effect statistical analysis to determine the existence of any matrix effects with the DART-MS, specifically in terms of ion suppression or enhancement. This chapter discusses these experimental considerations with the analysis of switchgrass samples with saccharification matrix.

4.2. SWITCHGRASS SACCHARIFICATION SAMPLES

Switchgrass samples were obtained from Eastern Kentucky University's Center for Renewable and Alternative Fuel Technologies (CRAFT), Richmond, KY. The samples were obtained by pretreatment of switchgrass with different methods as explained in Section 2.3. After pretreatment, the samples were subjected to enzymatic hydrolysis to extract the sugars. Each sample was obtained by pretreatment of 35 g of switchgrass which was subsequently hydrolyzed to generate the sugars. Blank solutions, i.e., solutions that have been subjected to the pretreatment and hydrolysis process but did not contain any switchgrass, were also obtained alongside the switchgrass samples. The samples were placed in 20 mL clear glass vials with Teflon septa and stored in the freezer before analysis. The color of these samples varied; from clear to light yellow.

4.2.1. Preliminary Analysis of Switchgrass Samples

Initially, switchgrass samples were analyzed to determine the type of spectral peaks generated in the sample matrix. This was imperative to confirm the type of six-carbon sugars that were present in the samples. Therefore, a comparison of the spectral peaks of the switchgrass samples was done against glucose standards. Three samples were selected randomly for analysis from three different particle sizes (ball milled, 1 mm, and 2 mm). Similarly, three blank solutions were randomly picked for analysis. A 1.0 mL aliquot of each sample and blank solution were drawn and placed into 1.5 mL clear glass vials and then stored in the refrigerator (4°C) until analysis occurred.

For analysis, samples were removed and allowed to equilibrate to room temperature before any run was made. Samples were then analyzed without any

modification or dilution with the DART-MS. Settings for the DART source and the mass spectrometer were optimized in a similar fashion as described in Chapter three (Sections 3.4.2). Each sample, including the blank solutions, was analyzed by spotting 1.0 μL on the glass tip placed in the moving rail. Three separate trials were done for each sample to determine the consistency of the mass spectra obtained. **Figure 4.1** shows a representative mass spectrum obtained from a switchgrass-saccharification sample with the DART-MS.

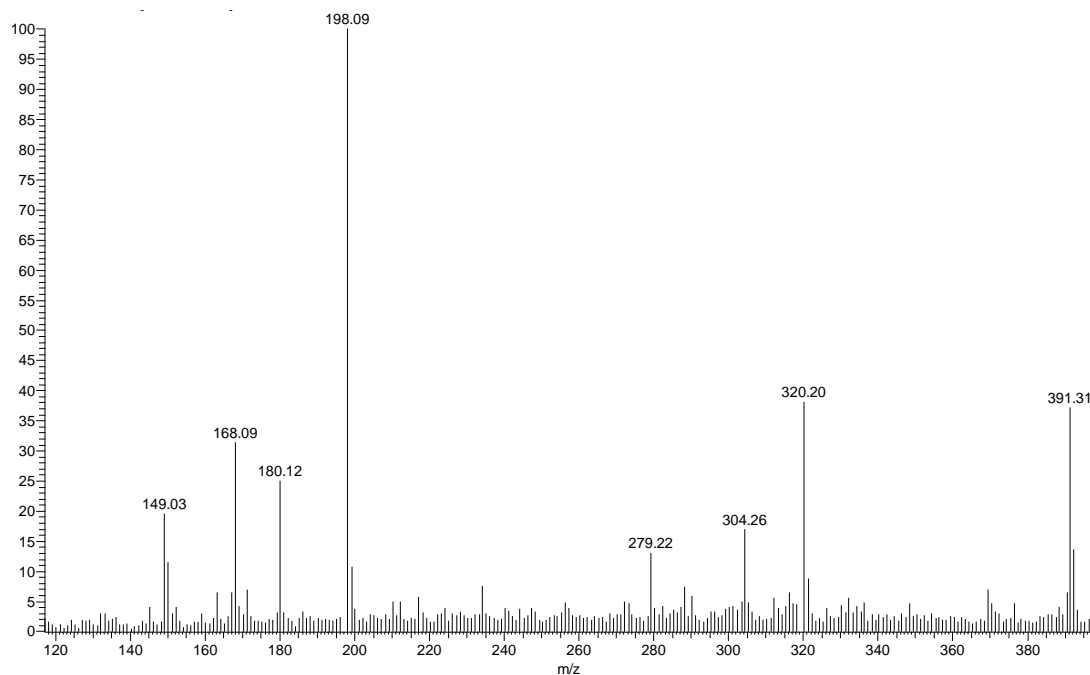


Figure 4.1. A full scan mass spectrum of a switchgrass-saccharification sample showing the generated peaks present using the DART-MS. The analyte of interest (m/z 198) is preliminary designated as the six-carbon sugar.

It was observed the spectral peaks were consistent for each switchgrass-saccharification sample. In each mass spectrum, the base peak was at m/z 198 along with other common peaks that were not considered background peaks were at m/z 149, 168,

180, 279, 320, and 391 because such peaks were not observed with pure sugar standard solutions. The peaks at m/z 180 and 198 were tentatively assigned as six-carbon sugar present in the sample aliquots. This was confirmed by carrying out MS/MS analysis on the peak at m/z 198 with a CID energy of 30 normalized collision energy. Fragment peaks obtained included m/z 180 and 163 (**Figure 4.2**). These fragments were consistent with peaks obtained when MS/MS was performed on glucose standards (m/z 198), shown in **Figure 3.5**. The other tentatively assigned sugar peak was observed at m/z 168. This peak was generated from the five-carbon sugar xylose using the same tandem experiment with standards (xylose standards were previously analyzed, data not shown).

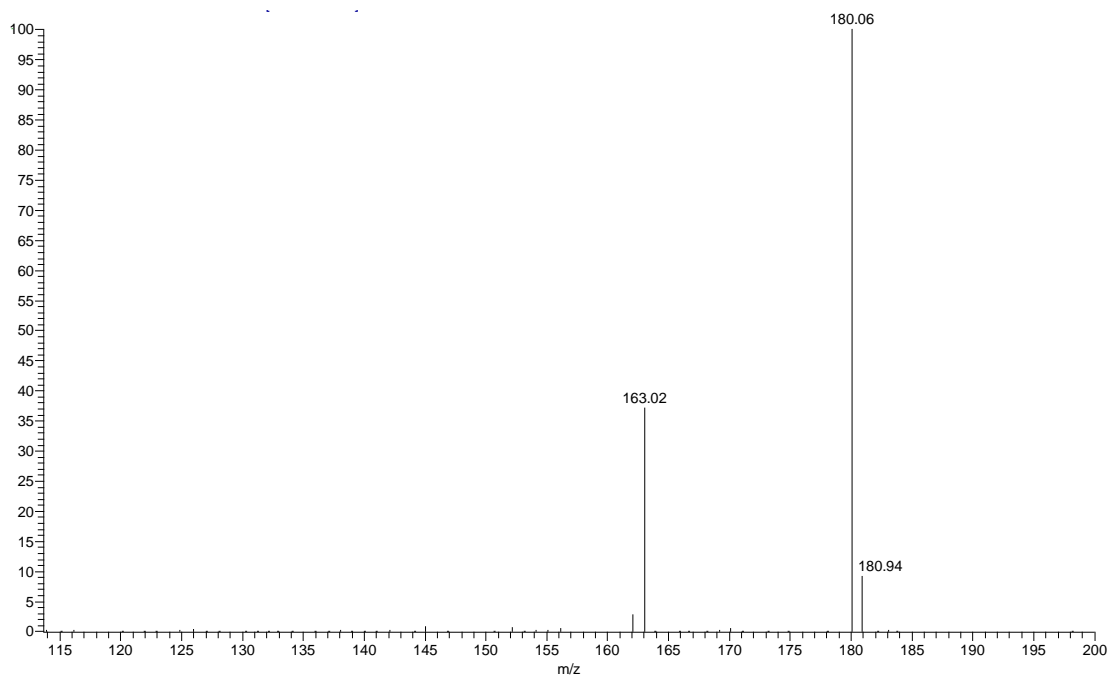


Figure 4.2. Product ions generated when m/z 198 from a switchgrass-saccharification sample was mass selected and then fragmented giving the tandem mass spectrum (that can be compared with glucose standards).

The other prominent peaks were labeled as matrix components found in the samples since fragmentation patterns did not correlate to any sugar analytes of interest. With the presence of matrix components, validation of the quantitation method was necessary to determine if these components had any effect on the analytes, e.g. ion suppression or enhancement.

4.2.2. Analysis of Blank Solution from Saccharification Process

The blank solutions were also analyzed in a similar fashion as the switchgrass-saccharification samples. An interesting aspect was observed from the mass spectra obtained for all three blank solutions analyzed; a base peak at m/z 198. Since this was unexpected, the m/z 198 peak was fragmented to determine the product ions generated and the fragmentation profiles of the blank solutions were almost identical to the glucose standards profiles (small differences were noticed when MS³ was done). Subsequently, it was determined the commercially available enzyme mix used for switchgrass hydrolysis reportedly has glucose, however; the exact concentration was not known. Glucose in the enzyme mix can be removed by dialysis. In order to remove the glucose in the enzyme by dialysis, an Amicon filter can be used.¹⁶¹ However, a filter unit was not used in the current saccharification process and implementation of this dialysis step would be an additional sample preparation (and minimal sample preparation is desired). The implication is each switchgrass-saccharification sample will contain a relatively equal amount of six-carbon sugar (glucose) derived from the commercial enzyme mix. Quantitative analysis of these samples would then need to take the sugar concentration from blank solutions into consideration.

4.2.3. Limit of Detection and Limit of Quantitation Determination

The limit of detection (LOD), or detection limit, is the lowest concentration level determined to be statistically different from a blank (at a 99% level of confidence). The LOD is when the signal of the analyte is three times the noise. LOD is matrix, instrument, method, and analyte specific and requires a well-defined analytical method for its determination and provides a useful mechanism for comparing different laboratories capabilities with identical methods as well as different analytical methods within the same laboratory. The limit of quantitation (LOQ), or lower limit of quantitation, is the level above which quantitative results may be obtained with a specified degree of confidence and defined as ten times the standard deviation of the results for a series of replicates used to determine a justifiable limit of detection. The LOQ is also matrix, instrument, method, and analyte dependent.

To determine the LOD using the calibration curve method for the current study, a set of replicate glucose standard samples (at least seven) with a blank were analyzed for at least three times. An estimate of the lowest concentrated sample (non-blank) in the calibration curve (1.00×10^{-5} M) was made to be close to the limit of detection. The standard deviation was then calculated for the lowest sample on the calibration curve, excluding the blank. Since the limit of detection deals with a peak three times the signal-to-noise ratio (S/N), and if the blank is taken as the y-intercept, Equation 4.1 can be used in the calibration curve in determining the LOD. Substituting the equation of the linear curve into Equation 4.1 gives Equation 4.2, which can be used to solve for x to give the LOD, expressed as x_{LOD} in Equation 4.3.¹⁶²

$$y = 3s + b \quad \text{Equation 4.1}$$

$$3s + b = mx + b \quad \text{Equation 4.2}$$

$$x_{LOD} = \frac{3s}{m} \quad \text{Equation 4.3}$$

In Equation 4.1, b is the y-intercept, and s is the standard deviation of the lowest concentration on the calibration curve. The LOD for glucose standards can then be estimated using the equations provided above. Using Equation 4.3, the standard deviation of the signal for the lowest concentration (0.00396) and the slope from the calibration curve in **Figure 3.15** (2035.2), the LOD can be determined as shown in Equation 4.4.

$$\text{LOD} = (3 \times 0.00396)/2035.2 = 5.84 \times 10^{-6} \text{ M} \quad \text{Equation 4.4}$$

In order to verify the calculation above, an experimental confirmation needs to be done to determine whether the calculated LOD is close to the detector signal produced at the estimated concentration. To fine-tune LOD determination, replicates of glucose standards whose concentrations were lower than the low-concentration sample in the calibration curve were prepared. This was done to determine their S/N to determine if their signals were less than three times greater than the noise. **Figure 4.3** shows the signals produced by the lowest concentration point previously used in the calibration curve, shown in **Figure 3.15** (1.00×10^{-5} M) as well as other glucose standards below that point (3.50×10^{-6} , 4.00×10^{-6} , and 5.00×10^{-6} M solutions of glucose standards), which were analyzed together with the lowest concentration value in the calibration curve. From **Figure 4.3**, it is observed that analysis of glucose concentrations near (or below) the

calculated LOD gave an experimental signal with at least an S/N of 3 or less and in all the subsequent experiments performed (data not shown).

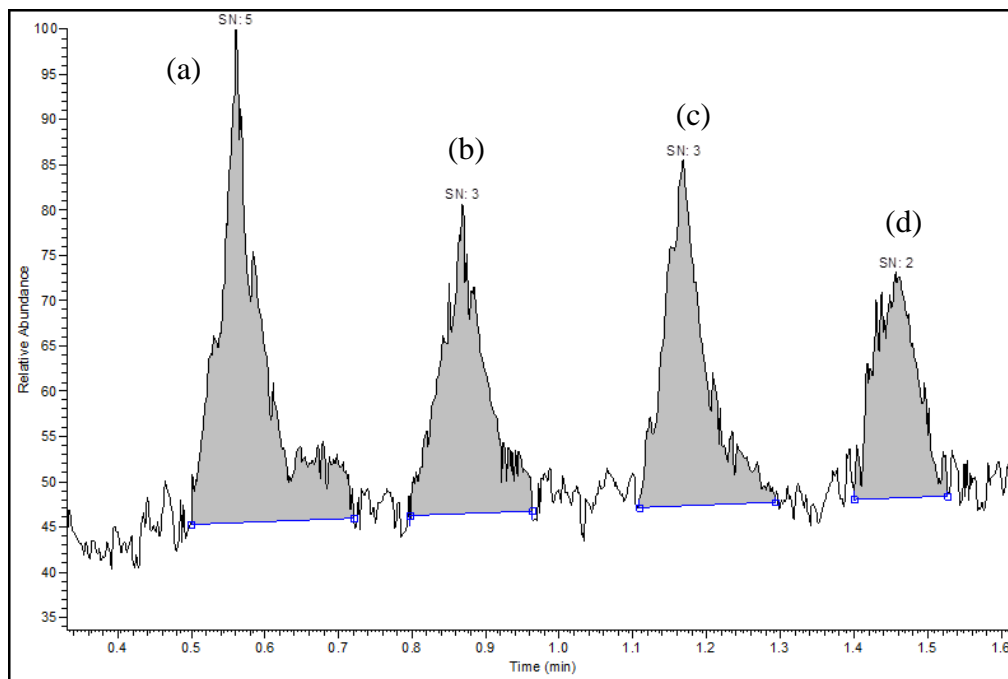


Figure 4.3. A representative chromatographic peaks showing the signal to noise ratio (S/N) for different concentrations of glucose (a) 1.00×10^{-5} M, (b) 5.00×10^{-6} M, (c) 4.00×10^{-6} M, and (d) 3.50×10^{-6} M.

A similar procedure is used to determine the LOQ except that three should be replaced by ten in Equations 4.1 – 4.3. In most case cases, the LOQ is only estimated by observing the signal peaks at a concentration in which the S/N is at least 10. The S/N produced by 1.00×10^{-5} M in **Figure 4.3** was in the range of 5 and 10. This was estimated to be the LOQ. However, the calculated LOQ was found to be 1.95×10^{-5} M when ten is substituted for three in Equation 4.4 ($LOD = 10s/m$). Since the volume of the glucose standard spiked on the glass tips was only 1.0 μ L, the precise concentration of the LOD

can be determined. By using the molecular mass of glucose and considering the volume of the sample applied, the LOD and LOQ were calculated to be 1.05 *ng* and 3.51 *ng* of glucose, respectively.

4.3. MATRIX EFFECTS ANALYSIS

4.3.1. Introduction

In Chapter 3, a calibration curve for glucose standards was generated with a linear range of 1.00×10^{-5} to 3.00×10^{-3} M, however, those sugar standard solutions were prepared in methanol/water (50:50 v/v) solutions. While the generated calibration curves were reproducible over a number of days, with respectable R^2 values, the switchgrass samples analyzed in this study contained matrix components with the analyte of interest. The existence of matrix has the potential to influence instrumental response of the six-carbon sugars in switchgrass samples, i.e. matrix effect, and needs to be evaluated with respect to quantitation results. In order to evaluate the presence of matrix effects, glucose standard solutions of different concentrations were prepared using blank saccharification solutions, solutions prepared in the same manner as saccharification samples without adding switchgrass. These solvents had the same proportions of buffers and enzyme mix as those used in the hydrolysis of the switchgrass samples. Calibration curves from glucose standards prepared from these blank solutions would then be compared with the calibration curves generated from standard solutions prepared in methanol/water solvents using the same instrumental conditions.

4.3.2. Calibration Curves Comparison

Using methanol/water (50:50, v/v) as solvent, three replicate sets of glucose standard solutions were prepared in the concentration range of 1.00×10^{-5} to 3.00×10^{-3} M. Each set consisted of seven different concentrations (**Table 4.1**) spiked with an internal standard (deuterated glucose) where the final concentration was 4.00×10^{-4} M. Additional replicate standards with the same concentration range were prepared using a blank enzyme solvent (BES), hereafter referred to as a blank solvent, also spiked with the same internal standard, final concentration of 4.00×10^{-4} M. The blank solvent in which the standards were made was prepared by diluting the blank samples with methanol/water (50:50, v/v) solvent to a final concentration of 1% BES. A 1% BES concentration was chosen because (1) the detector signal was relatively measurable, and (2) matrix effects were expected to be less at this concentration. In addition to the six concentration values, each set had an accompanying blank solution that was not spiked with any glucose standard but still contained the internal standard. This would be a signal response for a theoretical 'zero' concentration and can be used for corrections purposes, specifically to subtract the signal obtained as a result of the blank solvent.

Both sets of standards, those in methanol/water and in 1% BES, were analyzed and each set had three replicates (there was a total of nine replicate samples). The peak area ratios were obtained for each run and the three replicates from each set were averaged for each concentration. Calibration curves were then generated for each set of standards. The purpose of these runs was to compare and determine if the slopes of the two curves were significantly different. **Table 4.1** shows data for the two sets of analysis and the respective calibration curves generated are shown in **Figure 4.4**. By simple

observation of the two curves, the slopes (best fit with least squares) appear to differ but do converge to a point.

Table 4.1. The peak area ratios of glucose standards made in methanol/water and 1% blank enzyme solvent (BES) and their respective standard deviations. ^athe corrected PAR is that obtained by subtracting the PAR of the blank. ^bis the standard deviation of the corrected PAR.

Methanol/water Standards			1% BES Standards		
Concentration (M)	Average PAR	STDEV	Average PAR	Average Corrected ^a PAR	STDEV ^b
1.00 x 10 ⁻⁵	0.06116	0.00693	0.25272	0.05717	0.01502
6.00 x 10 ⁻⁵	0.14769	0.00472	0.36685	0.17129	0.00781
1.00 x 10 ⁻⁴	0.20543	0.00977	0.43038	0.23482	0.00216
6.00 x 10 ⁻⁴	1.44350	0.03841	1.62290	1.42735	0.01766
1.00 x 10 ⁻³	2.15672	0.04069	2.41834	2.22279	0.05047
2.00 x 10 ⁻³	4.26406	0.01950	4.30377	4.10822	0.18462
3.00 x 10 ⁻³	6.28637	0.02358	6.32478	6.12923	0.03140
0 (blank)	-	-	0.19556	0	0

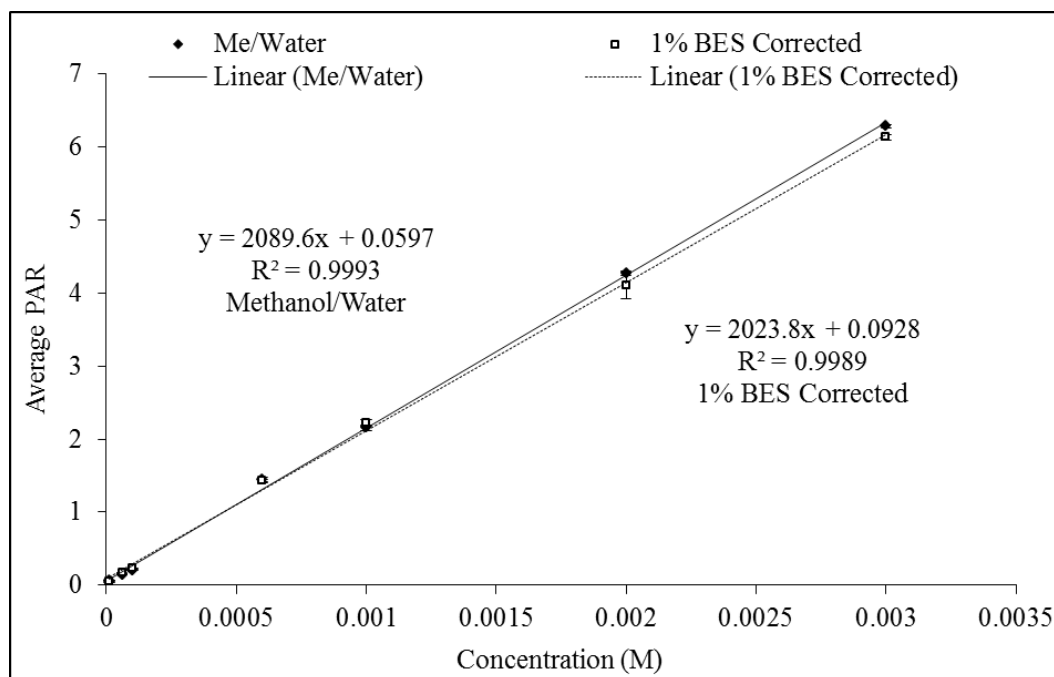


Figure 4.4. Calibration curves generated from glucose standards with and without the blank solvent with respective calculated slopes.

In order to statistically determine whether the slopes of the two calibration curves are significantly different or not, the Student's *t*-test was applied. A Student's *t*-test (commonly referred to as the *t*-test) is a commonly used technique for testing a hypothesis on the basis of a difference between replicate measurements. In simpler terms, the *t*-test determines a probability on whether two populations are significantly the same (or different) with respect to the variable tested. A null hypothesis in statistics states that two sets of measurements are not significantly different. Statistical analysis can generate a probability that observed difference between two set of measurements can reject the null hypothesis within a certain level of confidence (a null hypothesis is customarily rejected if there is less than a 5% chance that the observed difference arises from random variations. With this criterion, there is a 95% chance that a conclusion is correct).¹⁶⁰

Using statistical analysis, values of *x* and *y* that generate the best-fit (least squares) trend line (as indicated in **Table 4.1**) can be used to calculate the predicted values, \hat{X} and \hat{Y} , respectively, from the straight lines. The \hat{Y} value is solved from the equations of the curves ($y = mx + b$, where *m* is the slope and *b* the *y*-intercept for each of the curves) by using the corresponding *x* values from each curve. After solving for the \hat{Y} values, the next step is to calculate the residual sum of squares (SS_{res}) for each curve by using Equation 4.5.

$$SS_{res} = \sum_{i=1}^n (y_i - \hat{Y}_i)^2 \quad \text{Equation 4.5}$$

The criterion used here is that of least squares, which considers the vertical deviation of each point from the line (i.e., the deviation we describe here as $(y_i - \hat{Y}_i)$), and defines the

best-fit line as that which results in the smallest value for the sum of the squares of these deviations for all values of y_i and \hat{Y}_i . That is, $\sum_{i=1}^n (y_i - \hat{Y}_i)^2$ is to be a minimum, where n is the number of data points composing the sample.

Once the SS_{res} has been determined, the mean square residual (MS_{res}) is computed using Equation 4.6 as a function of the residual degrees of freedom. MS_{res} defines the mean variance around the curves.

$$MS_{res} = \frac{SS_{res}}{n - 2} \quad \text{Equation 4.6}$$

where n is the number of data points composing the sample (at different concentrations), therefore, $n - 2$ is the residual degree of freedom defined by the difference of the total degrees of freedom and the regression degrees of freedom. From the mean square variance, the standard error of estimate, $S_{y \cdot x}$, (occasionally termed the “standard error of the regression”) can be found according to Equation 4.7. The standard error of estimate is an overall indication of the accuracy with which the fitted regression function predicts the dependence of y on x .¹⁶³

$$S_{y \cdot x} = \sqrt{MS_{res}} \quad \text{Equation 4.7}$$

The $S_{y \cdot x \text{ pooled}}$ (Equation 4.8) is used to calculate the pooled variance between the methanol/water standards curve and the 1% BES curve. The $S_{y \cdot x \text{ pooled}}$ is a pooled standard deviation making use of both sets of data (the matrix-free and matrix-diluted data).

$$S_{y \cdot x \text{ pooled}} = \sqrt{\frac{(n_1 - 2)(S_{y \cdot x(1)})^2 + (n_2 - 2)(S_{y \cdot x(2)})^2}{n_1 + n_2 - 4}} \quad \text{Equation 4.8}$$

In Equation 4.8, $(S_{y \cdot x(1)})^2$ and $(S_{y \cdot x(2)})^2$ are the variances in the matrix-free (methanol/water) and matrix-diluted (1% BES) data sets, respectively, and the factor $(n_1 + n_2 - 4)$ represents the pooled number of degrees of freedom (the subscripts 1 and 2 refers to the two regression lines being compared).

Once the $S_{y \cdot x}$ has been determined, one can calculate the variance for the slopes of each curve, $S_{b(p)}$, using Equation 4.9.^{163, 164}

$$S_{b(p)} = S_{y \cdot x \text{ pooled}} \sqrt{\frac{1}{(\sum x^2)_1} + \frac{1}{(\sum x^2)_2}} \quad \text{Equation 4.9}$$

In Equation 4.9, $(\sum x^2)$ is the sum of squares of \hat{X}_i ($i = 1$ to n) values defined as $\sum_{i=1}^n (x_i - \hat{X}_i)^2$ and the subscripts 1 and 2 refer to the two regression lines, the matrix-free and matrix-diluted lines, respectively, being compared.

After computing the $S_{b(p)}$, the last step will be calculating the $t_{\text{calculated}}$ value (Equation 4.10) for the slopes to determine if the slopes are significantly different or not.

$$t_{\text{calculated}} = \frac{|b_1 - b_2|}{S_{b(p)}} \quad \text{Equation 4.10}$$

where $|b_1 - b_2|$ is the absolute value of the difference of the slopes for matrix-free and matrix-diluted calibration curves. The $t_{\text{calculated}}$ from Equation 4.10 is compared with the t value in the Student's t table (t_{table}). If $t_{\text{calculated}}$ is greater than t_{table} at the 95% confidence level, the two slopes are considered to be significantly different. There is a 5% chance that the two sets of data were drawn from populations with the same population mean. **Tables 4.2** shows a summary of the statistical parameters and Appendix A (**Tables A1** and **A2**) shows how the statistical data has been computed.

Table 4.2. Pooled standard errors and t test results for the statistical comparison of linear trend line fits to calibration curves from the matrix-free standards and matrix-diluted standards.

Statistical Parameters	Matrix-free Standards	Matrix-diluted Standards
Residual sum of squares (SS_{res})	0.0251	0.0366
Mean square residual (MS_{res})	0.0050	0.0073
Standard error of estimate ($S_{y \cdot x}$)	0.0709	0.0856
Pooled standard error ($S_{y \cdot x \text{ pooled}}$)	0.0786	
Pooled error of slopes ($S_{b(p)}$)	1327.9	
$t_{calculated}$	0.050	
t_{table} (95% confidence)	2.228	
Matrix-free = matrix-diluted slope?	Yes	

From the statistical analysis, the $t_{calculated}$ value is 0.050 whereas the t_{table} at a 95% confidence level is 2.228 for ten degrees of freedom ($n_1 + n_2 - 4$, where $n_1 = n_2 = 7$). Since $t_{calculated} < t_{table}$ it follows that the slopes of the curves are not different.¹⁶⁰ In fact, the low value of $t_{calculated}$ indicates the slopes are quite similar. This evaluation concludes that no significant matrix effect exist so no significant suppression/enhancement of the instrumental response was observed for the matrix-diluted (1% BES) standards overall. The absence of matrix effects could be attributed to the dilution carried out on the matrix blank solvent and any matrices present would be very low in concentration to cause any effect on the instrumental signal. Therefore, calibration curves of standards made from methanol-water would be equivalent as 1% matrix-diluted standards for the determination of unknown six-carbon sugars in the real test samples (switchgrass samples). However, the slopes of the two lines (**Figure 4.4**) tend to diverge as the concentration increases and this divergence may lead to false results in a specific

concentration range. Statistical analysis is needed to test the accuracy for specific concentration ranges in the overall dynamic range.

4.4. METHOD ACCURACY AND RECOVERY

4.4.1. Introduction

The accuracy of an analytical method is how close a measured value of an analyte will be to the 'true value' for the sample, where the 'true value' is one that is either an adopted or accepted certified reference value. There are four ways for determining accuracy of an analytical method: i) Accuracy can be assessed by analyzing a sample of known concentration (e.g., a control sample or certified reference material) and comparing the measured value with the true value as supplied with the material.¹⁶⁵ ii) Compare results from a new method with results from an existing alternate method that has been adopted to be accurate. iii) A recovery study is performed by spiking an analyte in a blank sample matrix. In this method, spiked samples are normally prepared in triplicate and their concentrations should cover the range of interest and should include concentrations close to the quantitation limit, mid-range, and one at the high end of the calibration curve. The analyte levels in the spiked samples should be determined using the same quantitation procedure that will be used in the final method. (i.e., the same number and levels of standards, same number of samples, and standard injections, etc.)¹⁶⁵ For this accuracy assessment, care in sample preparation should be taken to mimic the actual sample preparation as closely as possible. If validated correctly, the recovery factor determined for different concentrations can be used to correct the final results. iv) A fourth approach is the standard addition technique where a series of increasing amounts

of standard are added to divided sample aliquots. This technique can be employed for samples where matrix effects are prevalent and not possible to obtain a blank sample matrix without the presence of the analyte.

4.4.2. Recovery of Control Sample Analytes Spiked into Blank Matrices

Since statistical analysis indicates the lack of matrix effects at low dilution levels (Section 4.3.2.), the next experimental procedure is to investigate the recovery efficiencies of sugar standards spiked in BES matrix. Since the BES matrix was readily available, the third approach (previously described in Section 4.4.1) was used to assess accuracy and recoveries. In order to determine the recovery and extraction efficiency, a standard sample set must be generated and analyzed with a separately prepared quality control sample set. For the standards sample set, six different concentrations of glucose standards were prepared ranging from 1.00×10^{-4} to 3.00×10^{-3} M. These standards were prepared in 1% BES and all were spiked with the internal standard so as to have a final concentration of 4.00×10^{-4} M. A blank sample was also prepared together with the standards for purposes of subtraction of the signal obtained from 1% BES. The quality control (QC) samples set were also prepared in 1% BES (blank matrix). However, a separate, freshly prepared stock solution of glucose (as described in Section 3.2.3.) was used to obtain the amount of glucose spiked in the blank matrix solutions for preparing the QC samples (QCs). The QCs were also prepared in triplicate at three different levels over the range of the standards concentration, a low concentration (at least three times the lowest data point in the calibration curve), a mid-range concentration, and high concentration (about 0.75 times the highest concentration in the calibration curve). All

the QCs were spiked with the internal standard to have a final concentration of 4.00×10^{-4} M. Since the overall dynamic range for the standards was 1.00×10^{-4} to 3.00×10^{-3} M, the high concentration QC sample (HQC) was defined to be 2.50×10^{-3} M, the mid-range concentration QC (MQC) was 1.50×10^{-3} M, and the low concentration QC (LQC) was 5.00×10^{-4} M. The generated calibration curve will be used to obtain calculated values of the glucose from these control samples set to determine percent (%) recovery efficiencies.

Analysis was performed on three replicates for the standards and each QC set, example: HQC was analyzed three times, each time with a different set of standards set such that an independent value was determined against each standard set, HQC1, HQC2, and HQC3 (where 1, 2, and 3 represent the three replicates of HQC). The peak area ratio (PAR) was determined (the ratio is the peak area generated from spiked glucose divided by the peak area of the internal standard) using the Xcalibur software for each run and an average PAR computed. Since a blank enzyme solution was used, the PAR and the average PARs were corrected to subtract the signal from the blank matrix solution. A calibration curve was generated for each run; the calibration curve will be used to determine the “recovery” concentration of the quality control samples from the matrix. Similar runs were performed for MQC and LQC samples where a total of nine runs were measured for the QC samples. In **Table 4.3**, the average corrected PARs are shown for the standard solutions with the three different QCs concentrations. Calibration curves generated from this table are shown in **Figures 4.5 – 4.7**. The resulting best-fit equation of the calibration curve was then used to determine the concentration of the QCs (**Table 4.3**).

Table 4.3. Peak area ratios and the respective standard deviations from standards spiked into a blank matrix solution analyzed with QCs at three levels of concentration (low, mid, and high). ^aThe blank was used to correct the PAR in each run and its values are not included.

Standards spiked into blank enzyme solution (matrix–diluted)						
	HQC (2.50×10^{-3} M)		MQC (1.50×10^{-3} M)		LQC (5.00×10^{-4} M)	
Concentration (M)	Average PAR	Standard Deviation	Average PAR	Standard Deviation	Average PAR	Standard Deviation
3.00×10^{-3}	6.1383	0.1462	6.1955	0.0866	6.17928	0.1277
2.00×10^{-3}	4.0520	0.2351	4.1380	0.1344	4.1270	0.1627
1.00×10^{-3}	2.2260	0.0532	2.2362	0.0270	2.2557	0.0469
8.00×10^{-4}	1.8593	0.0670	1.8495	0.1624	1.8810	0.04192
4.00×10^{-4}	1.1024	0.0235	1.1314	0.0513	1.1620	0.0352
1.00×10^{-4}	0.2558	0.0190	0.2661	0.0630	0.2701	0.0446
0 (blank) ^a	-	-	-	-	-	-
QC Sample	5.1556	0.1014	3.1591	0.08138	1.2481	0.0263

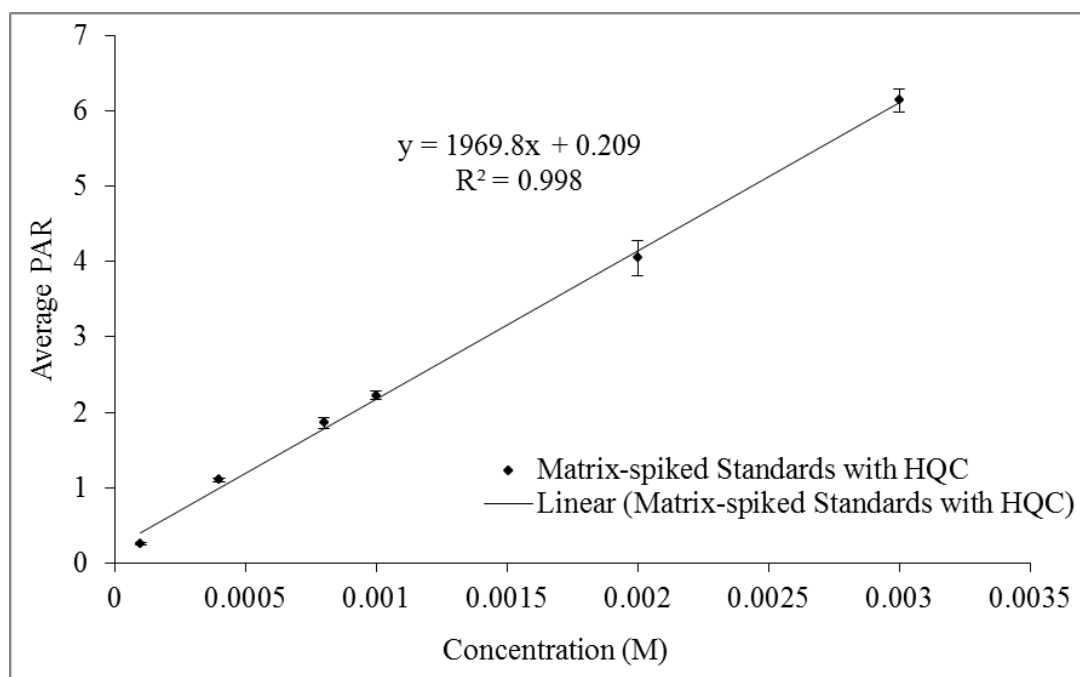


Figure 4.5. A calibration curve obtained by analyzing blank matrix solutions spiked with glucose standards with high concentration QCs.

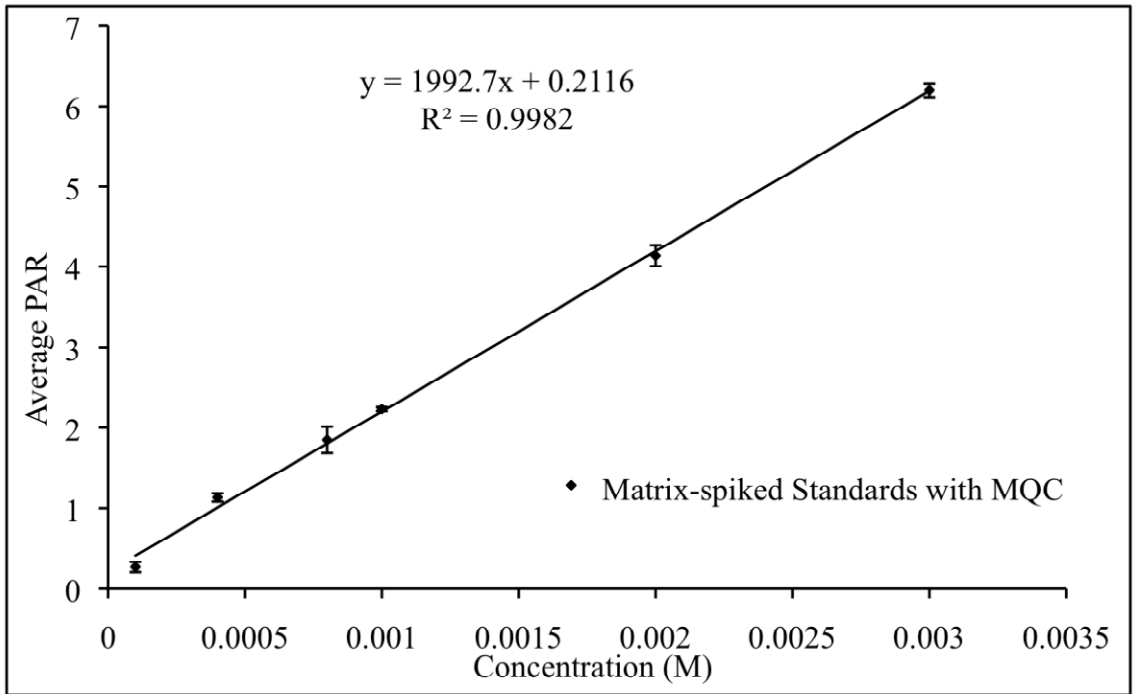


Figure 4.6. A calibration curve obtained by analyzing blank matrix solutions spiked with glucose standards with mid-range concentration QCs.

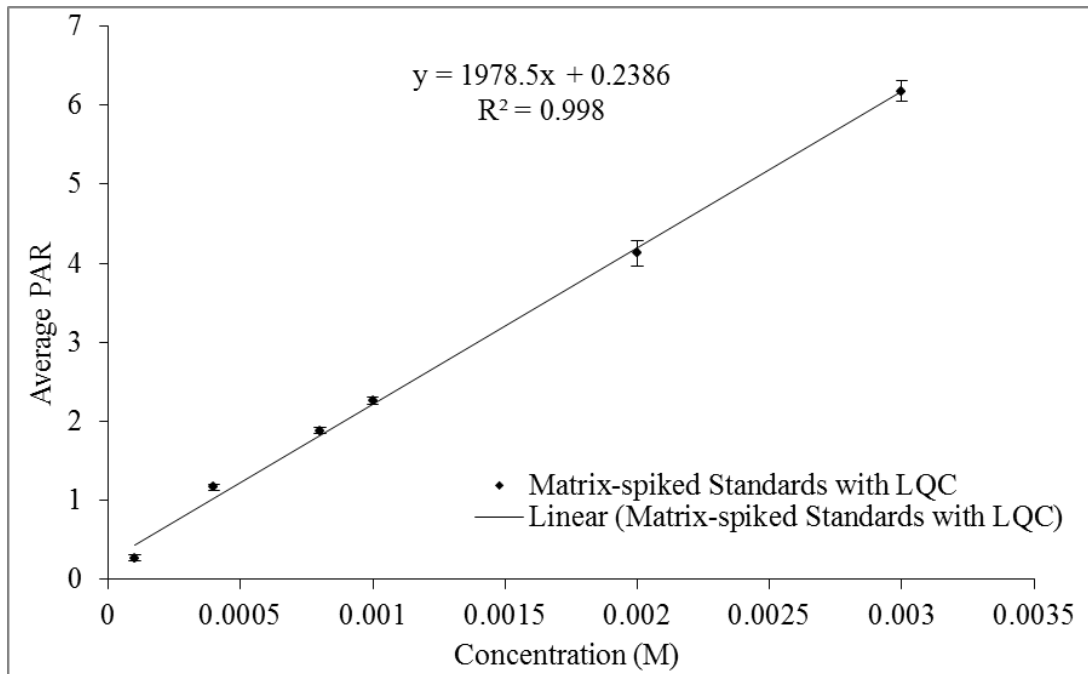


Figure 4.7. A calibration curve obtained by analyzing blank matrix solutions spiked with glucose standards with low concentration QCs.

From **Table 4.3**, the average PAR for each QC sample was used to calculate the concentration of the glucose recovered from the blank matrix solution by using the equation of the line of each calibration curve. Since the concentrations of the QCs are known, Equation 4.11 determines a percent recovery.

$$\text{Percent Recovery} = \frac{\text{Calculated Concentration}}{\text{Actual Concentration}} \times 100 \% \quad \text{Equation 4.11}$$

An example of an accuracy criteria for an assay method is that the mean recovery will be $100 \pm 2\%$ at each concentration over a range of 80–120% of the target concentration. Apart from this criterion, there are published acceptable recovery percentages as a function of the analyte concentration and the acceptable recovery % range for the analytes used in this study is 97–103%.¹⁶⁶ Using the equations of the calibration curves and Equation 4.11, the percent recoveries were calculated and the results are shown in **Table 4.4**. The average PAR used to compute the “calculated concentration” for each QC sample was from three replicate runs in each QC concentration level. Individual percent recoveries were calculated for every single run at each concentration level and their respective average percent recoveries calculated. From **Table 4.4**, the average percent recoveries ranged from 98.6% to 102.0%. The standard deviations of the percent recoveries were found to be in the range of 2.2 to 4.2 (**Table 4.4**) for the three levels of concentrations of the QC samples. The ultimate conclusion from this recoveries data is that standards spiked in matrix did not affect the recoveries of the analytes in the same matrix. This confirms one can null any matrix effects in the analytical method developed. It also proves the accuracy of the method in determining unknown concentrations of sugar samples that mimic saccharification samples.

Table 4.4. Data generated when determining the percent recovery of control samples spiked into blank matrix samples. ^aAverage PAR was obtained from three replicate runs of the QCs. ^bSD is the standard deviation.

Recovery Calculation of QC Samples Spiked into Blank Enzyme Solution (matrix–diluted)			
QC Samples	HQC	MQC	LQC
Trend Line Equation	$y = 1968.8x + 0.2090$	$y = 1992.7x + 0.2116$	$y = 1978.5x + 0.2386$
R ²	0.998	0.9982	0.998
Average PAR ^a	5.1556	3.1591	1.2481
SD ^b of Average PAR	0.1014	0.0814	0.0263
Calculated Concentration (M)	2.51×10^{-3}	1.48×10^{-3}	5.10×10^{-4}
Actual Concentration (M)	2.50×10^{-3}	1.50×10^{-3}	5.00×10^{-4}
Percent Recovery (%)	100.4	98.6	102.0
SD of Percent Recovery	2.5	2.2	4.2

Similar experiments were performed when standard glucose solutions were prepared in pure methanol/water (50:50 v/v) with the concentration range 1.00×10^{-4} to 3.00×10^{-3} M. The QC samples analyzed previously were also analyzed with the standards made from the matrix-free (methanol/water) solvents. This series of experiments will determine if the concentrations and recoveries of the QC samples obtained with pure standards would be different from those determined from standards spiked into matrix. Even though the overall slopes of the two trend lines (for standards in matrix-free vs. matrix-diluted) were statistically determined not to be significantly different, further investigations was deemed necessary since slopes of the two trend lines diverge as the concentration increased, as shown in **Figure 4.4**. Therefore, these studies will determine, statistically, if quantitation of unknowns will be more accurate when matrix-free solvents are used versus using matrix-diluted solutions at specific concentration ranges.

Standards in matrix-free (methanol/water) solvents were prepared in triplicate and run with the QCs. Each concentration level of the QCs was analyzed in triplicate and their average PAR computed, **Table 4.5** shows the obtained data. Percent recovery calculations were also calculated using Equation 4.11 and the results are shown in **Table 4.6** (calibration curves obtained from these standards are shown in **Figures 4.8 – 4.10**). The average percent recoveries for the QCs were found to range from 94.9 to 103.0% with average standard deviations ranging from 1.8 to 5.3. When compared with the recovery values for the QCs analyzed with standards prepared in matrix–diluted solutions (**Table 4.4**), the QCs recoveries obtained with the standards in matrix-free solvents spanned a wider range (with a wider range of standard deviations as well). While an overall matrix effect was shown not to be present when comparing the two slopes, it appears that significant deviation does exist on the higher concentration range. This deviation does influence the accuracy and precision of the measured results. As previously stated, one can null any matrix effects in the analytical method developed if standards for generating the calibration curves were prepared in the same matrix.

Table 4.5. Peak area ratios and the respective standard deviations from standards prepared from matrix-free (methanol/water) solvents analyzed with QCs at three levels of concentration (low, mid, and high). ^aThe blank was used to correct the PAR of the QCs, which were spiked into a blank matrix.

Standards spiked into pure solvent (matrix-free)						
	HQC (2.50×10^{-3} M)		MQC (1.50×10^{-3} M)		LQC (5.00×10^{-4} M)	
Concentration (M)	Average PAR	Standard Deviation	Average PAR	Standard Deviation	Average PAR	Standard Deviation
3.00×10^{-3}	6.2562	0.1777	6.3304	0.2632	6.2643	0.0586
2.00×10^{-3}	4.2548	0.0418	4.1991	0.0833	4.2010	0.0966
1.00×10^{-3}	2.1540	0.0676	2.1317	0.0830	2.1500	0.0402
8.00×10^{-4}	1.9421	0.1588	1.8356	0.0390	1.7992	0.0305
4.00×10^{-4}	1.1228	0.0305	1.1244	0.0150	1.1590	0.1189
1.00×10^{-4}	0.2218	0.0128	0.2173	0.0154	0.2190	0.0127
0 (blank) ^a	0.1630	0.0322	0.1796	0.0727	0.1811	0.0300
QC	5.0100	0.0945	3.0798	0.1466	1.2056	0.0276

Table 4.6. Data generated when determining the percent recovery of control samples spiked into matrix-diluted samples. The QCs were analyzed with glucose standards prepared from matrix-free solvents. ^aAverage PAR was obtained from three replicate runs of the QCs. ^bSD is the standard deviation.

Recovery Calculation for QC Samples Analyzed with Standards in Pure Solvents			
QC Samples	HQC	MQC	LQC
Trend Line Equation	$y = 2032.5x + 0.1858$	$y = 2056.4x + 0.1378$	$y = 2033.6x + 0.1579$
R ²	0.9973	0.9979	0.9976
Average PAR ^a	5.0095	3.0798	1.2056
SD ^b of Average PAR	0.0945	0.1466	0.0276
Calculated Concentration(M)	2.37×10^{-3}	1.43×10^{-3}	5.15×10^{-4}
Actual Concentration(M)	2.50×10^{-3}	1.50×10^{-3}	5.00×10^{-4}
Percent Recovery (%)	94.9	95.4	103.0
SD of Percent Recovery	1.8	5.3	2.2

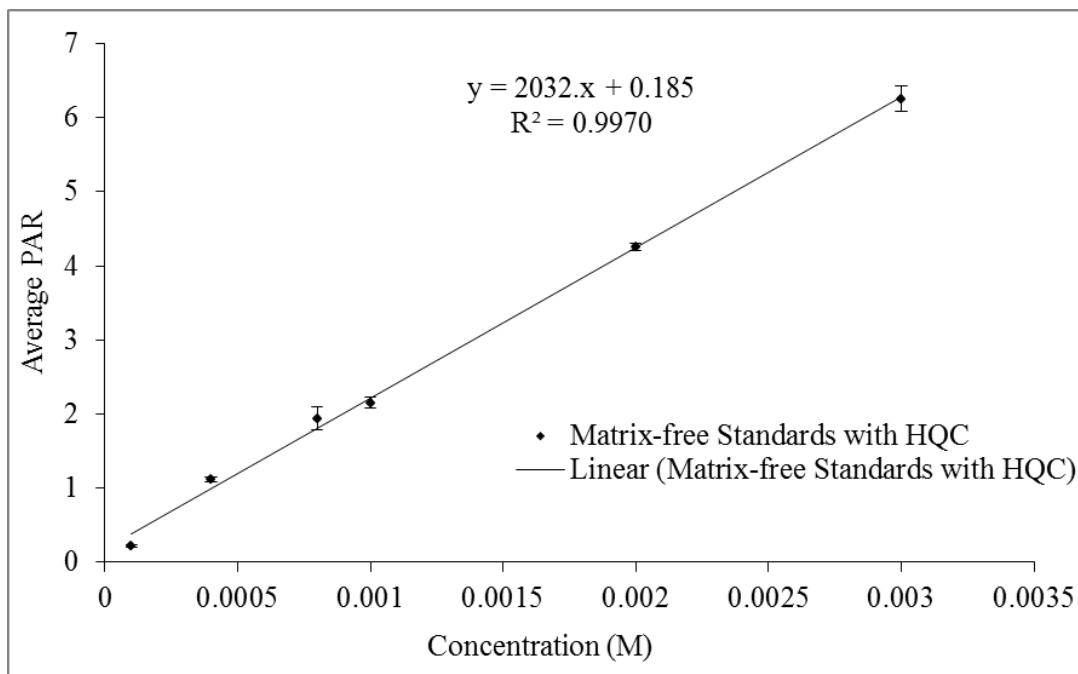


Figure 4.8. A calibration curve was obtained by analyzing glucose standards in pure solvents with high concentration QCs.

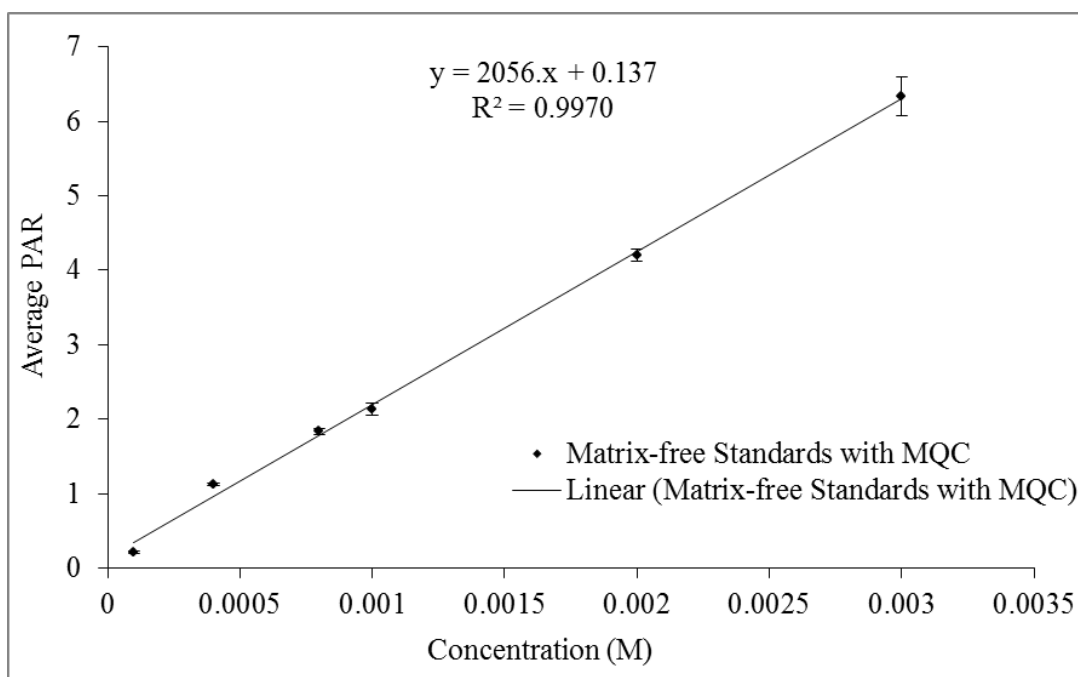


Figure 4.9. A calibration curve was obtained by analyzing glucose standards in pure solvents with mid-range concentration QCs.

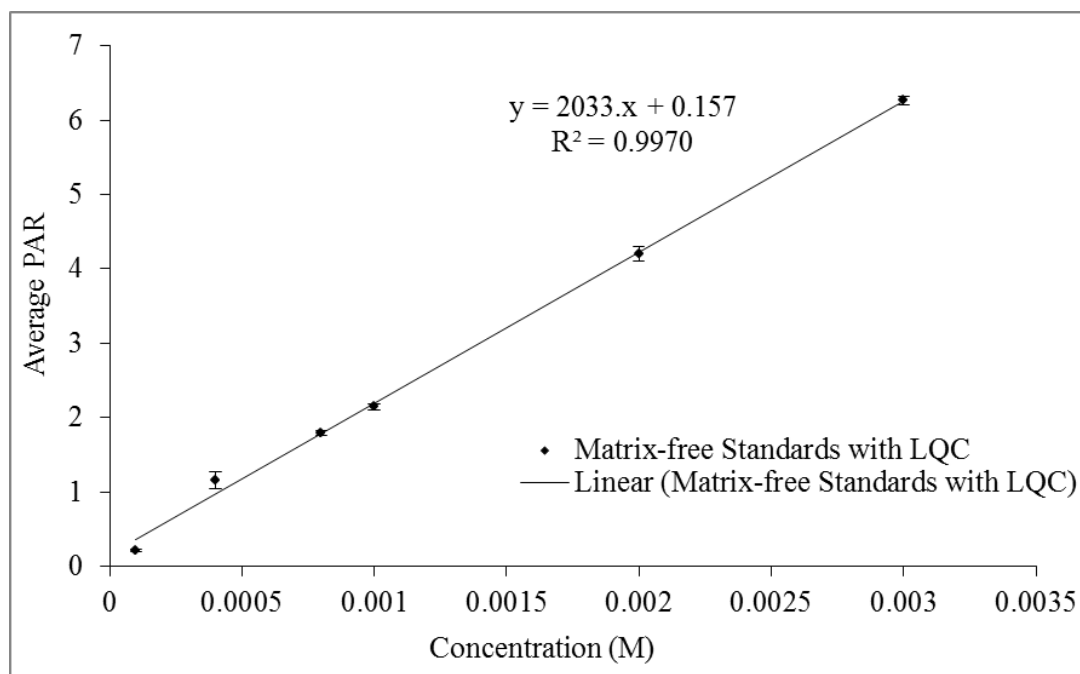


Figure 4.10. A calibration curve was obtained by analyzing glucose standards in pure solvents with low concentration QCs.

The divergence of the calibration lines with respect to percent recoveries (as well as concentration, see Appendix B, **Figures B1 – B3**) can be evaluated statistically to determine if accuracy of the results is influenced when obtained from the matrix-free versus matrix-diluted standards. To determine if the concentrations for the two different sets of measurements (matrix-free versus matrix-diluted) agree within experimental error or if they are significantly different at the three levels of concentrations, replicate measurements are compared using the Student's *t*-test. The data used to calculate the percent recoveries were also used to carry out this statistical computation.

The PAR for each run of the QCs (whose concentrations were known) at the three levels of concentration was obtained and used to compute the “calculated concentration” from the two sets of standards (matrix-free and matrix-diluted). To compare the

“calculated concentrations” from the two sets of measurements, the average calculated concentrations are first determined at each QC level. The \bar{x}_1 and \bar{x}_2 are assigned as the average “calculated concentration” in the matrix-free set and matrix-diluted set (at each concentration level), respectively. Each set of measurement has its own uncertainty and we assume the population standard deviation (σ) for each set to be essentially the same. **Table 4.7** shows the data (concentration expressed in M) used for this analysis, where the label numbers 1, 2, and 3 indicate the three replicates for each QC. The s_1 and s_2 are assigned as the standard deviations for the matrix-free and matrix-diluted sets, respectively.

For the two sets of data consisting of n_1 and n_2 (where $n = 3$ for each set) measurements (with averages \bar{x}_1 and \bar{x}_2), we calculate the value of t with the formula

$$t_{\text{calculated}} = \frac{|\bar{x}_1 - \bar{x}_2|}{S_{\text{pooled}}} \sqrt{\frac{n_1 n_2}{n_1 + n_2}} \quad \text{Equation 4.12}$$

where $|\bar{x}_1 - \bar{x}_2|$ is absolute value of the difference of the means of the two sets and S_{pooled} (Equation 4.13) is a pooled standard deviation making use of both sets of data:¹⁶⁰

$$S_{\text{pooled}} = \sqrt{\frac{\sum_{\text{set1}} (x_i - \bar{x}_1)^2 + \sum_{\text{set2}} (x_j - \bar{x}_2)^2}{n_1 + n_2 - 2}} = \sqrt{\frac{s_1^2 (n_1 - 1) + s_2^2 (n_2 - 1)}{n_1 + n_2 - 2}} \quad \text{Equation 4.13}$$

In Equation 4.13, s_1 and s_2 are the standard deviations for the matrix-free and matrix-diluted standard sets. Using Equations 4.12 and 4.13, the $t_{\text{calculated}}$ values were computed from the data in **Table 4.7** for each level of concentration of the QCs. These values are compared with the t values in the Student's t table (t_{table}) for $n_1 + n_2 - 2$ degrees of freedom as shown in **Table 4.8**.

Table 4.7. Replicate sets of measurements for the calculated concentration of the QCs at different levels of concentrations using the matrix-free and matrix-diluted standards. ^aSD is the standard deviation.

QC Samples	Matrix-free Set		Matrix-diluted Set	
	PAR	Calculated Concentration	PAR	Calculated Concentration
HQC1	4.9761	2.40×10^{-3}	5.1479	2.52×10^{-3}
HQC2	4.9362	2.32×10^{-3}	5.0582	2.45×10^{-3}
HQC3	5.1162	2.40×10^{-3}	5.2606	2.57×10^{-3}
<i>Mean</i> (\bar{x}_1)		2.37×10^{-3}	<i>Mean</i> (\bar{x}_2)	
<i>SD</i> ^a (s_1)		4.45×10^{-5}	<i>SD</i> (s_2)	
MQC1	2.9543	1.35×10^{-3}	3.0846	1.47×10^{-3}
MQC2	3.2410	1.50×10^{-3}	3.2460	1.52×10^{-3}
MQC3	3.0442	1.45×10^{-3}	3.1467	1.45×10^{-3}
<i>Mean</i> (\bar{x}_1)		1.43×10^{-3}	<i>Mean</i> (\bar{x}_2)	
<i>SD</i> (s_1)		7.89×10^{-5}	<i>SD</i> (s_2)	
LQC1	1.2322	5.28×10^{-4}	1.2783	5.34×10^{-4}
LQC2	1.2077	5.07×10^{-4}	1.2359	4.93×10^{-4}
LQC3	1.1770	5.11×10^{-4}	1.2301	5.03×10^{-4}
<i>Mean</i> (\bar{x}_1)		5.15×10^{-4}	<i>Mean</i> (\bar{x}_2)	
<i>SD</i> (s_1)		1.10×10^{-5}	<i>SD</i> (s_2)	

Table 4.8. *t* test results for the statistical comparison of QCs calculated concentration in two sets of standard samples (matrix-free and matrix-diluted) at the three levels of QCs concentrations.

QC Levels	S_{pooled}	$t_{\text{calculated}}$	t_{table} (95% confidence)	Do Measurements Agree?
HQC	2.71×10^{-5}	6.240	2.776	No
MQC	3.02×10^{-5}	1.923	2.776	Yes
LQC	8.40×10^{-6}	0.766	2.776	Yes

From the results shown in **Table 4.8**, the *t*-test calculation failed with the high concentration QCs showing a significant difference does exist between the two measurements but was successful in MQC and LQC levels, showing that no significant difference was present for the mid-range and low concentration QCs. In the HQC level, the $t_{\text{calculated}}$ is 6.240 whereas the t_{table} for four degrees of freedom ($n_1 + n_2 - 2$, $n = 3$ for each set of measurements) is 2.776 at a 95% confidence level. The $t_{\text{calculated}}$ for the mid-range and low concentration QCs were 1.923 and 0.766, respectively. These results indicate that the measurements obtained from the high concentration QCs from the two sets of standards are significantly different because $t_{\text{calculated}} > t_{\text{table}}$. This is revealed by the divergence of the trend lines that was described previously. Therefore, to obtain accurate measurements from unknowns, it is important that the appropriate range of concentrations to be used in the analysis be chosen. Even though there is some observed divergence in the calibration trend lines (when the two curves are put on the same plot) at low concentrations (**Figures B1** and **B2**, Appendix B) the *t*-test analysis shows that the calculated concentrations for the two sets of measurements are not significantly different.

CHAPTER FIVE

CONCLUSIONS AND FUTURE DIRECTIONS

5.1. INTRODUCTION

The extent of biofuels research has undergone a dramatic increase in the last two decades resulting from decreasing petroleum reserves and other non-renewable fossil fuels. Contributing factors also include the insecure dependence on foreign oil reserves as a source of transportation fuel as well as the environmental impact that occurs in the production and consumption of these fossil fuels. The utilization of biomass as a source of renewable energy has been extensively studied with the hope of replacing fossil fuels where the focus has been the development of energy crops that do not compete with food crops (e.g. corn). Herbaceous perennial crops (e.g. switchgrass) have been shown to be a good model energy crop candidate for the United States resulting from unique ecological, physical characteristics, and ability to thrive well in the temperate climate of North America.

Overcoming the degradation recalcitrance of biomass is the biggest challenge in the utilization of biomass as a source of fuel. Technologies have been developed to facilitate such degradation, but are the most expensive process in the production of energy fuels from biomass. Improvement of these technological processes for converting biomass into biofuels has been the focus of many researchers and a variety of pretreatment options are now being used to achieve this conversion with minimal costs. However, the efficiency of such conversion processes cannot be ascertained unless a

robust analytical process is available to quantify the byproducts of the degradation process. It was the goal of this research to develop a fast, easy, and robust method for the quantitation of sugars obtained from switchgrass after pretreatment and subsequent enzymatic hydrolysis. Direct Analysis in Real Time, an ambient mass spectrometry technique, has analyzed sugars obtained from switchgrass after these pretreatment and hydrolysis steps (i.e. saccharification). Since no publications currently exist on the analysis of sugars using DART-MS (with respect to hydrolysis conversion), this study involved the optimization of instrumental parameters for this process to achieve accurate measurement of sugars.

5.2. METHOD CONCLUSIONS

5.2.1. DART Optimization and Validation

The initial experimental optimization of DART-MS for the analysis of sugars was effective in obtaining accurate and optimum measurements for the quantitation of samples. Being an ambient ionization source, DART ionization needs to be optimized since its dynamics is influenced by atmospheric substances as well as the climatic conditions in the analytical room. The optimization of the gas temperature, grid voltage, helium gas pressure, and linear rail voltage was necessary for obtaining consistent measurements with the DART ionization process. It was observed the signal intensity was directly proportional to the heater gas temperature where an optimum temperature of 450 °C was observed to give optimized signals in all measurements. The helium gas pressure was found not to have a significant effect on the signal produced from the variations observed at the different pressures tested. Similarly, grid voltage changes did

not produce significant changes in the signal produced. However, the linear rail speed was a significant factor since running samples using a slower linear rail speed gave the greatest signal resulting from long residence time when a sample was present in the ionization region. One additional important parameter that influenced ion efficiency (and the resulting mass spectrum produced) was the capillary temperature which was optimized at 200 °C to produce the least fragmentation of the peaks used for quantitation.

Analyzing replicate samples at different days allowed validation of the precision and robustness of the method. The use of an internal standard allows reproducible peak area ratios when compared over several days and showed the method can be used repeatedly with low variance. In the process of developing a range for sugar standard for quantitation, a linear range spanning one and a half order of magnitude was obtained and pivotal for quantitation of saccharification samples whose concentrations may vary widely. From the calibration curves, it was apparent that DART-MS can be used for accurate quantitation of sugars; the correlation coefficients were always greater than 0.995. A detailed analysis of matrix effects in switchgrass sample blanks was studied. Calibration curves from matrix-free standards versus matrix-diluted standards were compared and with peak correction, and their slopes were observed to be different, however; statistical analysis was performed and showed no significant matrix effects was present at the dilution levels applied. Student t -test computation was performed and a $t_{\text{calculated}}$ value of 0.050 was obtained as compared to the t_{table} value of 2.228 at a 95% confidence level for the two slopes. This showed that the slopes of the curves were not significantly different and matrix effects would not affect the results for quantitation.

Recoveries experiments performed using quality control samples gave acceptable average percent recoveries. The percent recoveries were performed using three levels of concentrations within the calibration curve; high, mid-range, and low concentration and a comparison of the recoveries from matrix-free and matrix-diluted standards was done. The average percent recoveries ranged from 94.9–103% and 98.6–102% in matrix-free and matrix-diluted standards, respectively. The recoveries from the matrix-diluted standards spanned a smaller range and were shown to provide more accurate measurements when compared to matrix-free standards and were still a better option to null any potential matrix effects at all concentration levels. Statistical computation using the *t*-test was done to determine if there were any differences in the calculated concentration of the control samples from both matrix-free and matrix-diluted standards due to the divergence observed on the curves at higher concentrations. The failing of the *t*-test at higher concentration proved that the divergence was quite significant and it would therefore give inaccurate results and a fine-tuning of the linear range was necessary for accurate quantitation. The DART-MS method was also applied in the determination of the detection limits for the sugar standards and was found to be in the parts per million (ppm) ranges.

5.2.2. Analytical Challenges of the Method

Even though DART-MS was found to be a simple and rapid method for the analysis of sugars, some limitations existed that affected the obtained results. The first challenge was related to the sensitivity of DART in ionizing substances found in the room in which the analysis was done. Even though the temperature of the room was

regulated and the door was always shut, volatile substances found in the building (these substances were present when general cleaning of the building was being done) were easily detected by DART-MS since ionization took place in open atmospheric conditions. This caused competition during analyte ionization and was problematic when the concentration of samples was low. This was prevalent in the determination detection limits of the method. With DART, limits of detection are influenced with environmental conditions of a room and additional control should be in place to avoid signal suppression by substances present in the atmosphere.

Secondly, the analytical process (as available at Eastern Kentucky University) involved a series of manual sample introduction. Unlike the automated techniques such as HPLC, the use of DART required a person perform the analysis and be present to actually perform the runs. Manual application of samples on glass tips was tedious and time consuming and additional time was also required for cleaning the reusable glass tips (e.g. budget restricted the tips to be disposable). An automated DART system having sample wells synchronized to the automated rail system would be an option to be considered to conserve time for personnel by reducing the time required for analysis. Other limitations of the method were related to the DART parameters settings defined by the instrument software. For example, the temperature was fixed at increments of 50 °C and it was not possible to make a temperature change less than 50 °C. This was advantageous especially when fine-tuning parameter optimization. However, based on the small variances of the measurements in this study fine-tuning of the temperatures (ability to change in 10 or 20 °C increments) may not create a dramatic difference in the overall result of measurements.

5.3. FUTURE DIRECTIONS

The optimization and validation of DART-MS for the quantitative analysis of saccharification sugars has opened the door for future experiments for these types of samples. The knowledge of the influence of certain parameters on the signal of the analytes is a stepping stone for other researchers who may want to use or adapt this method for analysis. Ultimately, the data obtained from this work will be indispensable for gaining a better understanding of the operation of the DART-MS technique for quantitative analysis.

5.3.1. Real Switchgrass Sample Analysis

The ultimate goal of this work was to quantify six-carbon sugars obtained from enzymatic hydrolysis of switchgrass following initial pretreatment processes. Even though time was not available to fully achieve this result, preliminary analysis of switchgrass samples indicated that the amount of sugars present in different aliquots originating from different pretreatments was varied. Future work will involve accurate quantification of these sugars after necessary dilutions are done to reduce/eliminate matrix effects. Since blank samples are readily available for this specific analysis, dilution of switchgrass samples into matrix blanks to mimic the matrix composition of the real samples will be an accurate procedure for analyte concentration determination. A defined linear range has been established in the quantitation process – using internal standards, and can be used to determine the peak area ratios of diluted switchgrass samples. The use of blanks will require peak area ratio adjustments/correction because blanks were found to contain a certain unknown concentration of the analyte of interest.

5.3.2. Comparison of Pretreatment Methods

Seven pretreatment methods were applied to switchgrass before enzymatic hydrolysis. The efficiency of each method will be determined by the amount of sugar harvested. Once an accurate concentration is determined for all the samples, a comparative analysis of the methods is done. This will provide valuable information to the biofuel industry in terms of selecting a cost-effective method for degradation of switchgrass. More efficient pretreatment methods can also be proposed for other biomass promising feedstocks.

Before pretreatment was done, switchgrass samples were grinded to various powder sizes (ball milled, 1 mm, and 2 mm sizes). A comparison of the switchgrass samples in terms of the initial sizes can also be done to determine if the size of the powder particles had any effect of the final concentration of six-carbon sugars. This will provide valuable information to the biorefinery industry about the most effective mechanical comminution technique for biomass size reduction.

5.4. CLOSING REMARKS

Since its introduction, DART has proven to be a technique of choice among ambient ionization techniques. While this method has been used mainly for qualitative analysis, this study has proved that the technique is equally useful in quantitative analysis. For the first time, this study had validated DART-MS as a method that can be used for quantitation of sugars in lignocellulosic biomass. This is just the beginning of an ongoing biofuel research work. Being a relatively new analytical method, DART-MS has been shown to have the potential of providing accurate quantitative data required for

biofuel advancement. With switchgrass being the focus of this study, DART-MS can also be applied to other lignocellulosic feedstocks for the advancement of the biofuel industry.

LIST OF REFERENCES

1. Bradshaw, M. J. Global Energy Dilemmas: A Geographical Perspective. *The Geographical Journal*. **2010**, 176, 275-29.
2. EIA (US Energy Information Administration) Annual Energy Outlook 2011. <http://www.eia.gov/forecasts/aeo/pdf/0383%282011%29.pdf> (accessed July 23, 2011).
3. Serrano-Ruiz, J. C.; Dumesic, J. A. Catalytic Routes for the Conversion of Biomass into Liquid Hydrocarbon Transport Fuels. *Energy Environ. Sci.* **2011**, 4, 83-99.
4. EIA Annual Energy Review 2009. <http://www.eia.gov/aer/pdf/aer.pdf> (accessed July 25, 2011).
5. Eurostat, Statistical Aspects of the Energy Economy 2008, Issue Number 55/2009. http://epp.eurostat.ec.europa.eu/cache/ITY_OFFPUB/KS-SF-09-055/EN/KS-SF-09-055-EN.PDF (accessed July 23, 2011).
6. EIA Annual Energy Review 2010. <http://www.eia.gov/aer/pdf/aer.pdf> (accessed July 30, 2011).
7. Muneer, M. A. T. Energy Supply, its Demand and Security Issues for Developed and Emerging Economies. *Renewable and Sustainable Energy Reviews*. **2007**, 11, 1388-1413.
8. BP Statistical review of World Energy 2010. <http://bp.com/statisticalreview>, (accessed August 2, 2011).
9. Paterson, N. R. Global Warming: A Critique of the Anthropogenic Model and its Consequences. *Geoscience Canada*. **2011**, 38, 41-48.
10. Outka, U. Siting Renewable Energy: Land Use and Regulatory Context. *Ecology Law Quarterly*. **2010**, 37, 1041-1105.
11. Helmut T. Photovoltaic Hydrogen Generation. *International Journal of Hydrogen Energy*. **2008**, 33, 5911-5930.
12. Resch, G.; Held, A.; Faber, T.; Panzer, C.; Toro, F.; Hass, R. Potentials and Prospects for Renewable Energies at Global Scale. *Energy Policy*. **2008**, 36, 4048-4056.
13. Sullivan, P. W.; Blair, N. in *Modeling the Benefits of Storage Technologies to Wind Power*, Proceedings of the American Wind Energy Association (AWEA) WindPower 2008 Conference, June 2008, Golden, CO.
14. Pelc, R.; Fujita, R. M. Renewable Energy from the Ocean. *Marine Policy*. **2002**, 26, 471-479.
15. Kreith F.; Goswami, D. Y. *Handbook of Energy Efficiency and Renewable Energy*, CRC Press: Taylor and Francis Group, Boca Raton, FL, 2007.

16. Ragauskas, A. J. *et al.* The Path Forward for Biofuels and Biomaterials. *Science*. **2006**, *311*, 484-489.
17. Alonso, D. M.; Bond, J. Q.; Dumesic, J. A. Catalytic Conversion of Biomass to Biofuels. *Green Chem.* **2010**, *12*, 1493-1513.
18. Abbasi, T.; Abbasi, S. A. Biomass Energy and the Environmental Impacts Associated with its Production and Utilization. *Renewable and Sustainable Energy Review*. **2010**, *14*, 919-937.
19. Caldbeck, B. *et al.* US Canola Digest, Ed., Dansby, A. Vol. 4, Number 3, 2009.
20. Cocks, F. H. *Energy Demand and Climate Change: Issues and Resolutions*. Wiley-VCH Verlag GmbH & Co. Weinheim. 2009.
21. Brune, M. *Coming Clean: Breaking America's Addiction to Oil and Coal*, Sierra Club Books, 2008.
22. Smeets, E. M. W.; Bouwman, L. F.; Stehfest, E.; Vuuren, D. P. V.; Posthuma, A. Contribution of N₂O to the Greenhouse Gas Balance of First-Generation Biofuels. *Global Change Biology*. **2009**, *15*, 1-23.
23. Papini, A.; Simeone, M. C. Forest Resources for Second Generation Biofuel Production. *Scandinavian Journal of Forest Research*. **2010**, *25*, 126-133.
24. Tilman, D.; Hill, J.; Lehman, C. Carbon-negative Biofuels from Low-Input High-Diversity Grassland Biomass. *Science*. **2006**, *314*, 1598-1600.
25. Saxena, R. C.; Adhikari, D. K.; Goyal, H. B. Biomass-based Energy Fuel through Biochemical Routes: A Review. *Renewable and Sustainable Energy Reviews*. **2009**, *13*, 167-178.
26. Rakshit, S. K. Sustainable Transport of Second Generation Liquid Biofuels: The Way Forward. *Journal of Renewable and Sustainable Energy*. **2010**, *2*, 031010.
27. Aresta, M.; Dibenedetto, A.; Barberio, G. Utilization of Macro-Algae for Enhanced CO₂ Fixation and Biofuels Production: Development of a Computing Software for an LCA Study. *Fuel Processing Technology*. **2005**, *86*, 1679-1693.
28. Jing, L.; Con, S.; Pengcheng, F. Metabolic Engineering of Algae for Fourth Generation Biofuels Production. *Energy & Environmental Science*. **2011**, *4*, 2451-2466.
29. Searchinger, T.; Heimlich, R.; Houghton, R.; Dong, F.; Elobeid, A.; Fabiosa, J.; Tokgoz, S.; Hayes, D.; Yu, T. Use of U.S. Croplands for Biofuels Increases Greenhouse Gases through Emissions from Land Use Change. *Science*. **2008**, *319*, 1157-1268.
30. Pimentel, D.; Marklein, A.; Toth, M.A.; Karpoff, M. N.; Paul, G. S.; McCormack, R.; Kyriazis, J.; Krueger, T. Food Versus Biofuels: Environmental and Economic Costs. *Human Ecology*. **2009**, *37*, 1-12.
31. Chisti, Y. Biodiesel from Microalgae. *Biotechnology Advances*. **2007**, *25*, 294-306.

32. Scharlemann, J. P. W.; Laurance, W. F. Environmental Science: How Green are Biofuels? *Science*. **2008**, *319*, 43-44.
33. Francis, G.; Edinger, R.; Becker, K. A Concept for Simultaneous Wasteland Reclamation, Fuel Production, and Socio-Economic Development in Degraded Areas in India: Need, Potential and Perspectives of Jatropha Plantations. *Natural Resources Forum*. **2005**, 12-24.
34. Hamelinck, C.; Faaij, A. Outlook for Advanced Biofuels. *Energy Policy*. **2006**, *34*, 3268-3283.
35. Chari, K. B.; Abbasi, S. A. Study on the Aquatic and Amphibious Weeds of Oussudu Lake. *Hydrology Journal*. **2005**, *28*, 89-98F.
36. Abbasi, S. A.; Abbasi, N. The Likely Adverse Environmental Impacts of Renewable Energy Sources. *Applied Energy*. **2000**, *65*, 121-144.
37. Smil, V. Nitrogen in Crop Production: An Account of Global Flows. *Biogeochemical Cycles*. **1999**, *13*, 647-662.
38. Gitay, H. A.; Suarez, T. In: W. D. J.; Dokken, Ed. in *Climate Change and Biodiversity. IPCC Technical Paper V*. Intergovernmental Panel on Climate Change: Geneva, 2002.
39. Perez, J.; Dorado, J. M.; Rubia, T. D.; Martinez, J. Biodegradation and Biological Treatment of Cellulose, Hemicellulose, and Lignin: An Overview. *Int. Microbiol.* **2002**, *5*, 53-63.
40. Kumar, P.; Barrett, D. M.; Delwiche, M. J.; Stroeve, P. Methods for Pretreatment of Lignocellulosic Biomass for Efficient Hydrolysis and Biofuel Production. *Ind. Eng. Chem. Res.* **2009**, *48*, 3713-3729.
41. Kuhad, R. C.; Singh, A.; Eriksson, K. E. Microorganisms and Enzymes Involved in Degradation of Plant Fiber Cell Walls. *Adv. Biochem. Eng./Biotechnol.* **1997**, *57*, 45-125.
42. Kumar, M. N. S.; Mohanty, A. K.; Erickson, L.; Misra, M. Lignin and Its Application with Polymers. *J. Biobased Materials and Bioenergy*. **2009**, *3*, 1-24.
43. Lee, J. Biological Conversion of Lignocellulosic Biomass to Ethanol. *Journal of Biotechnology*. **1997**, *56*, 1-24.
44. Chang, V. S.; Nagwani, M.; Kim, C.; Holtzaple, M. T. Oxidative Lime Pretreatment of High-Lignin Biomass. *Applied Biochemistry and Biotechnology*. **2001**, *94*, 1-28.
45. Wright, L.; Turhollow, A. Switchgrass Selection as a "Model" Bioenergy Crop: A History of the Process. *Biomass and Bioenergy*. **2010**, *34*, 851-868.
46. McLaughlin, S. B.; Kszos, L. A. Development of Switchgrass (*Panicum virgatum*) as a Bioenergy Feedstock in the United States. *Biomass and Bioenergy*. **2005**, *28*, 515-535.

47. McLaughlin, S. B.; Walsh, M. E. Evaluating Environmental Consequences of Producing Herbaceous Crops for Bioenergy. *Biomass and Bioenergy*. **1998**, *14*, 317-324.
48. Rinehart, L. Switchgrass as a Bioenergy Crop. P. Driscoll, Ed. *ATTRA –National Sustainable Agriculture Information Service*. **2006**, 1-12.
49. Lemus, R.; Brummer, E. C.; Moore, K. J.; Molstad, N. E.; Burras, C. L.; Baker, M. F. Biomass Yield And Quality of 20 Switchgrass Populations in Southern Iowa, USA. *Biomass and Bioenergy*. **2002**, *23*, 433-442.
50. Cherney, J. H.; Johnson, K. D.; Volenec, J. J.; Anliker, K. S. Chemical Composition of Herbaceous Grass and Legume Species Grown for Maximum Biomass Production. *Biomass*. **1988**, *17*, 215-238.
51. Wright, L. L. Production Technology Status of Woody and Herbaceous Crops. *Biomass and Bioenergy*. **1994**, *6*, 191-209.
52. Parrish, D. J.; Fike, J. H. The Biology and Agronomy of Switchgrass for Biofuels. *Critical Reviews in Plant Sciences*. **2005**, *24*, 423-459.
53. Murray, L. D.; Best, L. B.; Jacobsen, T. J.; Braster, M. L. Potential Effects on Grassland Birds of Converting Marginal Cropland to Switchgrass Biomass Production. *Biomass Bioenergy*. **2003**, *25*, 167-175.
54. Roth, A. M.; Sample, D. W.; Ribic, C. A.; Paine, L.; Undersander, D. J.; Bartelt, G. A. Grassland Bird Response to Harvesting Switchgrass as a Biomass Energy Crop. *Biomass Bioenergy*. **2005**, *28*, 490-498.
55. Harper, C. A.; Keyser, P. D. Potential Impacts on Wildlife of Switchgrass Grown for Biofuels. UT Extension #SP704-A. <https://utextension.tennessee.edu/publications/Documents/SP704-A.pdf> (Accessed July 22, 2011).
56. Zhiqin, M. Carbon Sequestration by Switchgrass. PhD. Dissertation, Auburn University, Auburn, AL. 1999: <http://adsabs.harvard.edu/abs/1999PhDT.....73M> (Accessed June 19, 2011).
57. Samson, R. A.; Omielan, J. A. *Switchgrass: A Potential Biomass Energy Crop for Ethanol Production*, In: *The Thirteenth North American Prairie Conference*, Windsor, Ontario, 1992, pg. 253-258.
58. Parrish, D. J.; Wolf, D. D.; Fike, J. H.; Daniels, W. L. Switchgrass as a Biofuels Crop for The Upper Southeast: Variety Trials and Cultural Improvements. Final Report for 1997-2001, ORNL/SUB-03-19XSY163/01, Oak Ridge National Laboratory, TN, 2003.
59. Wright, L. Screening of Herbaceous Species for Energy Crop Production: Final Report 1985-1990, ORNL/Sub/85-27411/5. Oak Ridge National Laboratory, Oak Ridge, TN 1990.

60. Stout, W. L.; Jung, G. A.; Shaffer, J. A. Effects of Soil and Nitrogen on Water use and Efficiency of Tallfescue and Switchgrass under Humid Conditions. *Soil Science Society American Journal*. **1988**, *52*, 429-434.
61. Moser, L. E.; Vogel, K. P. Switchgrass, Big Bluestem, and Indiangrass. In: *Forages Vol 1, An Introduction to Grassland Agriculture*, ed. R. F. Barnes, D. A. Miller, and C. J. Nelson. Iowa State University Press, Ames, IO, 1995.
62. Zheng, Y.; Pan, Z.; Zhang, R. Overview of Biomass Pretreatment for Cellulosic Ethanol Production. *Int. J. Agric. & Biol. Eng.* **2009**, *2*, 51-68.
63. McMillan, J. D. Pretreatment of Lignocellulosic Biomass. In *Enzymatic Conversion of Biomass for Fuel Production*; Himmel, M. E.; Baker, J. O.; Overend, R. P. eds.; American Chemical Society, Washington, 1994.
64. Palmqvist, E.; Hahn-Hagerdal, B. Fermentation of Lignocellulosic Hydrolyzates. II: Inhibitors and Mechanisms of Inhibition. *Bioresource Technol.* **2000**, *74*, 25-33.
65. Wyman, C. E. Biomass Ethanol: Technical Progress, Opportunities, and Commercial Challenges. *Annu. Rev. Energy Env.* **1999**, *24*, 189-226.
66. Millet, M. A.; Baker, A. J.; Satter, L. D. Physical and Chemical Pretreatments for Enhancing Cellulose Saccharification. *Biotech. Bioeng. Symp.* **1976**, *6*, 125-153.
67. Ma, H.; Liu, W. W.; Chen, X.; Wu, Y. J.; Yu, Z. L. Enhanced Enzymatic Saccharification of Rice Straw by Microwave Pretreatment. *Bioresource Technology*. **2009**, *100*, 1279-1284.
68. Lu, Y. P.; Yang, B.; Gregg, D.; Saddler, J. N.; Mansfield, S. D. Cellulase Adsorption and Evaluation of Enzyme Recycle During Hydrolysis of Steam-Exploded Softwood Residues. *Appl. Biochem. Biotechnol.* **2002**, *99*, 7553-7564.
69. Isci, A.; Himmelsbach, J. N.; Pometto III, A. L.; Raman, D. R.; Anex, R. P. Aqueous Ammonia Soaking of Switchgrass followed by Simultaneous Saccharification and Fermentation. *Appl. BiochemBiotechnol.* **2008**, *144*, 69-77.
70. Wang, Z.; Keshwani, D. R.; Redding, A. P.; Cheng, J. J. Alkaline Pretreatment of Coastal Bermudagrass for Bioethanol Production, In *ASABE Annual International Meeting*, Rhode Island. 2008.
71. Sun, Y.; Cheng, J. Hydrolysis of Lignocellulosic Materials for Ethanol Production: A Review. *Bioresource Technol.* **2002**, *83*, 1-11.
72. Xu, J.; Cheng, J. J. Pretreatment of Switchgrass for Sugar Production with the Combination of Sodium Hydroxide and Lime. *Bioresource Technology*. **2011**, *102*, 3861-3868.
73. Goldstein, I. S.; Pereira, H.; Pittman, J. L.; Strouse, B. A.; Scaringelli, F. P. The hydrolysis of Cellulose with Superconcentrated Hydrochloric Acid. *Biotechnol. Bioeng.* **1983**, *13*, 17-25.

74. Israilides, C. J.; Grant, G. A.; Han, Y. W. Sugar Level, Fermentability, and Acceptability of Straw Treated with Different Acids. *Appl. Environ. Microbiol.* **1978**, *36*, 43-46.
75. Dien, B. S.; Jung, H-J. G.; Vogel, K. P. *et al.* Chemical Composition and Response to Dilute-Acid Pretreatment and Enzymatic Saccharification of Alfalfa, Reed Canarygrass, and Switchgrass. *Biomass Bioenergy.* **2006**, *30*, 880-891.
76. Ladisch, M. R.; Lin, K. W.; Voloch, M.; Tsao, G. T. Process Consideration in the Enzymatic Hydrolysis of Biomass. *Enzyme Microb. Technol.* **1983**, *5*, 82-102.
77. MacLellan, J. Strategies to Enhance Enzymatic Hydrolysis of Cellulose in Lignocellulosic Biomass. *Basic Biotechnology.* **2010**, *6*, 31-35.
78. Pathak, A. N.; Ghose, T. K. Cellulases I, Sources and Technology. *Process Biochem.* **1973**, *8*, 35-38.
79. Taherzadeh, M. J.; Karimi, K. Enzyme-based Hydrolysis Processes for Ethanol from Lignocellulosic Materials: A Review. *BioResources.* **2007**, *2*, 707-738.
80. Tengborg, C.; Galbe, M.; Zacchi, G. Influence of Enzyme Loading and Physical Parameters on the Enzyme Hydrolysis of Steam-Pretreated Softwood. *Boitechnol.Prog.* **2001**, *17*, 110-117.
81. Taherzadeh, M. J.; Karimi, K. Process for Ethanol Production from Lignocellulosic Materials I: Acid-Based Hydrolysis Processes. *BioResources.* **2007**, *2*, 472-499.
82. Linde, M.; Galbe, M.; Zacchi, G. Simultaneous Saccharification and Fermentation of Steam-Pretreated Barley Straw at Low Enzyme Loadings and Low Yeast Concentration. *Enzyme Microb. Technol.* **2007**, *40*, 1100-1107.
83. Shehaan, J. S.; Himmel, M. E. Outlook for Bioethanol Production from Lignocellulosic Feedstocks: Technology Hurdles. *Agro. Food Ind. Hi-Tech.* **2001**, *12*, 54-57.
84. Miller, G. L. Use of *Dinitrosalicylic Acid Reagent for Determination of Reducing Sugars.* *Anal. Chem.* **1959**, *31*, 426-428.
85. Dubois, M.; Gilles, K. A.; Hamilton, J. K.; Rebers, P. A.; Smith, F. Colorimetric Method for Determination of Sugars and Related Substances. *Anal. Chem.* **1956**, *28*, 350-356.
86. Ko, J. H.; Huang, H.; Kang, G. W.; Cheong, W. J. Simultaneous Quantitative Determination of Monosaccharides Including Fructose in Hydrolysates of Yoghurt and Orange Juice Products by Derivatization of Monossaccharides with P-Aminobenzoic Acid Ethyl Ester Followed by HPLC. *Bull. Korean Chem. Soc.* **2005**, *26*, 1533-1538.
87. Gusakov, A. V.; Kondratyeva, E. G.; Sinitsyn A. P. Comparison of Two Methods for Assaying Reducing Sugars in the Determination of Carbohydrase Activities. *International Journal of Analytical Chemistry.* **2011**, *2011*, 1-4.

88. Hall, M. B. Challenges with Non-Fiber Carbohydrate Methods. *J. Anim. Sci.* **2003**, *81*, 3226-3232.
89. Fox, A.; Lau, P. Y.; Brown, A.; Morgan, S. L.; Zhu, Z.-T.; Lema, M.; Walla, M. D. Capillary Gas Chromatographic Analysis of Carbohydrates of *Legionella pneumophila* and Other Members of The Family *Legionellaceae*. *Journal of Clinical Microbiology.* **1984**, *19*, 326-332.
90. Silva, F. O. Microwave-assisted Derivatization of Glucose and Galactose for Gas Chromatographic Determination in Human Plasma. *Clinical Chemistry.* **2006**, *52*, 334-336.
91. Martinez-Castro, I. et al. Derivatization of Carbohydrates for GC and GC-MS Analyses. *Journal of Chromatography.* **2011**, *879*, 1226 -1240.
92. Karagoz, S.; Bhaskar, T.; Muto, A.; Sakata, Y. Comparative Studies of Oil Compositions Produced from Sawdust, Rice Husk, Lignin and Cellulose by Hydrothermal Treatment. *Fuel.* **2004**, *84*, 857-884.
93. Cayle, T.; Viebrock, F.; Schiaffino, J. Gas Chromatography of Carbohydrates. *Cereal Chemistry.* **1968**, *45*, 154-161.
94. Luo , P.; Luo, M. Z.; Baldwin, R. P. Determination of Sugars in Food Products: Using HPLC and Electrochemical Detection at a Cu Electrode. *J. Chem. Educ.* **1993**, *70*, 679-681.
95. Chavez-Servin, J. L.; Castellote, A. I.; Lopez-Sabater, M. C. Analysis of Mono- and Disaccharides in Milk-Based Formulae by High-Performance Liquid Chromatography with Refractive Index Detection. *J. Chromatography A.* **2004**, *1043*, 211-215.
96. Bernal, J. L.; Del Nozal, M. J.; Toribio, L.; Del Alamo, M. HPLC Analysis of Carbohydrates in Wines and Instant Coffees using Anion Exchange Chromatography Coupled to Pulsed Amperometric Detection. *J. Agric. Food Chem.* **1996**, *44*, 507-511.
97. Wei, Y.; Ding, M-Y. Analysis of Carbohydrates in Drinks by High-Performance Liquid Chromatography with a Dynamically Modified Amino Column and Evaporative Light Scattering Detection. *J. Chromatography.* **2000**, *904*, 113-117.
98. Wan, E. C.; Yu, J. Z. Determination of Sugar Compounds in Atmospheric Aerosols by Liquid Chromatography Combined with Positive Electrospray Ionization Mass Spectrometry. *J. Chromatography A.* **2006**, *1107*, 175-181.
99. Zhu, X.; Sato, T. The Distinction of Underivatized Monosaccharides using Electrospray Ion Trap Mass Spectrometry. *Rapid Commun. Mass Spectrom.* **2007**, *21*, 191-198.
100. Taormina, C. R.; Baca, J. T.; Asher, S. A.; Grabowski, J. J. Analysis of Tear Glucose Concentration with Electrospray Ionization Mass Spectrometry. *J. Am. Soc. Mass Spectrom.* **2007**, *18*, 332-336.

101. Choi, S-S.; Kim, J-C. Deuterium Effect on Ionization and Fragmentation Patterns of Monosaccharides Ionized by Atmospheric Pressure Chemical Ionization. *Carbohydrate Research*. **2010**, *345*, 408-413.
102. Bereman, M. S.; Williams, T. I.; Muddiman, D. C. Carbohydrate Analysis by Desorption Electrospray Ionization Fourier Transform Ion Cyclotron Resonance Mass Spectrometry. *Anal. Chem.* **2007**, *79*, 8812-8815.
103. Downard, K. *Mass Spectrometry: A Foundation Course*, Royal Society of Chemistry: Cambridge, UK, 2004.
104. Skoog, D. A.; Holler, F. J.; Nieman, T. A. *Principles of Instrumental Analysis*, Harcourt Brace & Company: Orlando, Florida, 1998.
105. De Hoffmann, E.; Stroobant, V. *Mass Spectrometry: Principles and Applications*, 3rd ed.; John Wiley & Sons: West Sussex, England, 2007.
106. Watson, J. T.; Sparkman, O. D. *Introduction to Mass Spectrometry: Instrumentation, Applications and Strategies for Data Interpretation*, John Wiley & Sons: West Sussex, England, 2007.
107. Harris, G. A.; Galhena, A. S.; Fernandez, F. M. Ambient Sampling/Ionization Mass Spectrometry: Applications and Current Trends. *Anal. Chem.* **2011**, *83*, 4508-4538.
108. Alberici, R. M.; Simas, R. C.; Sanvido, G. B.; Romao, W.; Lalli, P. M.; Benassi, M.; Cunha, I. B. S.; Eberlin, M. N. Ambient Mass Spectrometry: Bringing MS into the "Real World". *Anal. Bioanal. Chem.* **2010**, *398*, 265-294.
109. Huang, M. Z.; Yuan, C. H.; Cheng S. Y.; Cho, Y. T.; Shiea, J. Ambient Ionization Mass Spectrometry. *Ann. Rev. Anal. Chem.* **2010**, *3*, 43-65.
110. Hirabayashi, A.; Sakairi, M.; Koizumi, H. Sonic Spray Mass Spectrometry. *Anal. Chem.* **1995**, *67*, 2878-2882.
111. Cody, R. B.; Laramee, J. A.; Durst, H. D. Versatile New Ion Source for the Analysis of Materials in Open Air under Ambient Conditions. *Anal. Chem.* **2005**, *77*, 2297-2302.
112. Laramee, J. A.; Cody, R. B. Method for Atmospheric Pressure Analyte Ionization. U.S. Patent 7, 112, 785, September, 26, 2006.
113. Cody, R. B.; Laramee, J. A.; Durst, H. D. Direct Analysis in Real Time Mass spectrometry. *JEOL News*. **2005**, *40*, 8-12.
114. Cody, R. B. Observation of Molecular Ions and Analysis of Nonpolar Compounds with Direct Analysis in Real Time Ion Source. *Anal. Chem.* **2009**, *81*, 1101-1107.
115. Nilles, J. M.; Connell, T. R.; Stokes, S. T.; Durst, H. D. Explosives Detection using Direct Analysis in Real Time (DART) Mass Spectrometry. *Propellants, Explosives, Pyrotechnics*. **2010**, *35*, 446-451.
116. Song, L.; Dykstra, A. B.; Yao, H.; Bartmess, J. E. Ionization Mechanism of Negative Ion-Direct Analysis in Real Time: A Comparative Study with Negative

- Ion-Atmospheric Pressure Photoionization. *J. Am. Soc. Mass Spectrom.* **2009**, *20*, 42-50.
117. Song, L.; Gibson, S. C.; Bhandari, D.; Cook, K. D.; Bartmess, J. E. Ionization Mechanism of Positive-Ion Direct Analysis in Real Time: A Transient Microenvironment Concept. *Anal. Chem.* **2009**, *81*, 10080-10088.
 118. Yu, S.; Crawford, E.; Tice, J.; Musselman, B.; Wu, J. T. Bioanalysis without Sample Cleanup or Chromatography: The Evaluation and Initial Implementation of Direct Analysis in Real Time Ionization Mass Spectrometry for the Quantification of Drugs in Biological Matrixes. *Anal. Chem.* **2009**, *81*, 193-202.
 119. Nyadong, L.; Harris, G. A.; Balayssac, S.; Galhena, A. S.; Malet-Martino, M.; Martino, R.; Parry, R. M.; Wang, M. D.; Fernandez, F. M.; and Gilard, V. Combining Two-Dimensional Diffusion-Ordered Nuclear Magnetic Resonance Spectroscopy, Imaging Desorption Electrospray Ionization Mass Spectrometry, and Direct Analysis in Real-Time Mass Spectrometry for the Integral Investigation of Counterfeit Pharmaceuticals. *Anal. Chem.* **2009**, *81*, 4803-4812.
 120. Helmy, R.; Schafer, W.; Buhler, L.; Marcinko, S.; Musselman, B.; Guidry, E.; Jenkins, H.; Fleitz, F.; Welch, C. J. Ambient Pressure Desorption Ionization Mass Spectrometry in Support of Preclinical Pharmaceutical Development. *Org. Process Res. Dev.* **2010**, *14*, 386-392.
 121. Zhou, M.; Guan, W.; Walker, L. D.; Mezencev, R.; Benigno, B. B.; Gray, A.; Fernandez, F. M.; McDonald, J. F. Rapid Mass Spectrometric Metabolic Profiling of Blood Sera detects Ovarian Cancer with High Accuracy. *Cancer Epidemiol. Biomarkers Prev.* **2010**, *19*, 2262-2271.
 122. Navare, A. T.; Mayoral, J. G.; Nouzova, M.; Noriega, F. G.; Fernandez, F. M. Rapid Direct Analysis in Real Time (DART) Mass Spectrometric Detection of Juvenile Hormone III and its Terpene Precursors. *Anal. Bioanal. Chem.* **2010**, *398*, 3005-3013.
 123. Bennett, M. J.; Steiner, R. R. Detection of GHB in Various Drink Matrices via AccuTOF-DART™. *J. Forensic Sci.* **2009**, *54*, 370-375.
 124. Nilles, J. M.; Connell, T. R.; Durst, H. D. Quantitation of Chemical Warfare Agents using Direct Analysis in Real Time (DART) Technique. *Anal. Chem.* **2009**, *81*, 6744-6749.
 125. Nilles, J. M.; Connell, T. R.; Durst, H. D. Thermal Separation to Facilitate Direct Analysis in Real Time (DART) of Mixtures. *Analyst.* **2010**, *135*, 883-886.
 126. Nilles, J. M.; Connell, T. R.; Stokes, S. T.; Durst, D. H. Explosives Detection Using Direct Analysis in Real Time (DART) Mass Spectrometry. *Propellants, Explo. Pyrotech.* **2010**, *35*, 446-451.
 127. Bevilacqua, V. L.; Nilles, J. M.; Rice, J. S.; Connell, T. R.; Schenning, A. M.; Reilly, L. M.; Durst, H. D. Ricin Activity Assay by Direct Analysis in Real Time Mass Spectrometry Detection of Adenine Release. *Anal. Chem.* **2010**, *82*, 798-800.
 128. Jagerdeo, E.; Abdel-Rehim, M. Screening of Cocaine and Its Metabolites in Human Urine Samples by Direct Analysis in Real-Time Source Coupled to Time-of-Flight Mass Spectrometry After Online Preconcentration Utilizing

- Microextraction by Packed Sorbent. *J. Am. Soc. Mass Spectrom.* **2009**, *20*, 891-899.
129. Steiner, R. R.; Larson, R. L. Validation of the Direct Analysis in Real Time Source for Use in Forensic Drug Screening. *J. Forensic Sci.* **2009**, *54*, 617-622.
 130. Curtis, M. E.; Jones, P. R.; Sparkman, O. D.; Cody, R. B. Determination of the Presence or Absence of Sulfur Materials in Drywall Using Direct Analysis in Real Time in Conjunction with an Accurate-Mass Time-of-Flight Mass Spectrometer. *J. Am. Soc. Mass Spectrom.* **2009**, *20*, 2082-2086.
 131. Haunschmidt, M.; Klampfl, C. W.; Buchberger, W.; Hertsens, R. Determination of Organic UV Filters in Water by Stir Bar Sorptive Extraction and Direct Analysis in Real-Time Mass Spectrometry. *Anal. Bioanal. Chem.* **2010**, *397*, 269-275.
 132. Borges, D. L. G.; Sturgeon, R. E.; Welz, B.; Curtius, A. J.; Mester, Z. Ambient Mass Spectrometric Detection of Organometallic Compounds Using Direct Analysis in Real Time. *Anal. Chem.* **2009**, *81*, 9834-9839.
 133. Domin, M. A.; Steinberg, B. D.; Quimby, J. M.; Smith, N. J.; Greene, A. K.; Scott, L. T. Routine Analysis and Characterization of Highly Insoluble Polycyclic Aromatic Compounds by Direct Analysis in Real Time Mass Spectrometry (DART). *Analyst.* **2010**, *135*, 700-704.
 134. Jones, R. W.; Reinot, T.; McClelland, J. F. Molecular Analysis of Primary Vapor and Char Products during Stepwise Pyrolysis of Poplar Biomass. *Energy & Fuel.* **2010**, *24*, 5199-5209.
 135. Ackerman, L. K.; Noonan, G. O.; Begley, T. H. Assessing Direct Analysis in Real-Time-Mass Spectrometry (DART-MS) for the Rapid Identification of Additives in Food Packaging. *Food & Addit. Contam.* **2009**, *26*, 1611-1618.
 136. Vaclavik, L.; Rosmus, J.; Popping, B.; Hajslova, J. Rapid Determination of Melamine and Cyanuric Acid in Milk Powder using Direct Analysis in Real Time-Time-of-Flight Mass Spectrometry. *J. Chromatogr. A.* **2010**, *1217*, 4204-4211.
 137. Dane, A. J.; Cody, R. B. Selective Ionization of Melamine in Powdered Milk by using Argon Direct Analysis in Real Time (DART) Mass Spectrometry. *Analyst.* **2010**, *135*, 696-699.
 138. Vaclavik, L.; Zachariasova, M.; Hrbek, V.; Hajslova, J. Analysis of Multiple Mycotoxins in Cereals under Ambient Conditions using Direct Analysis in Real Time (DART) Ionization Coupled to High Resolution Mass Spectrometry. *Talanta.* **2010**, *82*, 1950-1957.
 139. Zachariasova, M.; Cajka, T.; Godula, M.; Malachova, A.; Veprikova, Z.; Hajslova, J. Analysis of Multiple Mycotoxins in Beer Employing (Ultra)-High-Resolution Mass Spectrometry. *Rapid Commun. Mass Spectrom.* **2010**, *24*, 3357-3367.
 140. Edison, S. E.; Lin, L. A.; Gamble, B. M.; Wong, J.; Zhang, K. Surface Swabbing Technique for the Rapid Screening for Pesticides using Ambient Pressure Desorption Ionization with High-Resolution Mass Spectrometry. *Rapid Commun. Mass Spectrom.* **2011**, *25*, 127-139.

141. Jeckelmann, N.; Haefliger, O. P. Release Kinetics of Actives from Chewing Gums into Saliva Monitored by Direct Analysis in Real Time Mass Spectrometry. *Rapid Commun. Mass Spectrom.* **2010**, *24*, 1165-1171.
142. Haunschmidt, M.; Klampfl, C. W.; Buchberger, W.; Hertsens, R. Rapid Identification of Stabilizers in Polypropylene using Time-of-Flight Mass Spectrometry and DART as Ion Source. *Analyst.* **2010**, *135*, 80-85.
143. Rothenbacher, T.; Schwack, W. Rapid and Nondestructive Analysis of Phthalic Acid Esters in Toys Made of Poly(vinyl chloride) by Direct Analysis in Real Time Single-Quadrupole Mass Spectrometry. *Rapid Commun. Mass Spectrom.* **2009**, *23*, 2829-2835.
144. Rothenbacher, T.; Schwack, W. Rapid Identification of Additives in Poly(vinyl chloride) Lid Gaskets by Direct Analysis in Real Time Ionization and Single-Quadrupole Mass Spectrometry. *Rapid Commun. Mass Spectrom.* **2010**, *24*, 21-29.
145. Dolnikowski, G. G.; Kristo, M. J. *et al.* Ion-trapping Technique for Ion/Molecule Reaction Studies in the Center Quadrupole of a Triple Quadrupole Mass Spectrometer. *Int. J. Mass Spec. Ion Proc.* **1988**, *82*, 1-15.
146. Schwartz, J. C.; Senko, M. W. A Two-Dimensional Quadrupole Ion Trap Mass Spectrometer. *J. Am. Soc. Mass Spectrom.* **2002**, *13*, 659-669.
147. Wong, P. S. H.; Cooks, R. G. *Ion Trap Mass Spectrometry*. Bioanalytical Systems Inc., 16, 1997.
148. Song Y. S.; Wu, G. X.; Song, Q. Y.; Cooks, R. G.; Ouyang, Z.; Plass, W. R. Novel Linear Ion Trap Mass Analyzer Composed of Four Planar Electrodes. *J. Am. Soc. Mass Spectrom.* **2006**, *17*, 631-639.
149. Douglas, D.; Frank, A.; Mao, D. Linear Ion Traps in MS. *Mass Spectrom. Rev.* **2005**, *24*, 1-29.
150. Shukla, A. K.; Futrell, J. H. Tandem Mass Spectrometry: Dissociation of Ions by Collisional Activation. *J. Mass Spectrom.* **2000**, *35*, 1069-1090.
151. Bessette, E. E.; Spivack, S. D.; Goodenough, A. K. *et al.* Identification of Carcinogen DNA Adducts in Human Saliva by Linear Quadrupole Ion Trap/Multistage Tandem Mass Spectrometry. *Chemical Research in Toxicology.* **2010**, *23*, 1234 -1244.
152. Koppelaar, D. W.; Barigana, C. J.; Denton, M. B.; Sperline, R. P.; Hieftje, G. M.; Schilling, G. D.; Andrade, F. J.; Barnes J. H. Mass Spectrometry Detectors. *Anal. Chem.* **2005**, *77*, 418A-427A.
153. Barnes, J. H.; Hieftje, G. M. Recent Advances in Detector-Array Technology for Mass Spectrometry. *International Journal of Mass Spectrometry.* **2004**, *238*, 33-46.
154. Robb, D. B.; Covey, T. R.; Bruins, A. P. Atmospheric Pressure Photoionization: An Ionization Method for Liquid Chromatography–Mass Spectrometry. *Anal. Chem.* **2000**, *72*, 3653-3659.

155. F. M. Penning. Ionization by metastable atoms. *Naturwissenschaften*. **1927**, *15*, 818.
156. R. T. Haftka, E. P. Scott, J. Cruz. Optimization and Experiments – A Survey. *Applied Mechanical Reviews*. **1998**, *51*, 435-448.
157. Harris, G. A.; Fernandez, F. M. Simulation and Experimental Investigation of Atmospheric Transport in Ambient Metastable-Induced Chemical Ionization Source. *Anal. Chem.* **2009**, *81*, 322-329.
158. Zhou, M.; McDonald, J. F.; Fernandez, F. M. Optimization of a Direct Analysis in Real Time/Time-of-Flight Mass Spectrometry Method for Rapid Serum Metabolomic Fingerprinting. *J. Am. Soc. Mass. Spectrom.* **2010**, *21*, 68-75.
159. Crawford, E. A.; Musselman, B. D.; Tice, J. *Enabling More Efficient Ion Collection in Surface Ionization Experiments*. Proceedings at the 56th ASMS Conference on Mass Spectrometry and Allied Topics, Denver, CO, June 1-5, 2008.
160. Harris, D. C. *Quantitative Chemical Analysis*, 8th ed.; W. H. Freeman & Co.: New York, 2010.
161. Brown, R. F.; Agbogbo, F. K.; Holtzapple, M. T. Comparison of Mechanistic Models in the Initial Rate Enzymatic Hydrolysis of AFEX-treated Wheat Straw. *Biotechnology for Biofuels*. **2010**, *3*, 1-13.
162. Zar, J. H. *Biostatistical Analysis*, 5th ed.; Prentice Hall: Upper Saddle River, New Jersey, 2010.
163. Shafer, W. D. The Identification and Quantitation of Seven Ergot Alkaloids from Bovine Lateral Saphenous Vein Tissue using Liquid Chromatography Mass Spectrometry. Master's Thesis, Eastern Kentucky University, Richmond, KY, 2007.
164. Gonzalez, A. G.; Herrador, M. A. A Practical Guide to Analytical Method Validation, Including Measurement Uncertainty and Accuracy Profiles. *Trends in Analytical Chemistry*. **2007**, *26*, 227 -238.
165. Green, J. M. A Practical Guide to Analytical Method Validation. *Anal. Chem.* **1996**, *68*, A305-A309.
166. Huber, L. *Validation and Qualification in Analytical Laboratories*, Interpharm Press; East Englewood, Colorado, 1998.

APPENDIX A

Statistical computation of parameters in matrix-free and matrix-diluted standards

Table A1. Computation of statistical values for calculation of Student's t (matrix-free standards). The specific symbols in the table are described in Section 4.3.2.

Standards in methanol/water (matrix-free)							
x (M)	y (PAR)	\hat{Y}	\hat{X}	$y - \hat{Y}$	$(x - \hat{X})$	$(y - \hat{Y})^2$	$(x - \hat{X})^2$
3.00×10^{-3}	6.2864	6.3285	3.10×10^{-3}	-0.0421	2.02×10^{-5}	1.80×10^{-3}	4.07×10^{-10}
2.00×10^{-3}	4.2641	4.2389	2.01×10^{-3}	0.0252	-1.20×10^{-5}	6.00×10^{-4}	1.45×10^{-10}
1.00×10^{-3}	2.1567	2.1493	1.00×10^{-3}	0.0074	-3.50×10^{-6}	5.50×10^{-5}	1.26×10^{-11}
6.00×10^{-4}	1.4435	1.3135	6.62×10^{-4}	0.1300	-6.20×10^{-5}	1.71×10^{-2}	3.87×10^{-9}
1.00×10^{-4}	0.2054	0.2687	6.97×10^{-5}	-0.0632	3.03×10^{-5}	4.00×10^{-3}	9.16×10^{-10}
6.00×10^{-5}	0.1477	0.1851	4.21×10^{-5}	-0.0374	1.79×10^{-5}	1.40×10^{-3}	3.20×10^{-10}
1.00×10^{-5}	0.0612	0.0806	6.97×10^{-7}	-0.0194	9.30×10^{-6}	3.78×10^{-4}	8.66×10^{-11}
						SS_{res}	0.0251
						MS_{res}	0.0050
						$S_{y \bullet x(1)}$	0.0709
						$\sum(x^2)_1$	5.76×10^{-9}

Table A2. Computation of statistical values for calculation of Student's t (matrix-diluted standards). The specific symbols in the table are described in Section 4.3.2.

Standards in 1% BES (matrix-diluted)							
x (M)	y (PAR)	\hat{Y}	\hat{X}	$y - \hat{Y}$	$(x - \hat{X})$	$(y - \hat{Y})^2$	$(x - \hat{X})^2$
3.00×10^{-3}	6.1292	6.1642	2.98×10^{-3}	-0.03497	-1.70×10^{-5}	0.00122	2.99×10^{-10}
2.00×10^{-3}	4.1082	4.1404	1.98×10^{-3}	-0.03219	-1.60×10^{-5}	0.00103	2.53×10^{-10}
1.00×10^{-3}	2.2228	2.1166	1.05×10^{-3}	0.10619	5.25×10^{-5}	0.01128	2.75×10^{-9}
6.00×10^{-4}	1.4273	1.3071	6.59×10^{-4}	0.12027	5.94×10^{-5}	0.01446	3.53×10^{-9}
1.00×10^{-4}	0.2348	0.2952	7.02×10^{-5}	-0.06036	-3.00×10^{-5}	0.00364	8.89×10^{-10}
6.00×10^{-5}	0.1713	0.2142	3.88×10^{-5}	-0.04294	-2.10×10^{-5}	0.00184	4.50×10^{-10}
1.00×10^{-5}	0.0572	0.1130	-1.80×10^{-5}	-0.05587	-2.80×10^{-5}	0.00312	7.62×10^{-10}
						SS_{res}	0.0366
						MS_{res}	0.0073
						$S_{y \bullet x(2)}$	0.0856
						$\sum(x^2)_2$	8.94×10^{-9}

APPENDIX B

Calibration curves generated from glucose standards prepared from both pure solvents (50:50 methanol/water, v/v) and matrix-diluted solvents (1% BES). The curves were used to determine the percent recoveries of quality control samples (QCs).

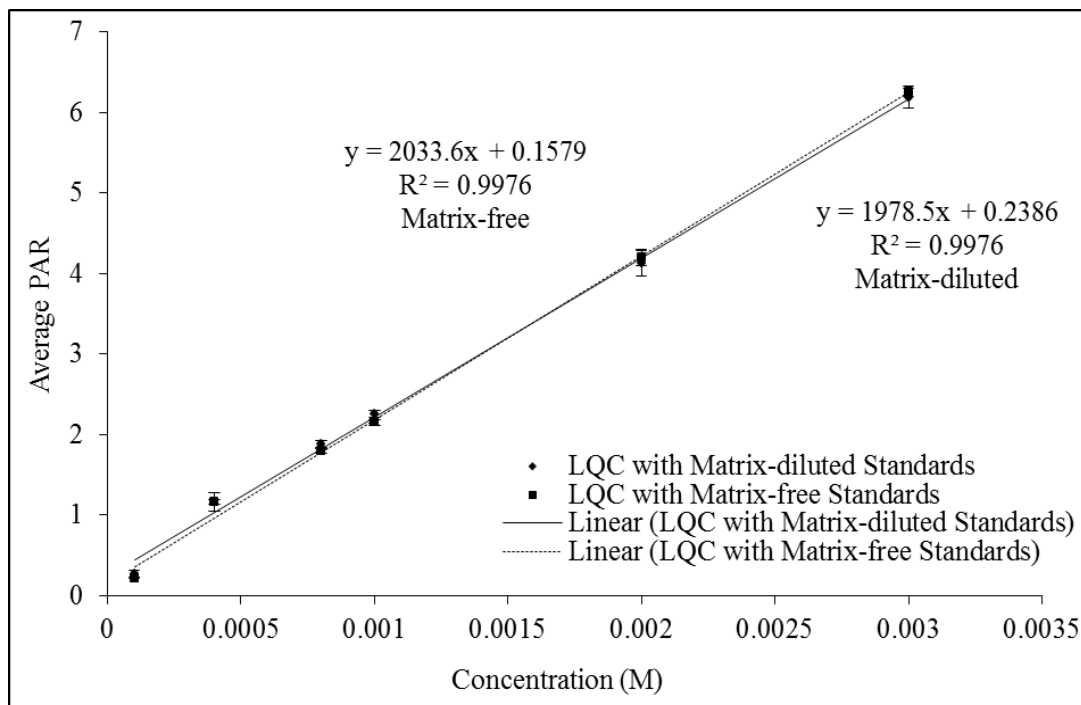


Figure B1. Trend lines generated from LQC recovery experiments with matrix-free and matrix-diluted glucose standards.

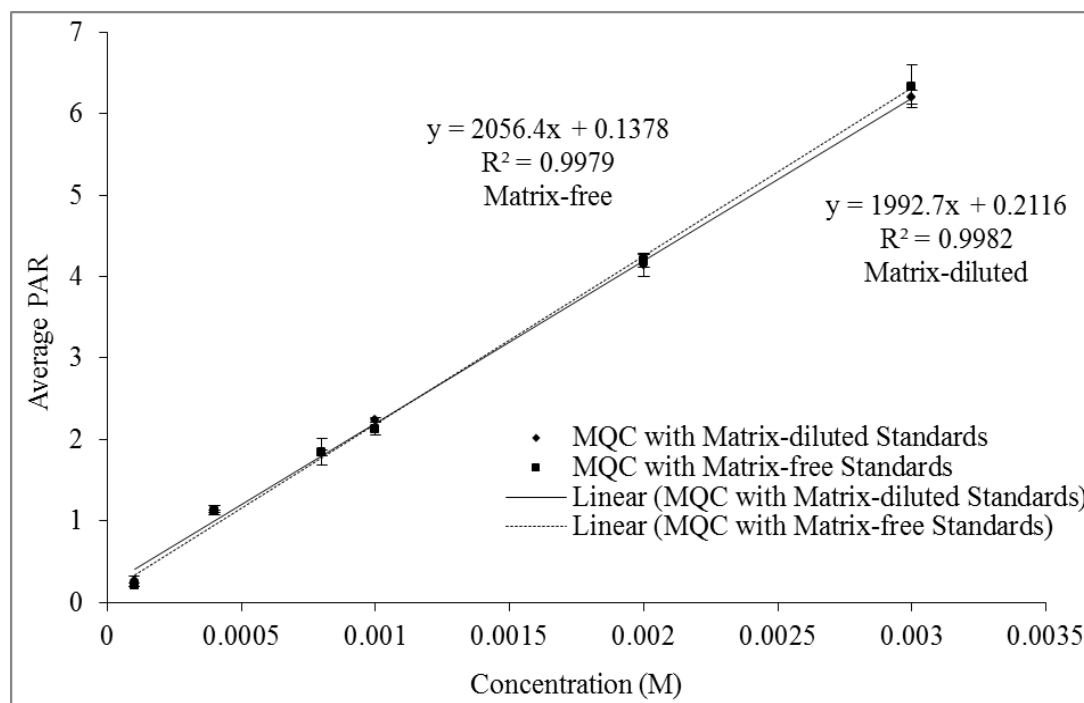


Figure B2. Trend lines generated from MQC recovery experiments with matrix-free and matrix-diluted glucose standards.

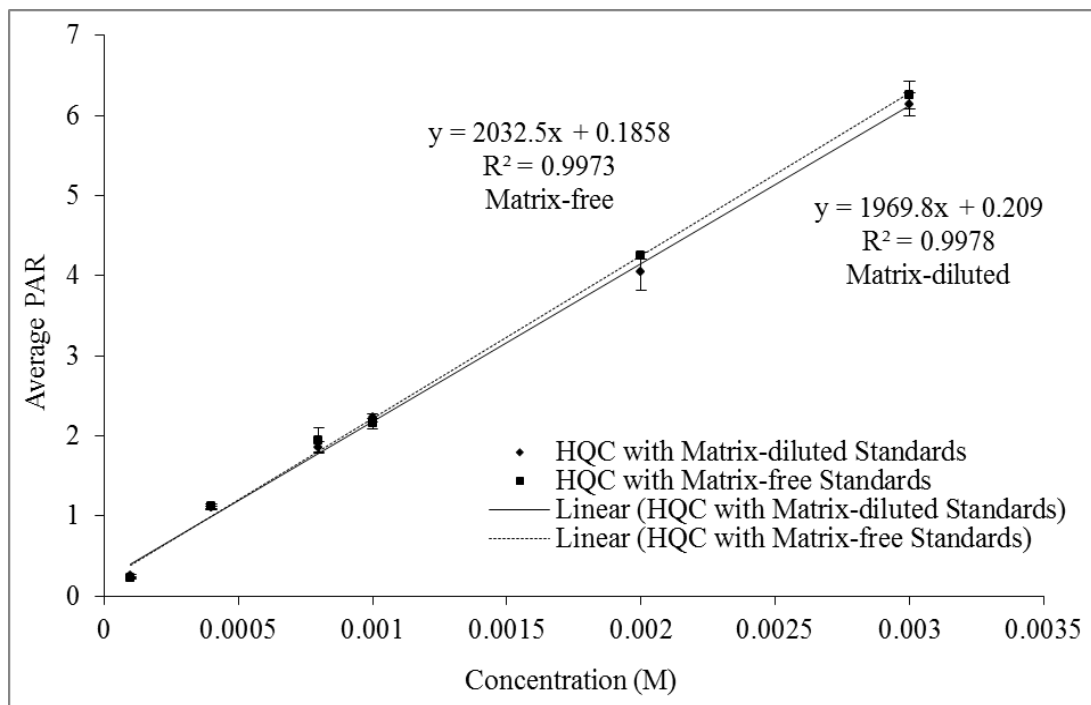


Figure B3. Trend lines generated from HQC recovery experiments with matrix-free and matrix-diluted glucose standards.